The Thesis committee for Kerry Lynn Kreitman

Certifies that this is the approved version of the following thesis:

NONDESTRUCTIVE EVALUATION OF REINFORCED CONCRETE STRUCTURES AFFECTED BY ALKALI-SILICA REACTION AND DELAYED ETTRINGITE FORMATION

Approved by

Supervising Committee:

Jinying Zhu, Supervisor

Kevin J. Folliard

NONDESTRUCTIVE EVALUATION OF REINFORCED CONCRETE STRUCTURES AFFECTED BY ALKALI-SILICA REACTION AND DELAYED ETTRINGITE FORMATION

by

Kerry Lynn Kreitman, B.S.C.E.

Thesis

Presented to the Faculty of the Graduate School of
The University of Texas at Austin
in Partial Fulfillment
of the Requirements
for the Degree of

Master of Science in Engineering

The University of Texas at Austin
August 2011

Dedication

To my parents and sister, for their unconditional love and support in everything

Acknowledgements

First, I'd like to extend appreciation to the Texas Department of Transportation for providing the funding to make this project possible. I would also like to thank my advisors, Dr. Jinying Zhu, Dr. Oguzhan Bayrak, and Dr. Kevin J. Folliard for all of their guidance throughout this project. Without their support and leadership, this project could not have happened. Additionally, I'd like to extend a special thank you to Dean Deschenes for all of his help along the way. His knowledge and experience was invaluable, and I appreciate him going out of his way to answer all of my questions.

To my fellow students on the project, Zach Webb and Eric Giannini, the following pages would be blank without your involvement in all aspects of this project. I cannot take sole credit for the any of the work that went into building the beams and NDT testing, as that was a group effort. Also, I greatly appreciate the help of the students at FSEL and 18B who pitched in during concrete pours and gave me advice on everything else. In particular, I would like to thank Seong-Hoon Kee for his guidance on the NDT front, as well as Nancy Larson, Catherine Hovell, Alejandro Avendaño, Jeremiah Fasl, James Kleineck, Neil Satrom and everyone else for making the lab fun!

The FSEL lab technicians were also vital to the success of this project. Special thanks to Andrew Valentine, who always helped me find better ways to do things as soon as I finished doing them. Additional thanks are extended to Blake Stasney and Dennis Fillip for unlocking doors for me early in the morning and helping with other tasks around the lab. Also, it would have been impossible to collect any data without Eric Schell and Mike Wason's knowledge of the magical world of electronics.

Finally, I'd like to thank my family for their continued support throughout all aspects of my life. My dad's love of math, science and problem solving has inspired me to pursue this particular course of study. My mom's caring and encouraging nature has always helped me achieve my goals. And my sister has always been there to help me with whatever I do, including proof-reading a good portion of this thesis in hopes that it can be easily understood.

August 12, 2011

NONDESTRUCTIVE EVALUATION OF REINFORCED CONCRETE STRUCTURES AFFECTED BY ALKALI-SILICA REACTION AND DELAYED ETTRINGITE FORMATION

Kerry Lynn Kreitman, M.S.E.
The University of Texas at Austin, 2011

Supervisor: Jinying Zhu

Alkali-silica reaction (ASR) and delayed ettringite formation (DEF) deterioration have been a problem for the concrete infrastructure in the state of Texas and around the world in recent decades. A great deal of research into the causes and mechanisms of the deterioration has helped to prevent the formation of ASR and DEF in new construction, but the evaluation and maintenance of existing structures remains a problem. The goal of this research is to investigate the use of several nondestructive testing (NDT) methods to evaluate the level of ASR and DEF deterioration in a structural element. Based on the results, recommendations are made as to which NDT methods have the most potential to be incorporated into the evaluation process.

Table of Contents

List of Tables

List of Figures

CHAPTER 1
Introduction

1.1 MOTIVATION

Alkali-silica reaction (ASR) and delayed ettringite formation (DEF) have been responsible for early deterioration of concrete structures around the world. This has been a particular problem for the infrastructure in the state of Texas in recent decades. Through several research programs, ASR and DEF have been largely eradicated in new construction, but the evaluation and maintenance of existing deteriorated structures remains a problem. Mitigation strategies and repairs have proved ineffective in the long-term, and replacement of all affected structures is not an economical option. However, laboratory research and load-testing of field structures have indicated that moderate levels of deterioration are unlikely to pose a threat to structural safety. Thus, effective evaluation techniques are valuable for the development of an economically feasible maintenance plan for these existing structures.

Despite the large volume of research pertaining to ASR and DEF in the literature, very little work has been done involving the use of nondestructive testing (NDT) methods to evaluate the deterioration in large-scale reinforced concrete elements. The behavior of field structures is affected by ASR and DEF differently than that of the small, often unreinforced, specimens tested in laboratories. This research aims to investigate the use of several NDT methods on near full-scale reinforced concrete specimens deteriorated by ASR and DEF, and to determine which methods are most suitable for the evaluation of existing field structures.

1.2 OBJECTIVES AND SCOPE

The Texas Department of Transportation (TxDOT) provided funding for a joint research project between the University of Texas at Austin and Texas A&M University to combine the knowledge and capabilities of both universities in the realms of ASR, DEF

and NDT. The primary objectives of the research were to (1) investigate the use of several NDT methods on a variety of large-scale test specimens deteriorated by ASR and DEF, and (2) make recommendations for the incorporation of NDT methods into the evaluation process for existing deteriorated structures. Structural testing of the specimens was also included as a secondary research objective. The research presented in this document covers a portion of this project completed in the first two years of the three-year project. All work was done at the Ferguson Structural Engineering Laboratory at the University of Texas.

This portion of the project began with performing a comprehensive literature review of previous research involving the use of NDT on specimens affected by ASR and DEF. Additional NDT methods that may potentially be used for evaluating the deterioration were also identified. Next, three near-full scale bent cap specimens were fabricated and conditioned outdoors to accelerate the deterioration. These specimens were monitored for approximately one year. Monitoring consisted of measuring the expansive strains caused by the deterioration, and performing several NDT methods as the deterioration progressed. Conclusions and recommendations were made based on the correlations between the NDT results and the level of deterioration.

1.3 ORGANIZATION

The details of the work completed in this two-year study are presented in the following chapters. Background information regarding the mechanisms of ASR and DEF and the effects of the deterioration on plain and reinforced concrete is provided in Chapter 2. A literature review of several NDT methods and their use on elements affected by ASR and DEF is given in Chapter 3. The test specimens and experimental program are described in detail in Chapter 4 and Chapter 5, respectively. All results from the monitoring program are presented and discussed in Chapter 6. Finally, conclusions and recommendations summarizing the findings of this research are made in Chapter 7.

CHAPTER 2
Background

2.1 OVERVIEW

In the past few decades, an outbreak of deterioration in highway structures brought on by alkali-silica reaction (ASR) and delayed ettringite formation (DEF) has occurred in Texas. A thorough description of this problem is provided by Deschenes (2009), with the key points summarized here.

This deterioration outbreak was largely caused by the increased use of cement with high early strength properties in both precast and cast-in-place elements, raising both the alkali content and the curing temperature to induce ASR and DEF. Deterioration has been found mostly in mass concrete structures, where elevated temperatures naturally form during hydration and curing, and in elements exposed to excessive moisture from runoff or nearby water sources. Several research projects have been funded by TxDOT in the past 15 years to investigate the prevention and mitigation of deterioration as well as the performance of affected structures. Large strides have been taken to prevent deterioration in new structures, but less success has been achieved with mitigation techniques and structural performance. The main concern now is with the evaluation of existing structures suffering from ASR and DEF, with a focus on determining the level of damage as well as the safety and performance implications of the deterioration.

This chapter begins with an overview of the mechanisms by which ASR and DEF occur (Section 2.2). Section 2.3 discusses the effects of deterioration on mechanical properties and behavior for both unreinforced and reinforced concrete. Finally, the major concerns that deterioration imposes on the safety and integrity of structures are highlighted in Section 2.4.

2.2 REACTION MECHANISMS

Though the effects are similar, specifically expansion and cracking, the mechanisms by which ASR and DEF occur in concrete are very different. Bauer et al. (2006) gives an in-depth explanation of the chemical reactions behind both deterioration processes. The following two sections summarize that work to give an overview of how ASR and DEF deteriorate concrete.

2.2.1 Alkali-Silica Reaction (ASR)

Deterioration from alkali-silica reaction (ASR) takes place in two stages, as illustrated in Figure 2-1. First, hydroxyl ions and alkalis from the cement paste react with silica from certain aggregates to form alkali-silica gel. The alkalis are typically sodium and potassium (Na^+ and K^+), while the silica is usually in non-crystalline or cryptoc-crystalline form (SiO_2). The gel is initially formed at the interface between the paste and the aggregate, although it can expand throughout both the paste and aggregate as deterioration progresses. Next, the gel absorbs available moisture and expands. When the tensile strength of the material is reached, cracks form in the cement paste and, in the case of high reactivity, in the aggregates as well. Because more moisture becomes available when cracks form and grow, the reaction can be self-propagating. It is important to note that if sufficient moisture is not available, the gel will not expand and deterioration will not occur. Thus, three components are required for deterioration by ASR: sufficient alkalis, reactive silica and the presence of moisture. Additionally, elevated temperatures tend to drive the reaction, encouraging more rapid deterioration.

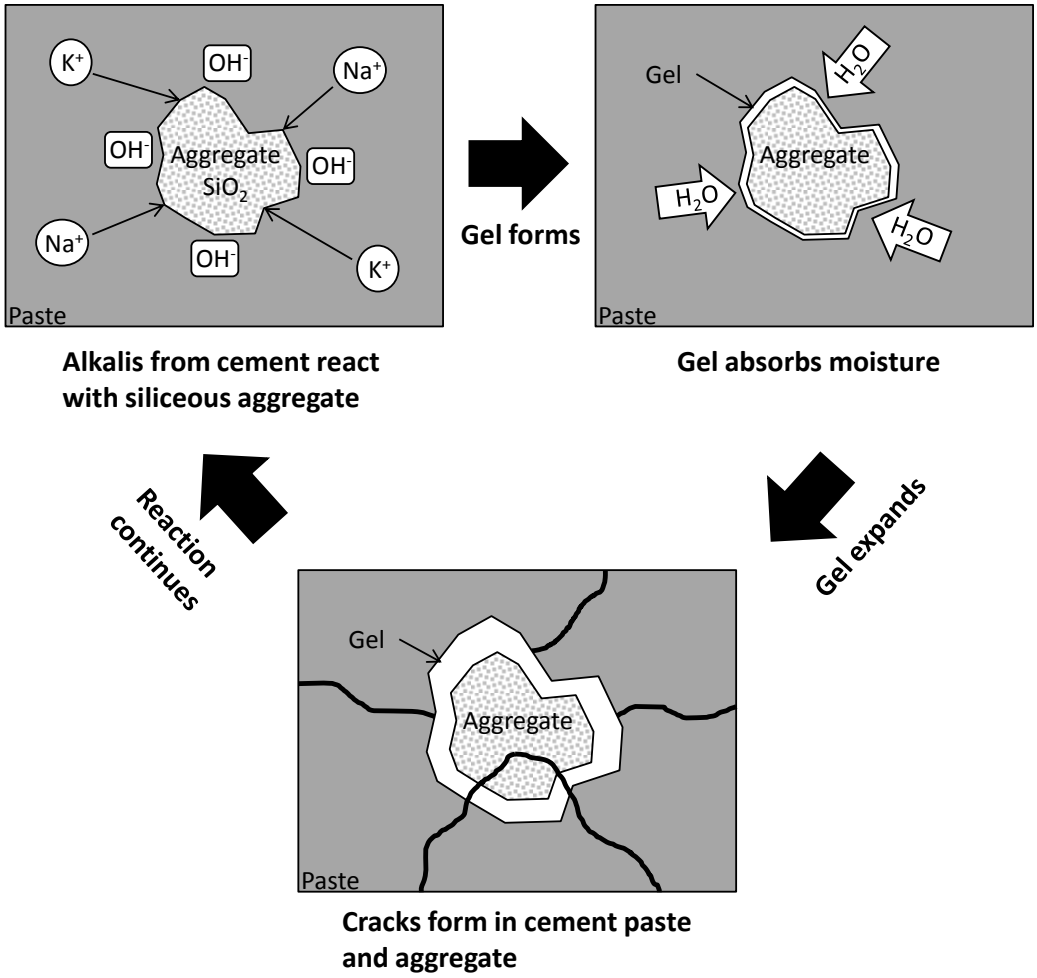

Figure 2-1: Alkali-Silica Reaction Mechanism

A great deal of research has been done to prevent ASR in new structures. Simple control of the materials used in the concrete mixture can diminish the chances of severe deterioration. Limiting the quantity of available alkalis and silica reduces both the likelihood and the magnitude of the reaction. This can be done by using low-alkali cement along with aggregates with lower silica contents or with less reactive forms of silica. Additionally, a portion of the cement can be replaced by fly ash, slag or silica fume to control or slow down the reaction. Fly ash reduces the availability of alkalis by more effectively binding them to the pore solution than cement alone. The presence of both slag and silica fume restricts the mobility of ions in the pore solution, limits the water permeability of the concrete, and reduces the pore solution pH.

2.2.2 Delayed Ettringite Formation (DEF)

Ettringite, a normal product of the concrete curing process, is formed by the combination of calcium aluminate and sulfate. At high curing temperatures, however, ettringite formation is inhibited. Instead, the compound forms slowly over time, causing expansive forces and cracking. This process is called delayed ettringite formation (DEF).

DEF deterioration, illustrated in Figure 2-2, also occurs in two stages. First, temperatures must exceed 158°F during curing of the concrete. At these high temperatures, the aluminates and sulfates that typically form ettringite are instead released into the pore solution. The aluminates combine with calcium to form products like monosulfoaluminate (an AFm phase), and the sulfates adsorb to other curing products (usually C-S-H gel). Then, over a long period of time, the sulfates dissolve back into the pore solution where they can move through the network of microcracks. The free sulfates react with the AFm phases to form ettringite, long after the curing process is complete.

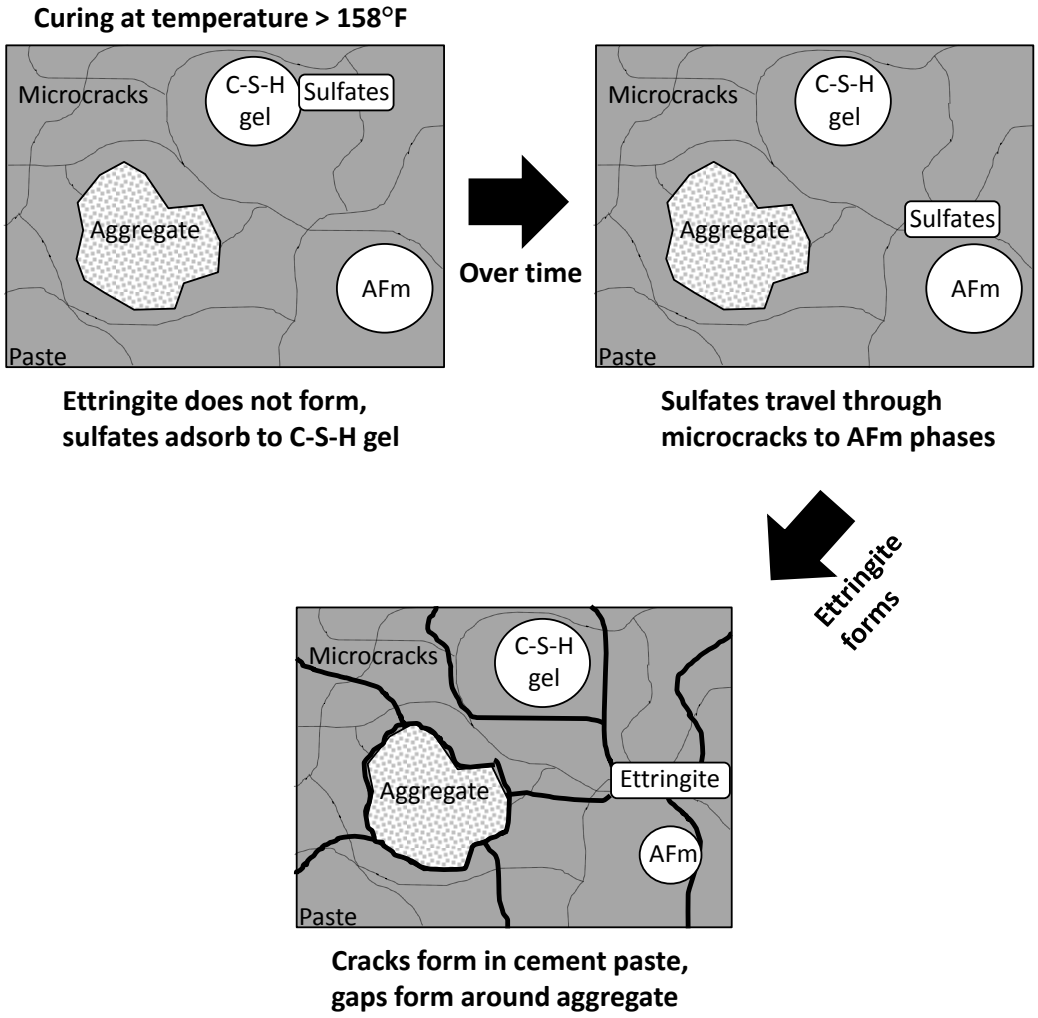

Figure 2-2: Delayed Ettringite Formation Mechanism

It is thought that expansion occurs as a result of the formation and growth of ettringite crystals in locations of limited space, such as the tips of microcracks. This applies pressure to the cement paste, causing cracking throughout the paste, similar to ASR. However, the aggregates do not expand or crack. Often gapping is seen as the paste expands away from the aggregate.

Deterioration due to DEF can be mitigated in several ways. Reducing curing temperatures below 158°F will essentially eliminate temperature-induced DEF. Note that in some cases, alternative forms of DEF can occur when sulfates are released from other sources after curing. Also, similar to ASR, replacing a portion of the cement with fly ash,

slag or silica fume can significantly inhibit DEF deterioration by limiting the mobility of water and dissolved ions and by altering the early hydration process.

2.3 EFFECTS OF ASR AND DEF DETERIORATION

Deterioration from ASR and DEF has a detrimental effect on the concrete material. As the reactions advance and the concrete expands, microcracks develop in the concrete core while significant cracking is observed on the surface. As a result, the strength and stiffness of the concrete are reduced. However, very different behavior is observed in reinforced concrete, as even a small amount of reinforcement can restrain the expansions to some degree. This is often described as having an effect analogous to prestressing.

Typical cracking patterns caused by ASR and DEF are presented in the next section, followed by a discussion of the mechanical properties and behavior of unreinforced and reinforced concrete deteriorated by ASR and DEF. Most of the information presented here is summarized from a report by The Institute of Structural Engineers (1992) on the structural implications of ASR. However, the structural effects of DEF are assumed to be very similar, because the two reactions induce similar expansion and cracking behavior.

2.3.1 Cracking

In an unrestrained element, expansion due to ASR and DEF causes distributed microcracking which is randomly oriented throughout the concrete core. At the surfaces, less reaction and expansion occurs, since alkalis typically have leached out over time. The difference in expansion between the cover and the core concrete causes wide surface cracks. Additionally, the concrete is not restrained from expanding in the out of plane direction, as it is by the surrounding concrete in all other directions. Thus, most surface expansion occurs in outward, rather than in-plane. Randomly oriented “map” cracking patterns can be observed on the surface of unreinforced elements, as shown in Figure 2-3a. However, reinforcement provides restraint to expansion in certain directions (see Section 2.3.2). For this reason, cracks on the surface of reinforced elements tend to be

oriented in the direction of the primary reinforcement, as illustrated in Figure 2-3b. These photos were taken of ASR and DEF deteriorated specimens from previous research at the University of Texas at Austin.

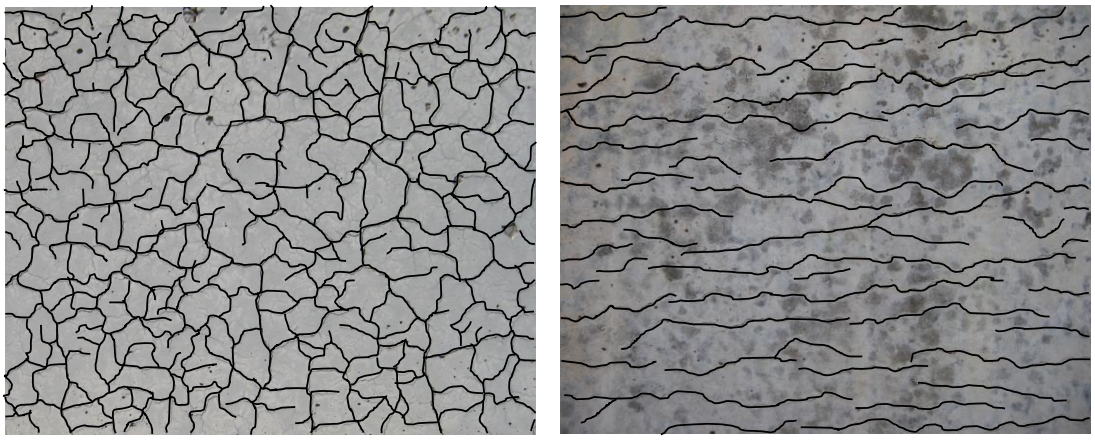

(a) *(b)*

Figure 2-3: Crack Patterns for (a) Unreinforced Element and (b) Reinforced Element with Primary Reinforcement in the Longitudinal Direction

2.3.2 Mechanical Properties and Behavior

The strength and stiffness of unreinforced concrete is reduced as a result of cracking from ASR and DEF. Both the tensile strength and elastic modulus show a maximum of a 50% reduction in the range of expansion typically seen in field structures (up to 2%). The compressive strength is less affected, showing a maximum loss of around 25%. Because the compressive strength of concrete in field structures is often significantly higher than the design strength, this loss is not typically a concern. However, results from several researchers are widely scattered, making it difficult to uniquely relate the loss in strength and stiffness to the amount of deterioration.

Coupled with the visible surface cracking, these results can be alarming to most engineers as well as the general public. Nevertheless, many structures around the world have suffered from ASR and DEF deterioration for decades with no severe performance problems. This is largely due to the presence of restraint from reinforcement in field structures, which limits the expansion in the direction in which the restraint is applied.

As the concrete in a reinforced element expands, the steel resists that expansion. The steel goes into tension, while the concrete undergoes counteracting compressive stresses. As in a prestressed element, this increases the stiffness, offsetting the loss in modulus caused by the cracking. Expansions in reinforced elements are significantly lower than unrestrained expansions, even at low reinforcement ratios. One researcher cited in the ISE report observed a 30% decrease in expansion at a reinforcement ratio of 0.1%, and a 75% decrease in expansion with a reinforcement ratio of 0.5%, as compared to unreinforced specimens (The Institute of Structural Engineers 1992).

Several small-scale studies have been performed to investigate the structural behavior of reinforced concrete. Clark (1989) gave a comprehensive critical review of the structural implications of ASR, including research on flexural and shear behavior as well as bond strength in reinforced and prestressed concrete beams and columns. General findings indicate that ASR deterioration causes little or no significant loss in stiffness, flexural strength, shear strength, or fatigue strength of reinforced or post-tensioned beams and columns with low axial loads. Not enough tests were performed on prestressed beams and heavily loaded columns to obtain conclusive results. Additionally, bond strength was not reduced in specimens with transverse reinforcement.

Most of the more recent studies confirmed these findings (Bungey 1991; Bach et al. 1992; Chana & Korobokis 1992; Ahmed et al. 1998; Fan & Hanson 1998; Monette et al. 2000). However, a few researchers reported a loss of flexural strength and stiffness, leading to some continued concern about the integrity of ASR-affected structures (Swamy & Al-Asali 1989; Hajighasemali et al. 2008). In addition to laboratory tests, a few load tests have been performed on field structures suffering from ASR and DEF damage around the world. Two such tests were described in detail by Deschenes (2009) and are briefly summarized here. First, in South Africa, two full-scale load tests were performed on a portal frame with severe visual damage from ASR (Blight et al. 1983). After loading to around 85% of the design strength, the frame was deemed adequate for stiffness and strength. In 1988, six years later, a second load test yielded very similar results, although crack widths had significantly increased since the first test. Also, in

Japan, full-scale load tests were conducted on two bridge piers showing signs of severe ASR deterioration (Imai et al. 1983). Two undamaged piers were tested as well. No significant loss of stiffness or capacity was reported for any of the piers.

Three large-scale studies of the structural effects of ASR and DEF in reinforced concrete were performed in the past decade at the University of Texas at Austin (Boenig 2000; Deschenes 2009; Larson 2010). Boenig (2000) tested prestressed box beams that were fabricated for use in a Texas bridge, but were never implemented due to signs of ASR and DEF deterioration. Testing yielded no significant reduction in flexural capacity. However shear capacities of nearly 15% lower than expected were found in the most heavily deteriorated beam. Deschenes (2009) fabricated two near full-scale bent caps with accelerated ASR and DEF deterioration, along with a third control specimen. The specimens were nearly identical to those in the current research, so for more details, see Chapter 4. Shear testing of these beams indicated that low to moderate levels of deterioration did not reduce the shear capacity. Additionally, load-induced shear cracks first appeared at much higher loads in the deteriorated beams than in the control. Larson (2010) tested 15 year old prestressed trapezoidal box beams with dapped ends that had been rejected for use in a Texas bridge due to void rotation and poor consolidation. During storage in the precast yard, these beams developed severe deterioration from ASR and DEF. Though shear tests were conducted, anchorage failure of the primary flexural reinforcement controlled the load-carrying capacity. In the most heavily damaged beam, the failure load was 15% lower than that of the beams exhibiting much less deterioration. However, all failure loads were at or above the predicted capacity of the beams.

2.4 STRUCTURAL CONCERNS

Although a great deal of research has already been performed on ASR and DEF in concrete, there are still many concerns about the behavior and safety of deteriorated structures. Most of these concerns lie in the serviceability realm, as large cracks pave the way for other deterioration processes to occur. Because engineers fear that laboratory and field testing may not have covered all possible cases, strength concerns also linger. The following sections describe these concerns.

2.4.1 Serviceability

The laboratory and field tests performed to this point have indicated that the most detrimental effects of ASR and DEF are likely serviceability problems. Firstly, the extensive surface cracking can be visually alarming, not only to engineers, but also to the general public. Severe cracking of concrete always invokes concern for the integrity of a structure. More importantly, the large surface cracks allow water and other contaminants to penetrate into the element, opening up the way for corrosion, freeze-thaw, and other deterioration mechanisms, which are often found in combination with ASR and DEF in field structures. The presence of any of these types of deterioration can ultimately lead to a loss in capacity.

Additionally, because load-induced cracks tend to form at higher levels of stress in elements deteriorated by ASR and DEF, less warning is given when the structure is nearing an overload. This is a minor effect of deterioration but should be taken into account when assessing a field structure.

2.4.2 Strength

Generally, research has indicated that the strength of structural elements with typical design details is not compromised by ASR and DEF deterioration. This is largely due to the presence of reinforcement which restrains the expansion and effectively prestresses the element (see Section 2.3.2). However, despite the countless laboratory tests that show no significant capacity loss, the sheer amount of material damage remains a safety concern.

Recently, a more pressing strength concern has been observed in Japan. Fracture of the transverse reinforcement has been found in structures exhibiting severe ASR deterioration (Miyagawa et al. 2006; Torii et al. 2008). In several bridge piers, fractures have occurred in the 90° bend of the stirrups, as shown in Figure 2-4. It is not clear whether these fractures are a direct result of ASR expansions, or of a combination of ASR and another type of deterioration such as corrosion or freeze-thaw. However, regardless of the cause, the fracture of rebar in an ASR-affected element is a major concern. Without the restraining effects of the reinforcement, a loss in strength and

stiffness may occur, as in unreinforced concrete. This calls into question the safety and integrity of the structure.

Rebar fracture in structures affected by ASR or DEF has not been reported outside of Japan. Due to different detailing practices, such as larger bend radii, rebar fracture may or may not be a realistic concern for Texas. This is being investigated as another portion of this project (Webb 2011).

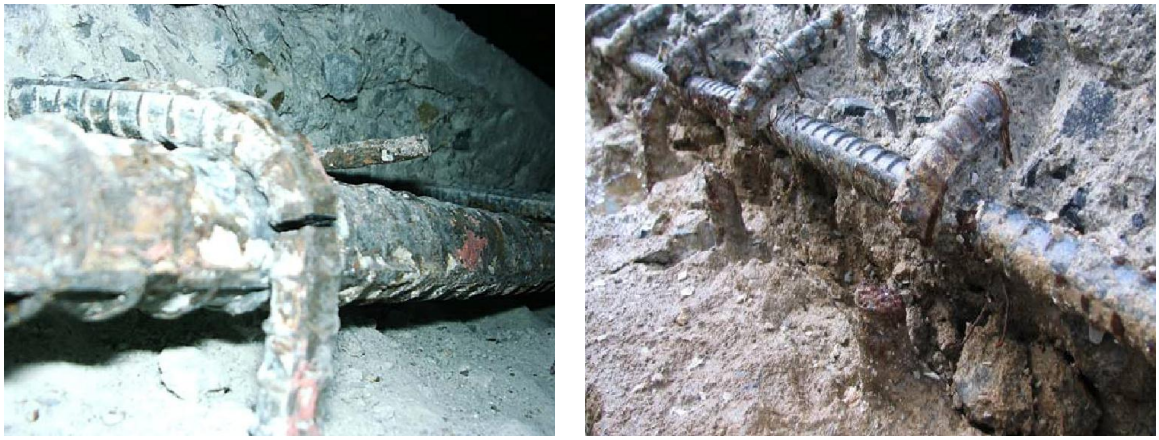

Figure 2-4: Fracture of Rebar in Bridge Piers in Japan Deteriorated by ASR (Miyagawa et al. 2006; Torii et al. 2008)

2.5 SUMMARY

ASR and DEF are chemical deterioration processes that cause expansion and cracking in concrete structures in Texas and around the world. From the great deal of research that has been done, it seems that the deterioration causes no significant loss in stiffness or strength in typically detailed structures because of the restraining effects of the reinforcing steel. Laboratory research and full-scale load tests on field structures generally have confirmed this. However, serviceability concerns arise with the development of large surface cracks, which allow contaminants such as water and de-icing salts to penetrate into the concrete, causing corrosion or freeze-thaw damage. Additionally, fracture of rebar may occur due to the large levels of expansion or as a result of other deterioration mechanisms. If the restraining effects of the reinforcement are removed due to rebar fracture, the structure may exhibit poor behavior or fail prematurely.

CHAPTER 3
Nondestructive Evaluation Methods

3.1 OVERVIEW

Several nondestructive evaluation, or testing, (NDE or NDT) methods have been developed for use in estimating the strength and stiffness of concrete, as well as detecting cracks, delaminations and voids that may or may not be visible from the surface. Most of these methods are based on the propagation properties of mechanical waves through the concrete. Many have already been used in laboratory and field testing to evaluate specimens exhibiting ASR and/or DEF deterioration.

In this chapter, an overview of elastic wave propagation in solids will first be given in Section 3.2. Sections 3.3 through 3.7 describe nine different NDT methods that have the potential to assess ASR and DEF deterioration. Any relevant results from the literature are also reviewed. The NDT methods described in this chapter can be organized into five categories:

1. Ultrasonic methods, including ultrasonic pulse velocity (UPV) and ultrasonic attenuation
2. The impact echo method
3. Resonant frequency methods, on small and large scale specimens
4. Surface wave methods, including spectral analysis of surface waves (SASW) and surface wave transmission (SWT)
5. Nonlinear behavior methods, including harmonic generation, resonant frequency shift and frequency modulation.

3.2 ELASTIC WAVE PROPAGATION IN SOLIDS

When a disturbance occurs on the surface of a solid material, the energy is transferred into the solid by mechanical waves. In nondestructive testing, the disturbance is usually created by impacting the surface with a hammer or steel ball, or by placing a

vibrating transducer on the surface. In a solid half space, the three main types of mechanical waves are compression waves, shear waves, and surface waves (also known as P-, S- and R- waves) respectively. Lamb waves belong to another family of waves that occur only in thin plates.

Compression and shear waves propagate through the body of the medium. In compression waves, the particles oscillate parallel to the direction of wave propagation, inducing compressive and dilational forces. Conversely, particles in shear waves vibrate perpendicular to the propagation direction (see Figure 3-1). Compression waves travel faster than shear waves and are used most often in nondestructive testing (Malhotra & Carino 2004).

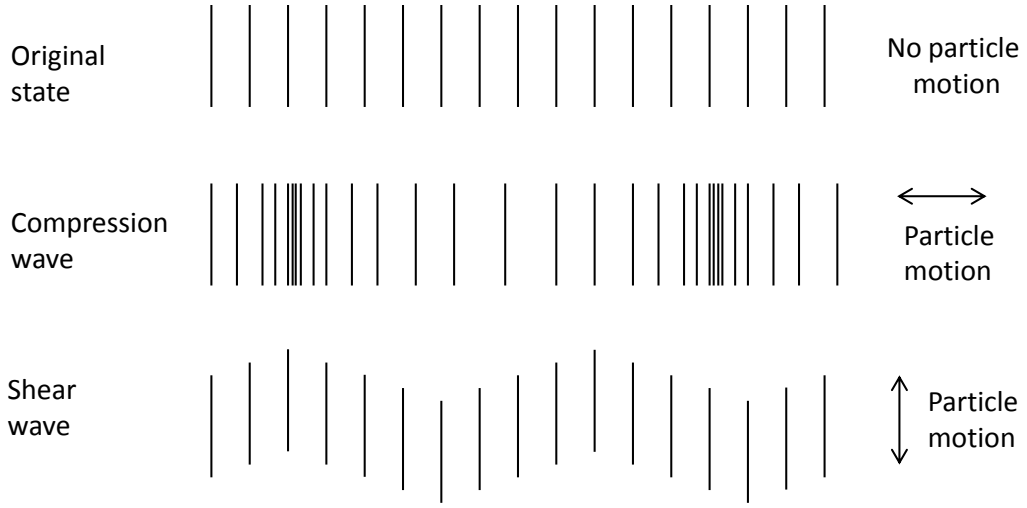

Figure 3-1: Compression and Shear Wave Propagation

Surface waves propagate along the surface of the medium, rather than in the body. As depicted in Figure 3-2, the particles experience both longitudinal and transverse motion while traveling along elliptical paths. The energy diminishes exponentially with depth, reaching about one-tenth of the surface amplitude at a depth of around 1.5 wavelengths (Malhotra & Carino 2004).

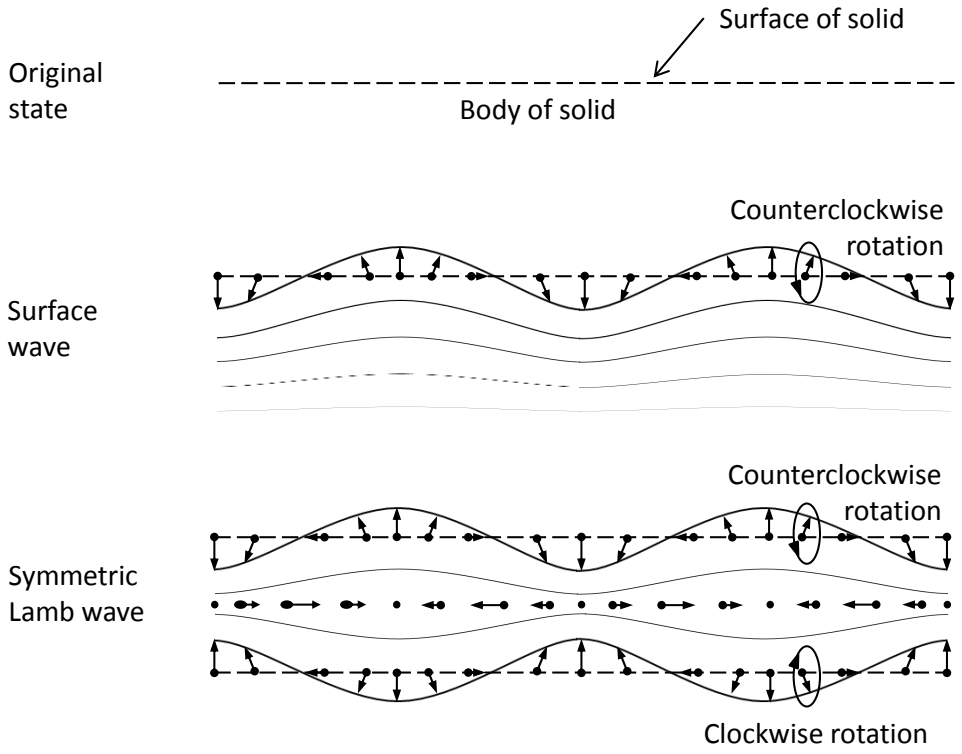

Figure 3-2: Surface and Lamb Wave Propagation

Lamb waves, which only exist in thin elements such as plates, can be thought of as elastic waves which are guided by the boundaries of the plate. They are formed through the interaction of compression and shear waves, and the individual particles translate in both the longitudinal and transverse directions, following elliptical paths (Gibson 2004). These waves can be symmetric or antisymmetric, and the particle motion of a symmetric Lamb wave is illustrated in Figure 3-2.

3.3 ULTRASONIC METHODS

Ultrasonic waves are high-frequency sound waves that exceed the human audible frequency range. For testing concrete, frequencies between 25 and 100 kHz are typically used. While all three main types of ultrasonic waves exist simultaneously in an element, the properties of compression waves are most often observed because they travel the fastest and tend to have higher energy (Malhotra & Carino 2004).

The compression wave velocity is often used as a simple indicator of uniformity and overall quality of concrete. The ultrasonic pulse velocity (UPV) method is based on this principle and is described in the following section. Additionally, the amount of energy dissipated as the wave travels through the concrete can be measured, as in the ultrasonic attenuation method described in Section 3.3.2.

3.3.1 Ultrasonic Pulse Velocity (UPV) Method

The most common technique that has been used to assess deterioration in concrete is the ultrasonic pulse velocity (UPV) method. As depicted in Figure 3-3, the test is performed by placing two transducers on opposite sides of the concrete specimen. The transmitter emits a series of ultrasonic pulses and the time it takes for each pulse to reach the receiver is measured. The velocity is then calculated by dividing the distance the wave has traveled by the measured time.

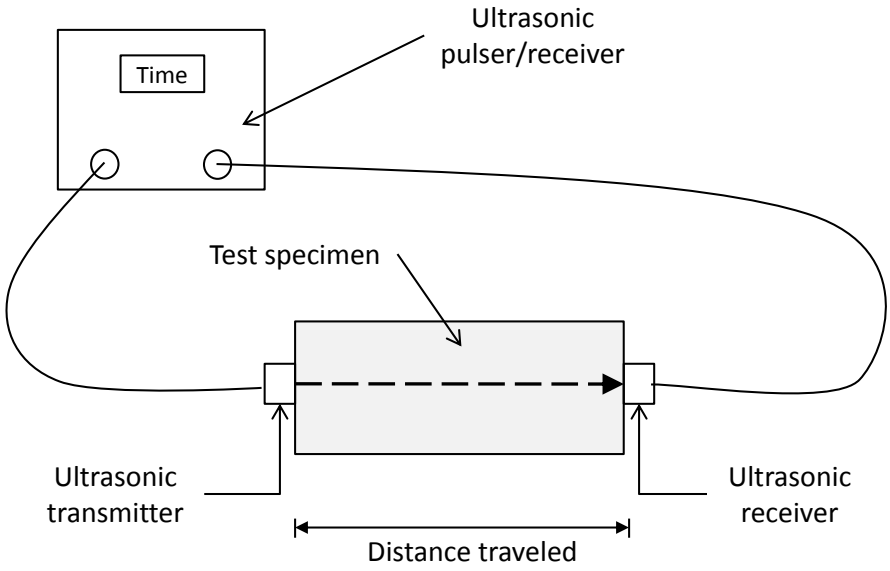

Figure 3-3: Ultrasonic Pulse Velocity Testing

3.3.1.1 Factors Affecting UPV Measurements

The velocity of a compression wave is dependent on the density and elastic properties of the material. For a perfectly elastic material of infinite dimensions, the P-wave velocity is (ACI Committee 228 1998):

$$V_p = \sqrt{\frac{E_d(1-\nu)}{\rho(1+\nu)(1-2\nu)}} \qquad \textit{Equation 3-1}$$

where V_p is the compression wave velocity through material with density ρ, and E_d and ν are the dynamic modulus of elasticity and Poisson's ratio, respectively. However, concrete is not a well-defined, homogeneous elastic material. The elastic properties and density of a particular concrete mixture, and thus the P-wave velocity, are largely affected by a variety of factors. These include the composition and uniformity of the concrete as well as environmental factors (Malhotra & Carino 2004).

The concrete composition has a significant effect on the compression wave velocity. Because the pulse velocity is generally lower in the paste than in the aggregates, a higher aggregate-cement ratio tends to yield a faster velocity. The type of aggregate may also influence the velocity. For example, a concrete mixture with crushed limestone aggregate will have higher compression wave velocity than a similar mixture with river gravel aggregate. Additionally, the presence of rebar in reinforced concrete will increase the velocity, because steel has a higher compression wave velocity than concrete. A high water-cement ratio tends to decrease the stiffness and thus lower the velocity.

The UPV method is often used to assess the quality and uniformity of concrete based on the presence of cracks and voids. It can be difficult to specifically locate small defects by measuring the compression wave velocity, but the method can indicate distributed damage in a certain region. As depicted in Figure 3-4, the shortest travel time will occur when the wave can pass unobstructed through the specimen. When passing through a defect, the wave will propagate more slowly, resulting in a longer total travel time. Additionally, traveling around a defect results in a longer travel path, and thus a longer travel time. If a defect is present that the wave can neither pass through, nor travel around, it would be impossible to measure the velocity at that location.

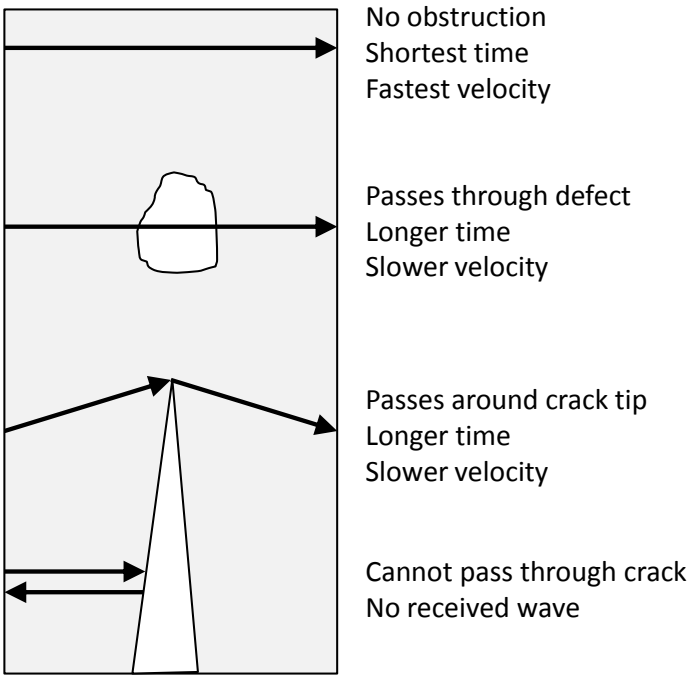

Figure 3-4: Paths of Ultrasonic Waves through Concrete (Adapted from ACI Committee 228 (1998))

Moisture content is the most significant environmental factor that affects the compression wave velocity through concrete. When fully saturated, a concrete specimen can have velocities up to 5% greater than a dry specimen of the same composition (Ohdaira & Masuzawa 2000). This can be explained by the fact that ultrasonic waves travel faster through water than through air. In the case of ASR, gel may also fill some of the cracks, resulting in an increased P-wave velocity as compared to a case with microcracks that are not filled with gel. The other major environmental factor, temperature, has been shown to be insignificant between about 40 and 85°F. For temperatures outside that range, correction factors have been empirically developed (Malhotra & Carino 2004). Also, the presence of load does not seem to affect the compression wave velocity under normal levels of stress. Direct compression tests have shown that the velocity will slightly increase up to a load that induces about 30% of the compressive strength, when microcracks begin to form. The velocity remains fairly constant as the microcracks develop until a load inducing around 70% of the compressive

strength is reached. At this point, the microcracks have developed into a dense network, resulting in a sharp decrease in velocity (S. Popovics & J. S. Popovics 1991).

In undamaged concrete, the compression wave velocity increases rapidly after placement as the concrete begins to harden. The velocity continues to increase through the curing process before leveling off to a relatively constant value. The time it takes to reach a steady velocity varies widely between concretes of different composition, but typically by 28 days the velocity has reached its peak value. In fact, most velocity gain occurs in the first day. Velocities between 3700 and 4200 m/s are typical for normal concrete, although high strength concrete can have P-wave velocities of over 5000 m/s (Malhotra & Carino 2004; Ravindrarajah et al. 2002).

3.3.1.2 Laboratory Studies

Several laboratory-based studies have investigated the effects of ASR deterioration on the compression wave velocity using the UPV method. All of the research addressed here was performed on small specimens, many unreinforced, with the largest cross sectional dimension being 5″. To accelerate the deterioration, all specimens were subjected to a harsh conditioning regime. The P-wave velocity was monitored over time, as was the expansion in at least one direction. Expansions reported here are the approximate average longitudinal expansions, taken in the same direction in which the velocity was measured (see Figure 3-5).

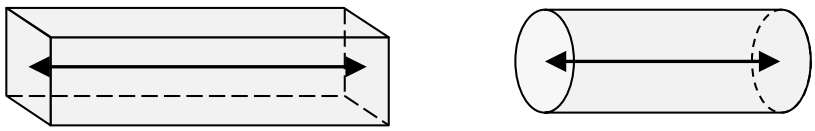

Figure 3-5: Direction of Expansion and UPV Measurements in Laboratory Studies

Empirical results from six different researchers are presented in Figure 3-6, which shows the relationships between compression wave velocity and longitudinal expansion (Rivard & Saint-Pierre 2009; Saint-Pierre et al. 2007; Ahmed et al. 1998; Bungey 1991; Pleau et al. 1989; Swamy & Al-Asali 1989). All percentage change values are based on the velocity reached after curing was complete. Note that no documentation was found

of research involving DEF and UPV. All of the results presented in this section pertain only to ASR.

Generally, all of these studies have found that the compression wave velocity begins to decrease at the onset of expansion. Some indicate that the velocity flattens out or shows tendencies to flatten out over time (Rivard & Saint-Pierre 2009; Saint-Pierre et al. 2007; Pleau et al. 1989). Others have also reported a subsequent increase in velocity at larger expansions, which may be a result of the cracks filling with ASR gel (Ahmed et al. 1998; Swamy & Al-Asali 1989). However, the reported results are quantitativly inconsistent between studies. The slopes of the curves, which can be interpreted as how sensitive the velocity measurement is to the level of expansion, are vastly different, as are the maximum losses in velocity and the level of expansion at which the curve begins to flatten out. These differences may be due to the variety in research parameters chosen for each study. Factors such as specimen size, type of reactive aggregate, total alkali content, reinforcement, and storage conditions varied widely between researchers. Table 3-1 summarizes these factors.

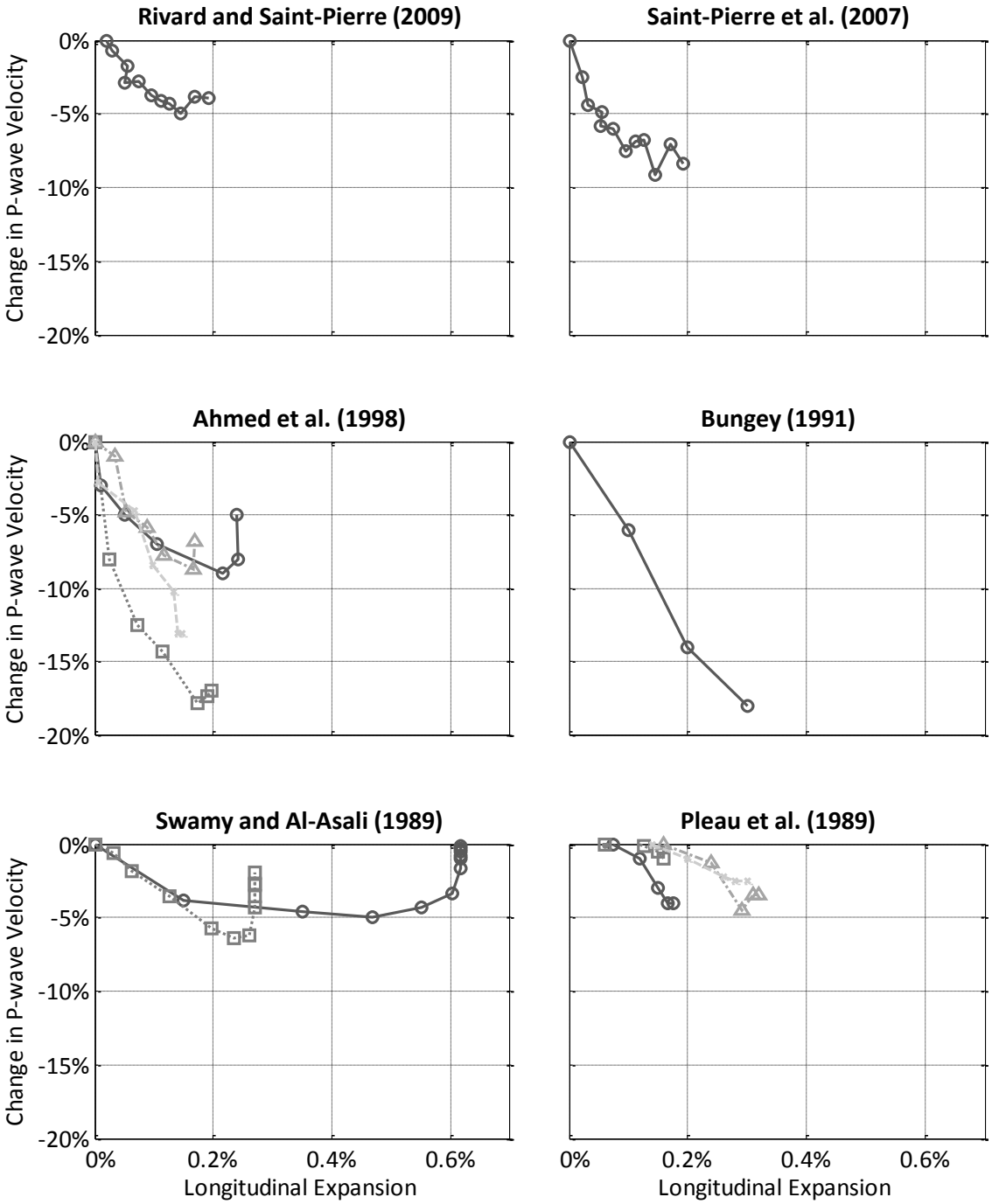

Figure 3-6: UPV Laboratory Results from Literature

Table 3-1: Variation in Research Parameters between UPV Laboratory Studies

Researcher	Specimen Size	Reactive Aggregate	Total Alkalis (kg Na_2O_{eq}/m^3)	Reinforcement	Storage Conditions
Rivard and Saint-Pierre (2009)	3x3x12" prisms, 4x8" cylinders	Spratt limestone	5.25	Unreinforced	At 100°F, over water
Saint-Pierre et al. (2007)	3x3x12" prisms, 4x8" cylinders	Spratt limestone	5.25	Unreinforced	At 100°F, in 1 mol NaOH solution
Ahmed et al. (1998)	3x5x51" beams	Thames Valley sand	7.0	Singly reinforced with and without stirrups	At 104°F, in water
Bungey (1991)	3x3x11" prisms	Fused silica	7.0	Unreinforced	At 68°F, in water
Swamy and Al-Asali (1989)	3x4x32" beams	Beltane opal and fused silica	5.2	Singly reinforced with no stirrups	At 68°F, in air at 96% RH
Pleau et al. (1989)	4x4x10" prisms	Spratt limestone	4.4	Unreinforced	At 73 or 100°F, in air at 100% RH or in 6% NaCL solution

3.3.1.3 Field Studies

A few hydraulic and bridge structures exhibiting ASR deterioration around the world have undergone long term monitoring programs which include UPV testing. However, like the laboratory studies, none of these structures were reported having any

damage from DEF. Compression wave velocity measurements were taken both on the structures themselves (in situ) and on drilled cores. In general, low velocities were reported, indicating deterioration. For example, P-wave velocities between 3450 and 3650 m/s were found in a bridge pier in Japan over the course of 7 years (Ono 2000).

Many researchers reported a wide variety of measured velocities within a structure. Rivard and Saint-Pierre (2009) drilled cores 46 feet deep into a 50 year old hydraulic structure in Canada, and reported a compression wave velocity variation between 3400 and 4700 m/s through the depth. There was no apparent pattern in the distribution of these measurements. Similarly, Alexander et al. (1992) found velocities ranging from 3900 to 4400 m/s, with an average around 4000 m/s, on cores taken from a portal frame in South Africa. Ishizuka et al. (1989) measured velocities between 2900 and 4800 m/s on drilled cores from a bridge pier in Japan. Alexander also reported an average near 4000 m/s for in situ UPV measurements on the same portal frame, and Ishizuka found a range of 2300 to 4500 m/s for in situ measurements of compression wave velocity on the bridge piers. Additionally, Ishizuka noted that the lowest measured in situ velocities were at locations of very large crack widths.

3.3.1.4 Interpreting UPV Results

The results of these field studies indicate that in-service structures may exhibit very different compression wave velocity behavior than laboratory specimens. Combined with the inconsistencies in the laboratory results, this makes it difficult to adequately evaluate field structures using the UPV method at this stage. Understanding the sources of the discrepancies and the inherent flaws in using this method is important, and may lead to better results in the future.

First and foremost, the wide range of measured velocities found in a single element indicate that field structures do not deteriorate as uniformly as do specimens built and monitored in the laboratory. This may be due in part to differences in moisture exposure in field structures, a factor that is easily controlled in a laboratory setting but can cause up to a 5% difference in velocity measurements. Additionally, information about the composition of the concrete is rarely available for field structures, so knowing

such parameters as the aggregate type or alkali content is only possible by coring samples and estimating.

Also, Rivard and Saint-Pierre (2009) mentioned that measuring the compression wave velocity on cores taken from a structure may yield different results than performing an in situ test. Removing the core from the structure changes the stresses on the sample and distances the core from the actual field conditions that the structure experiences. Thus, for the most relevant results, in situ measurements should be taken whenever possible.

One of the biggest weaknesses of many nondestructive testing methods for concrete is the need of a baseline to compare later results too. In this case, knowing what the velocity would be in an identical undamaged specimen is very helpful in estimating the amount of deterioration in an element affected by ASR or DEF. For example, both an undamaged and a severely deteriorated specimen could have P-wave velocities of 3800 m/s. Although it would almost certainly be possible to visibly distinguish between the two, the UPV measurement cannot make any distinction.

Finally, it may be difficult to obtain high-quality UPV results on field structures as a result of coupling issues on rough or dirty surfaces, limited access to certain regions of the structure, or low amplitude signals due to high attenuation and scattering in large structural elements.

3.3.2 Ultrasonic Attenuation Method

A few researchers have suggested that the attenuation, or energy loss, of ultrasonic pulses is more sensitive to ASR or DEF deterioration than the velocity (Saint-Pierre et al. 2007; Bungey 1991). To measure the ultrasonic attenuation, the same test setup is used as for the UPV method (see Figure 3-3), except the transmitted and received waveforms are saved for later analysis. The attenuation is measured from the frequency spectrum after performing a Fast Fourier Transform (FFT) on the received time domain signal. The value of the attenuation can vary over different frequencies, so the central frequency of the signal is often chosen. Saint-Pierre et al. (2007) provide a more detailed discussion of attenuation measurements.

Results from two studies investigating ultrasonic attenuation are shown in Figure 3-7 and Figure 3-8. Both studies were performed on small unreinforced concrete cylinders and prisms. Details about the testing parameters can be found in Table 3-1. In both cases, the attenuation shows about a 90% increase while the velocity decreases only 10-20% (note the difference in scale of the horizontal axes in Figure 3-7). This is an indication that attenuation may be a better assessment technique than velocity. However, unlike UPV testing, attenuation measurements can be affected greatly by the coupling of the transducers to the concrete.

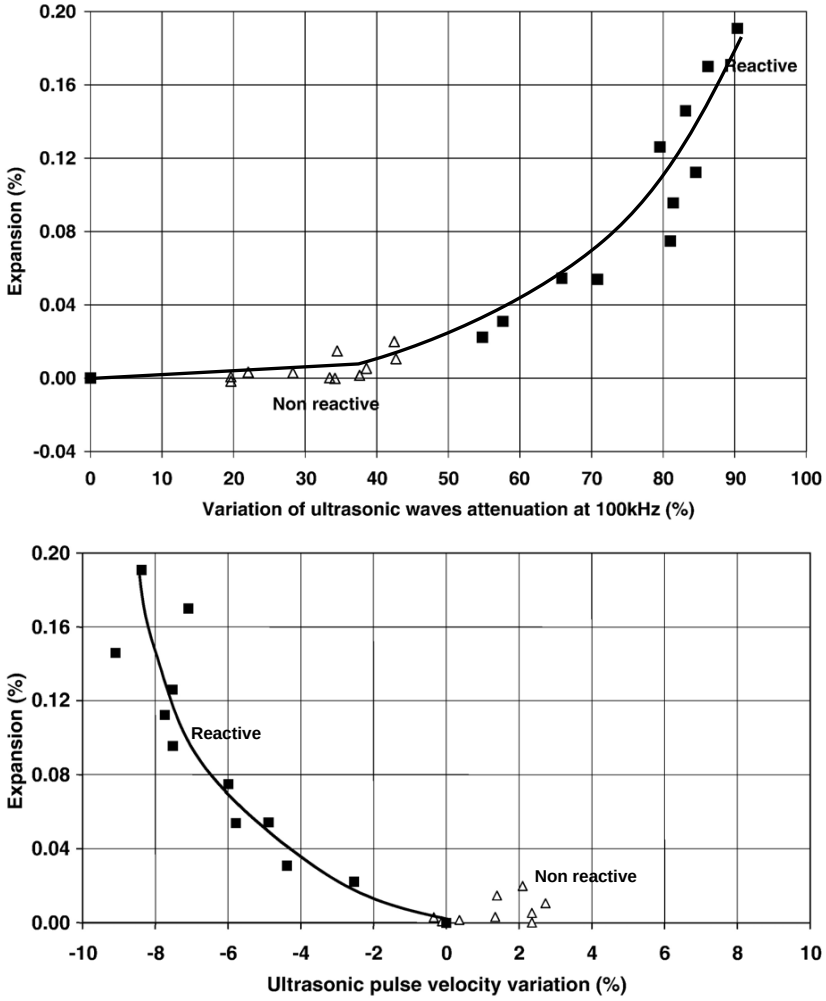

Figure 3-7: Comparison of Ultrasonic Velocity and Attenuation Results (Saint-Pierre et al. 2007)

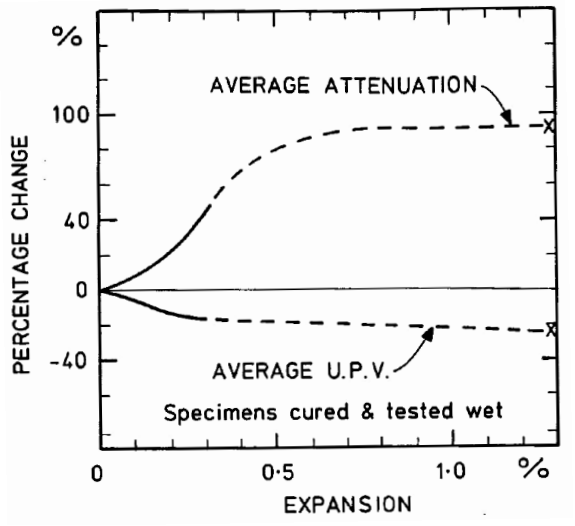

Figure 3-8: Comparison of Ultrasonic Velocity and Attenuation Results (Bungey 1991)

3.4 THE IMPACT ECHO METHOD

Although the impact echo method was originally developed to detect flaws in concrete slabs, it may have the potential to evaluate the distributed microcracking damage caused by ASR and DEF. The basic concept is to observe the surface motion of an element after a short-term mechanical impact, usually from a small steel ball or hammer. The impact induces stress waves into the material which reflect off boundaries and defects before returning to the receiver. Analyzing the surface motion caused by these reflections can indicate the presence or severity of deterioration from ASR or DEF in several ways. Two different theories explaining the impact echo method, the conventional and Lamb wave theories, are summarized in the following two sections. Section 3.4.3 discusses the effects of the impactor size, and Section 3.4.4 provides an overview of the use of the method in detecting distributed damage, as from ASR or DEF.

3.4.1 Conventional Theory

Conventional theory suggests that multiple reflections of the stress waves between the surfaces and any internal defects will be evident in the surface displacement measurements. For an undamaged, plate-like specimen, the wave will repeatedly reflect between the receiver and back surface, as depicted in Figure 3-9a. The time between

arrivals is constant, indicating periodic reflections. If a large internal defect is present, the wave will reflect between the defect and the receiver, resulting in a shorter time between arrivals (see Figure 3-9b).

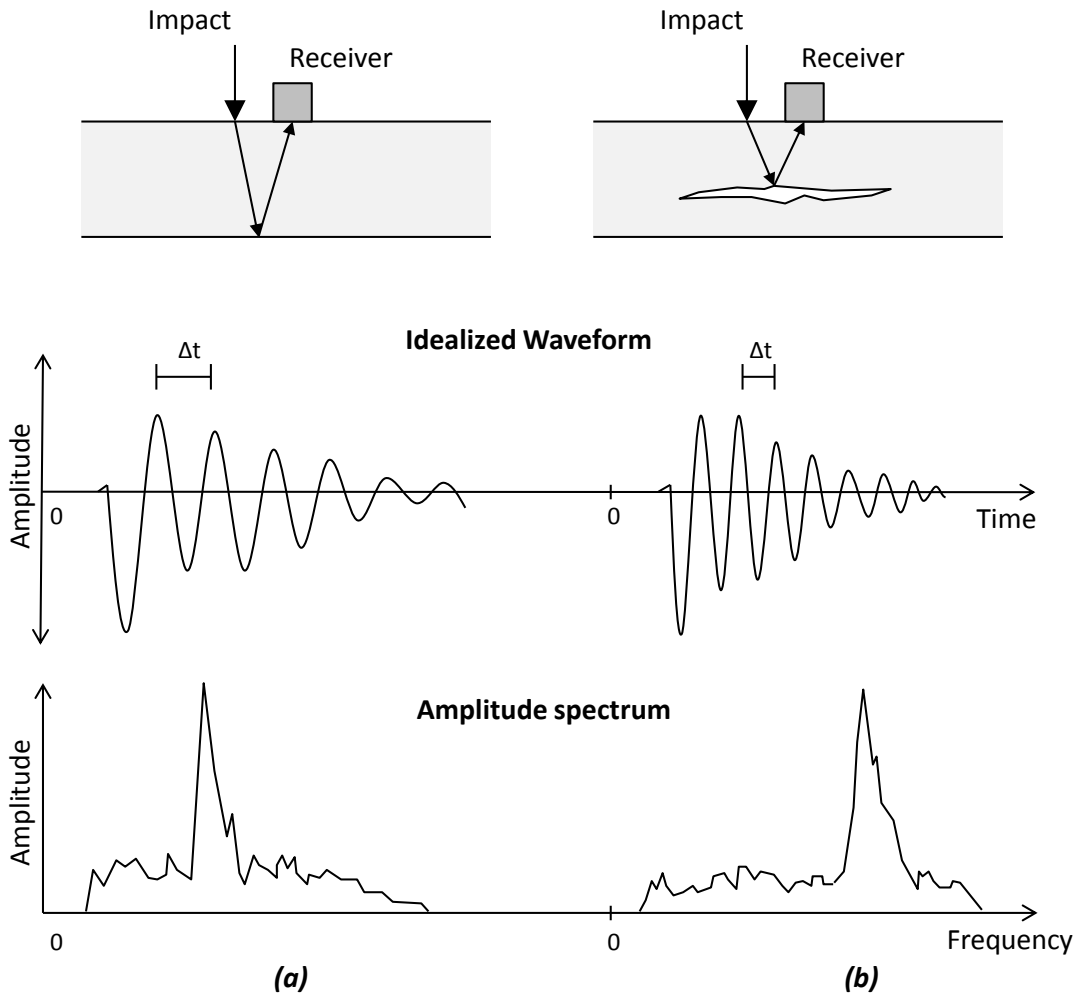

Figure 3-9: Conventional Impact Echo Theory (Adapted from Sansalone and Streett (1997)) (a) Undamaged Specimen and (b) Specimen with a Defect

Although the difference between these two signals is obvious from observing the time domain signal, the response is often more complex than the idealized waveforms shown here. This can make time domain analysis challenging. Using a Fast Fourier Transform (FFT) however, the signal can be transformed into the frequency domain, enabling a simpler analysis that clearly highlights the resonant frequencies as peaks in the spectrum. As can be seen in Figure 3-9, the undamaged specimen has a lower resonant

frequency than does the specimen with a defect. These frequencies are related to both the wave speed and the element thickness (or depth of defect) by (Sansalone 1997):

$$f = \frac{\beta V_p}{2D} \qquad \textit{Equation 3-2}$$

where f is the measured resonant frequency of an element of thickness or defect depth D, V_p is the compression wave velocity, and β is a shape factor dependent on the cross sectional geometry. Note that if the receiver is placed close to the impact source, the response will be dominated by compression waves, despite the presence of shear waves and surface waves. Often, the initial large amplitude surface wave is clipped or removed in the analysis.

The shape factor, β, accounts for the different vibrational modes induced in cross sections with different geometries. Values of β were determined by finite element and eigenvalue analysis for a variety of cross sectional shapes. For plate elements, for which this method was developed, β was thought to be equal to 1.0. However, computer analysis indicated a shape factor of 0.96. Sansalone explains that "this difference occurs because multiple reflections of P-waves excite a particular mode of vibration in the plate – the thickness mode – and the displacements caused by this mode produce the principal periodic patterns in the waveform" (Sansalone & Streett 1997). Though this theory gives no clear mathematical explanation for this slight reduction in the shape factor, this method is widely accepted in practice, has been upheld by experimental results and finite element modeling, and has its own ASTM standard (ASTM C1383 2004).

β varies between 0.75 and 0.96 for rectangular cross sections, depending on the aspect ratio. As depicted in Figure 3-10, the aspect ratio is defined as the depth-to-width ratio of the cross section, where the depth is measured parallel to the direction of the impact (Sansalone & Streett 1997). For an element to be classified as a plate, the aspect ratio must be less than 0.2. Schubert and Köhler (2008) argue that along with dependence on the cross sectional geometry, the correction factor is also a function of the time duration of the signal collected. Longer collection times allow for multiple reflections off of several boundaries, complicating the signal.

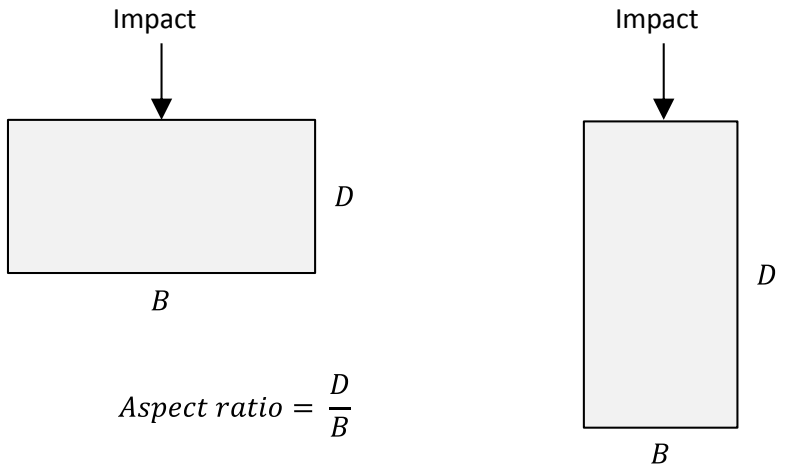

Figure 3-10: Definition of the Aspect Ratio in Impact Echo Testing

3.4.2 Lamb Wave Theory

Gibson and J. S. Popovics (2005) provide an alternate theory for the impact echo method, based on the propagation of Lamb waves (see Section 3.2), which offers a mathematical explanation for the shape factor of 0.96 in plate elements. This theory suggests that the dominant resonant mode, which Sansalone called the "thickness mode", is the non-propagating, first-order, symmetric Lamb wave vibrational mode. In a non-propagating Lamb wave, no energy is transmitted longitudinally and the particles undergo no rotation. Instead the energy is captured and sustained in stationary resonant vibration. These waves are said to have zero group velocity, since there is no associated energy propagation.

Gibson's Lamb wave theory has been upheld by both experimental and finite element tests. Values derived for the geometric correction factor ranged from 0.945 to 0.957 for plates, and are a function of Poisson's ratio. These results closely correspond to the empirically determined 0.96 β factor for plates in conventional theory.

3.4.3 Effect of Impactor Size

A key factor in impact echo testing is using the correct impactor. Typically, a steel ball of diameter between 3 and 15mm is used, inducing contact times ranging from 15 to 100μs (Sansalone & Streett 1997). The diameter of the impactor is directly related

to the contact time and inversely related to the maximum frequency that can be detected. Because the frequency, in turn, is inversely related to the thickness of the element or depth of the defect, larger impactors are used to detect deeper defects or the back surfaces of thicker elements. Conversely, smaller impactors can detect defects that are closer to the surface which reflect the wave at a higher frequency. These relationships are shown in Figure 3-11.

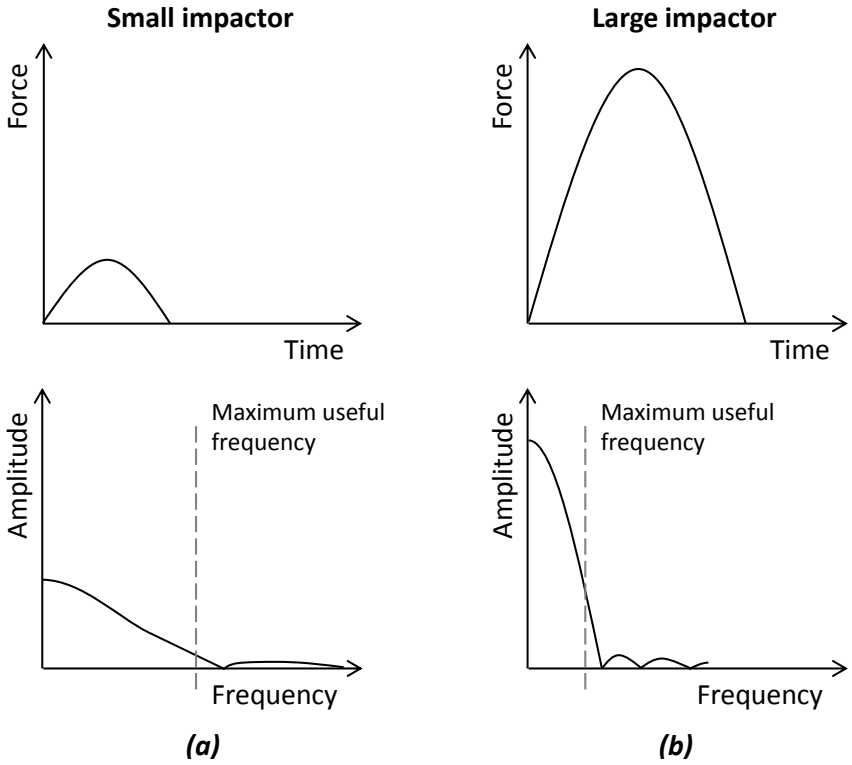

Figure 3-11: Impact Force Functions and Induced Frequency Ranges for (a) Small and (b) Large Impactor Diameters (Adapted from Sansalone and Streett (1997))

3.4.4 Detecting Distributed Damage with the Impact Echo Method

As described in Chapter 2, ASR and DEF cause distributed microcracking through the core of an affected concrete element. Though the impact echo method was initially developed to detect larger cracks and voids, two distinctly different techniques have been proposed to evaluate distributed deterioration, as from ASR or DEF. These techniques are centered around analysis in either the time domain or the frequency domain and are described in the following two sections.

3.4.4.1 Time Domain Analysis

The first technique to evaluate specimens with distributed damage using the impact echo method involves analysis in the time domain. This method focuses on the attenuation rate of the reflected compression waves, rather than on the wave velocity. Kesner et al. (2004) has proposed an exponential decay curve to approximate the rate of energy loss in consecutive wave reflections:

$$I = I_0 e^{-\alpha t} \qquad \textit{Equation 3-3}$$

where I is the stress wave intensity at time t, I_0 is the initial stress wave intensity and α is the decay constant. A typical idealized impact echo waveform is shown in Figure 3-12. The first portion is the surface wave, shown as a dotted line, followed by consecutive reflections of the compression wave, or signal cycles. For this analysis, the surface wave is ignored, and an exponential decay curve is fit through the peaks of the cycles. The decay constant, α, is determined from the best fit curve. Larger values of α indicate faster attenuation and more damage.

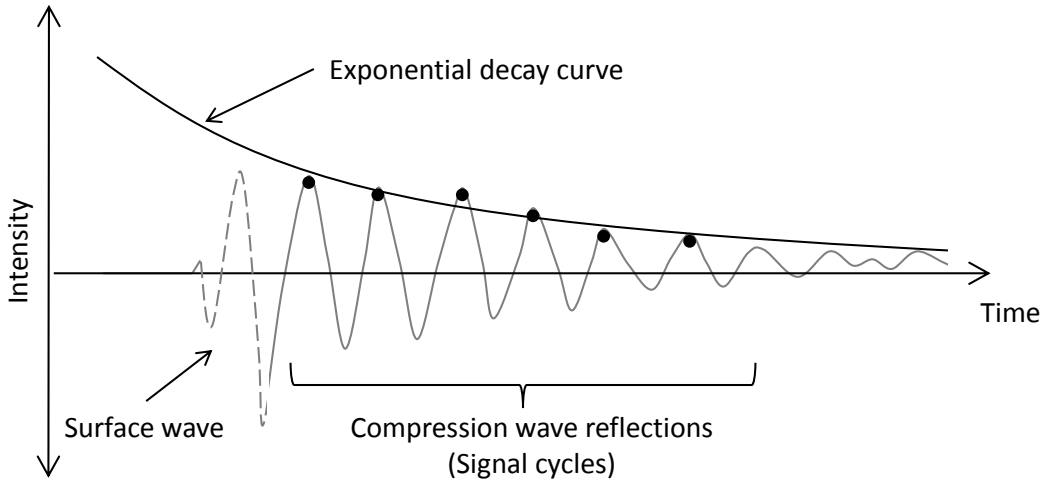

Figure 3-12: Impact Echo Attenuation Method (Adapted from Tinkey et al. (2000))

This method was developed by Kesner et al. using finite element modeling as well as laboratory and field testing on concrete specimens deteriorated by ASR and DEF. Typical results, shown in Figure 3-13, indicate that the laboratory results are significantly more scattered and irregular than those from the finite element modeling. However, as

the microcracking worsened, Kesner et al. detected a trend of decreasing decay constants, although the relationship is not linear. Damage estimation recommendations, summarized in Table 3-2, were made based on the decay constants and the number of discernable compression wave peaks. Although no results were presented, Kesner stated that the field tests "were consistent with" the laboratory and finite element testing.

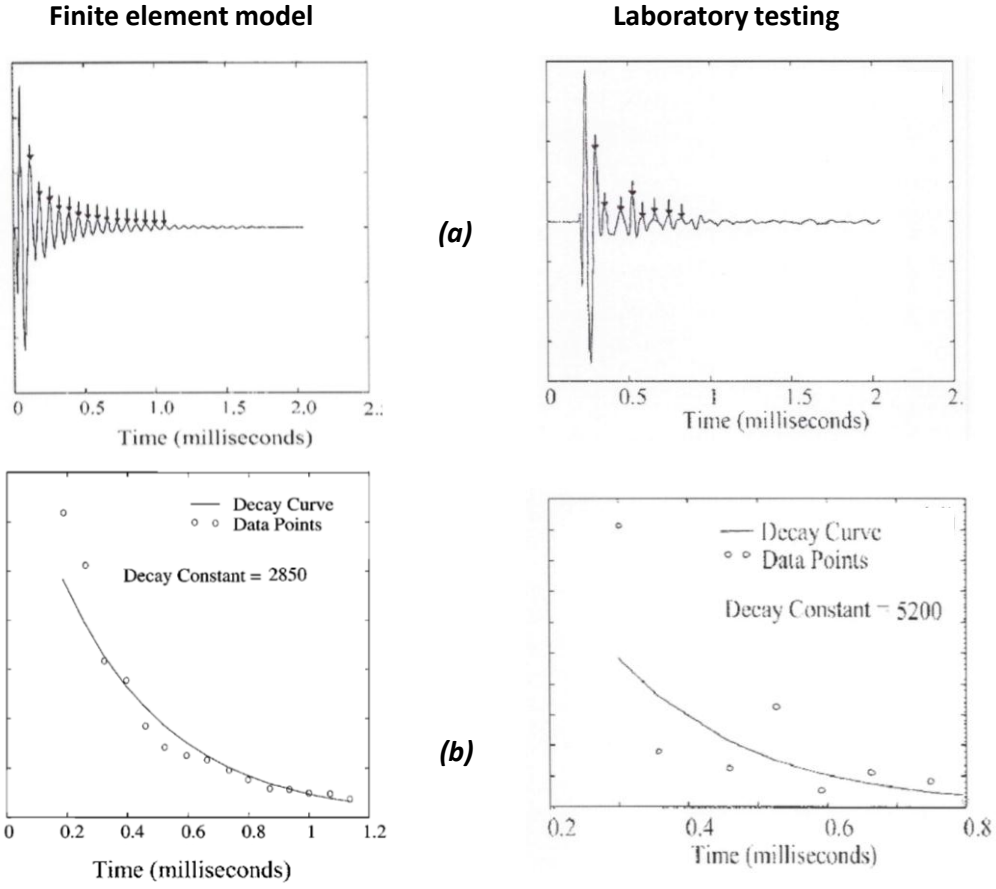

Figure 3-13: Typical Results from Kesner et al. (2004) (a) Waveforms and (b) Attenuation Analysis

Table 3-2: Damage Estimation by Impact Echo Attenuation Method (Kesner et al. 2004)

Decay Constant (1/s)	# of Compression Wave Peaks	Crack Density	Damage Level
Less than 3100	Greater than 13	Less than 0.5%	Little or none
3100 to 4000	11 to 13	0.5 to 1%	Minimal
4000 to 5000	9 to 11	1 to 2%	Moderate
Greater than 5000	Less than 9	Greater than 2%	Severe

Tinkey et al. (2000) also used this method to evaluate box girders subjected to ASR and DEF deterioration. The biggest difficulty encountered in this study was interpretation of the time domain signal. It was unclear how many peaks should be skipped to eliminate any effect of the surface wave, as well as how many signal cycles should be included. The decay constant from one time domain signal varied between 3,000 and 10,000 depending on whether one or two peaks were skipped to account for the surface wave and on the number of cycles included in the curve-fitting process (between 3 and 12 cycles).

Another difficulty inherent in the use of this method to assess distributed damage is that the time domain signal becomes complex as reflections from boundaries and defects make it difficult to pick out clear compression wave arrivals. Livingston et al. (2010) found that it was "not possible to evaluate the performance of this method for quantifying DEF-related damage" in bridges in Maryland without applying a bandpass filter to remove unwanted noise in the signal. After filtering, the signal was easier to interpret, but no direct conclusions were drawn from the measurements.

3.4.4.2 Frequency Domain Analysis

The second technique focuses on the frequency spectrum obtained after performing an FFT on the time domain signal. Two key features can be observed in the spectrum for damaged concrete as compared to an undamaged specimen. Firstly,

increasing amounts of noise may be observed as the level of internal microcracking intensifies in an element. Additional small peaks may form along the spectrum as a result of reflections from the distributed defects (Henriksen 1995). The amplitude of the peaks depends on the depth of the microcracks and on the impactor size, as noted in Section 3.4.3, making it difficult to quantitatively assess the damage. However, the presence of the peaks can be an indicator that distributed damage exists. An example of this phenomenon is given in Figure 3-14 below, which shows a frequency spectrum from a bridge deck subjected to ASR deterioration.

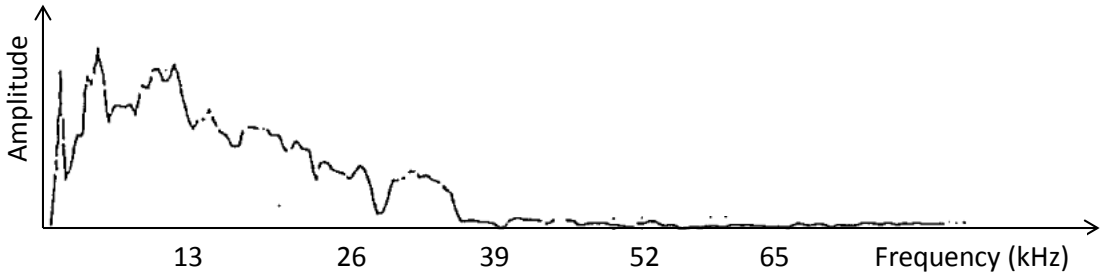

Figure 3-14: Example of a Noisy Frequency Spectrum (Henriksen 1995)

The second feature that can be observed from the frequency spectrum is a downward shift of the peak frequency as the specimen accumulates distributed damage. This indicates a loss of stiffness. Assuming the thickness remains constant, this results in a decrease in compression wave velocity, which is computed from the basic impact echo equation relating frequency, velocity and thickness (Equation 3-2, Section 3.4.1). It is important to note here that in order to calculate the velocity, the thickness must be known. Impact echo is often used in undamaged specimens to determine the compression wave velocity where only one side of the structure is accessible and UPV testing is not possible (Malhotra & Carino 2004).

In general, concrete composition and moisture content tend to have less effect on the impact echo results than on UPV measurements. This is because the low frequency stress waves induced by mechanical impact have much longer wavelengths than the size of aggregates and pores (Schubert & Köhler 2008). However, as with all NDT methods, environmental factors need to be taken into account when interpreting the results. An

additional source of error in the computed velocities comes from the β factor, which can be influenced by the time duration of the signal in non-plate elements (see Section 3.4.1).

The ability to apply this method in the field is uncertain. It can often be difficult to determine which frequency peak to choose from a noisy spectrum for velocity calculation. This is exhibited in the spectrum in Figure 3-14, in which there are several peaks of similar amplitude, and it is not clear which frequency to use for computing the velocity. Petersen (2000) actually detected an increase in the dominant frequency in a railroad tunnel exhibiting ASR deterioration, indicating that the compression wave velocity is faster than in undamaged portions of the tunnel. However, the frequency spectrum (see Figure 3-15) has a significant amount of noise, and it is possible that the peak corresponding to the back surface is one with lower amplitude.

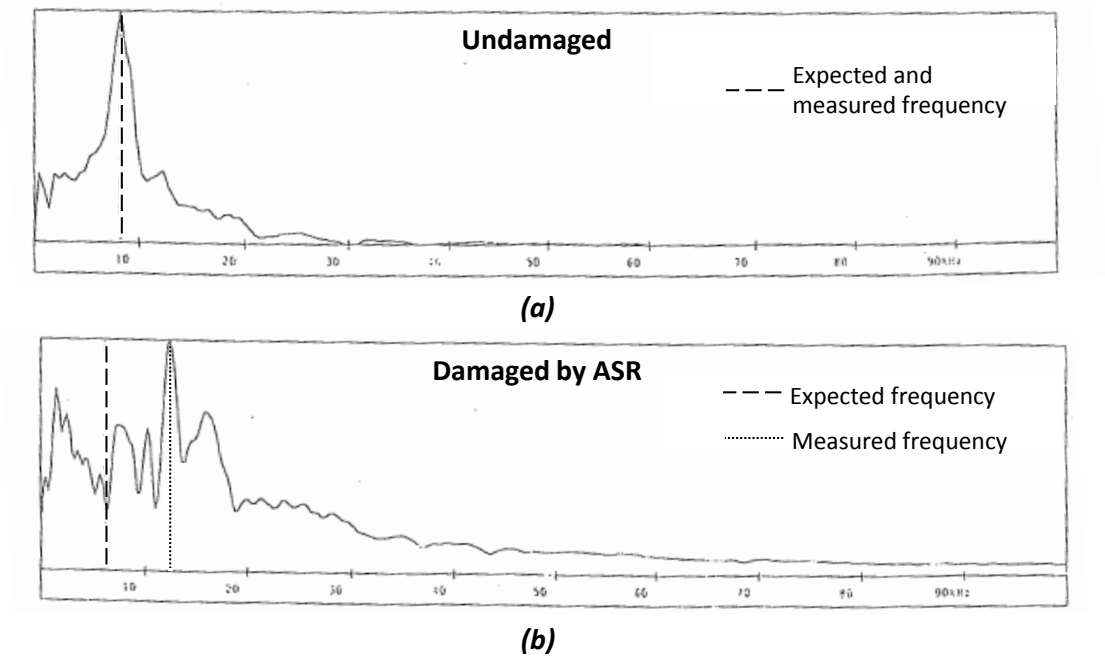

Figure 3-15: Typical Frequency Spectra from Petersen (2000) (a) Undamaged and (b) Damaged by ASR

3.5 RESONANT FREQUENCY METHOD

Because the resonant frequency of vibration is related to the stiffness of the structure, monitoring the various vibrational modes of an element may provide insight to the quality and integrity of the structure. Though the relationship is not linear, a decrease

in resonant frequency corresponds to a loss in stiffness, as the structure provides less resistance to motion. This section describes methods for measuring the various resonant frequencies of elements and applications to detecting deterioration in small samples and in large structures.

3.5.1 Resonant Frequencies of Small Specimens

The resonant frequencies of vibration are dependent on the elastic properties and shape of the element. Thus, a change in the resonant frequency could indicate the presence and severity of ASR and DEF deterioration.

Most commonly, resonant frequencies are measured on smaller specimens or on cores taken from a structure. ASTM C215 (2008) provides guidance for determining the fundamental transverse and longitudinal frequencies of concrete prisms and cylinders. As depicted in Figure 3-16, the specimen is subjected to a mechanical impact and the resulting vibrations are measured by an accelerometer. By locating the impact point and accelerometer as shown, the fundamental resonant frequencies will be dominant after performing an FFT of the signal. A typical time domain signal and its corresponding frequency spectrum are shown in Figure 3-17.

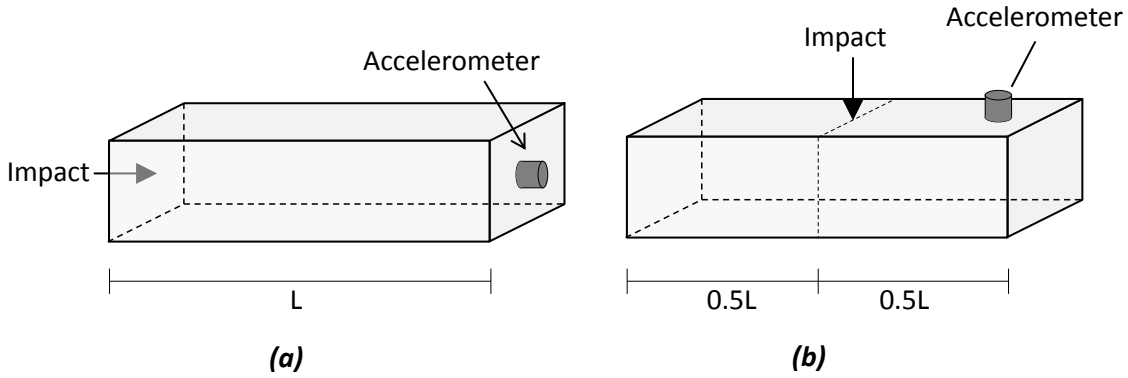

Figure 3-16: Resonant Frequency Test Setup for Measurement of (a) Longitudinal and (b) Transverse Resonant Frequency (Adapted from ASTM C215 (2008))

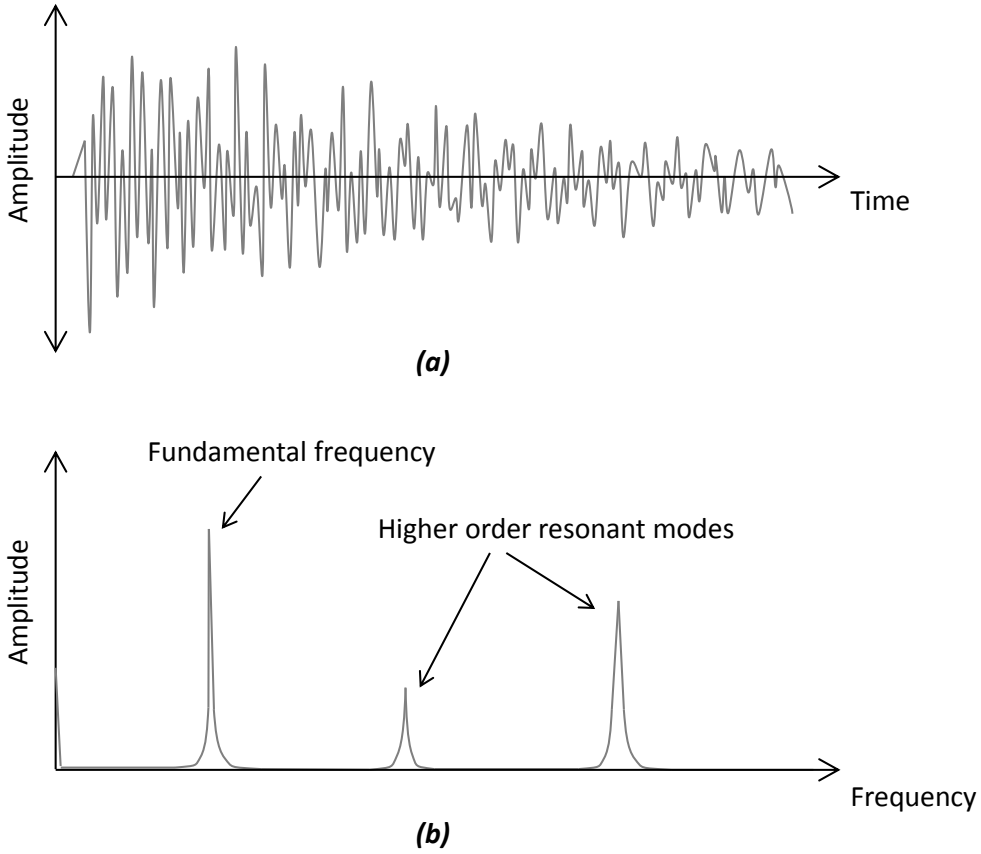

Figure 3-17: Typical Results from Resonant Frequency Testing (a) Time Domain Signal and (b) Frequency Spectrum

The dynamic elastic modulus, E_d, can be computed from resonant frequency testing by (ASTM C215 2008):

$$E_d = CMn^2 \qquad \textit{Equation 3-4}$$

where n is the measured fundamental frequency of a particular mode of free vibration, M is the mass of the element, and C is a constant based on the geometry. Note that this simple relationship is only valid for cylinders or rectangular prisms in free vibration.

Rivard and Saint-Pierre (2009) observed more than a 10% decrease of the longitudinal resonant frequency in ASR-damaged prisms and cylinders that had expanded nearly 0.2% longitudinally. Conversely the frequency increased by around 3% in similar undamaged specimens over the same time period (see Figure 3-18).

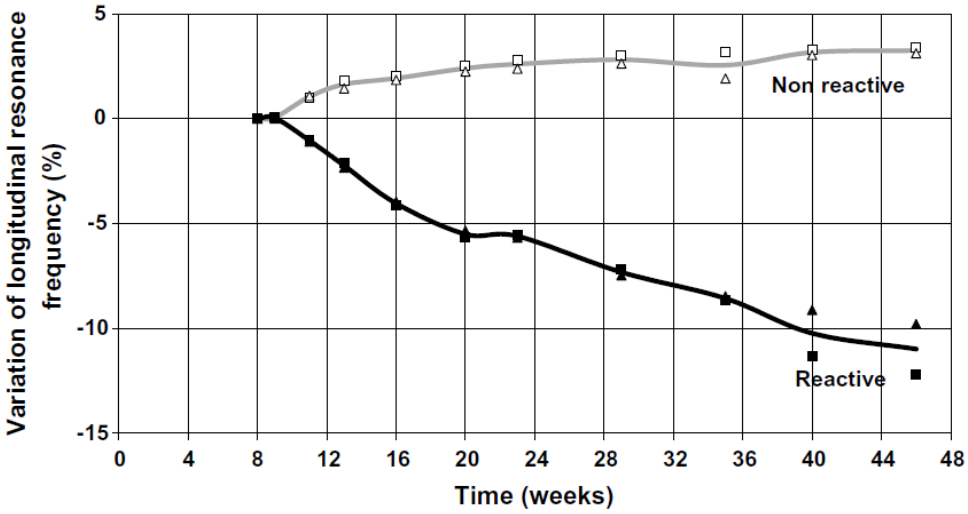

Figure 3-18: Resonant Frequency Variation in Cylinders and Prisms Deteriorated by ASR (Rivard & Saint-Pierre 2009)

3.5.2 Resonant Frequencies of Structures

An alternate approach was taken by Ono (1992) to measure the resonant frequency of T-shaped bridge piers in Japan subjected to ASR under regular traffic loading. As with small specimens, a lower resonant frequency was observed in piers that exhibited more ASR damage. Additionally, the dynamic elastic modulus computed from the resonant frequency of the piers was in some cases more than twice that measured on cores taken from the structure. These results may be promising for prediction of structural performance, since it has been shown that the mechanical properties of drilled cores are not good indicators of the behavior of the structure (see Chapter 2).

However, Ono notes that the ability to detect damage is limited to the members of the structure that participate most in the vibration of the fundamental mode. In this case, bending of the column dominated the vibration, so the tests were not able to detect deterioration in the beam. Also, it is often difficult to model the vibrational modes of structures in order to relate the measured frequencies to the stiffness. Irregular geometries, support conditions, and the presence of load complicate the analysis.

3.6 SURFACE WAVE METHODS

Analyzing the propagation of surface waves, rather than compression waves, in concrete is another nondestructive approach that may be able to detect ASR and DEF deterioration. The two parameters that are typically measured are the velocity and attenuation of the surface wave. The velocity is measured using the spectral analysis of surface waves (SASW) method while the energy transmission, which is the opposite of attenuation, is measured using the surface wave transmission (SWT) method. The details of the SASW and SWT methods are described in Sections 3.6.1 and 3.6.2, respectively.

The same test setup, shown in Figure 3-19, is used for both methods. Two receivers are placed on either side of the test region. The element is then impacted on one side, with the impact point in line with the receivers. To remove error in the measurements, the process is repeated with the impact point on the opposite side of the receivers.

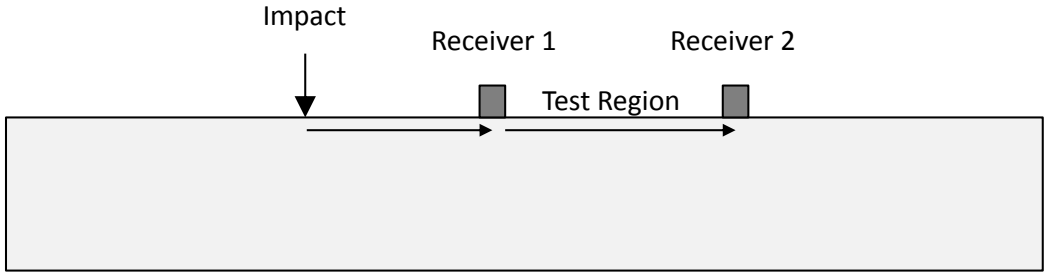

Figure 3-19: Surface Wave Test Setup

Typically, accelerometers are used as receivers. However, the quality of the results depends largely on the coupling of the accelerometer to the surface. In the field, surfaces are often rough, dirty or wet, making adequate coupling difficult. Recent research has indicated that a microphone placed close to the surface can accurately measure the surface displacement through slight changes of air pressure (Zhu 2005; Kee & Zhu 2010). These "air-coupled" sensors resolve coupling issues and yield very similar results to accelerometers. Additionally, using non-contact sensors can significantly speed up the testing process, as no time is spent achieving proper sensor coupling. However,

the microphones are sensitive to ambient noise, as from vehicular traffic or wind, so it is important to isolate the sensor as much as possible with sound insulation.

3.6.1 Spectral Analysis of Surface Waves (SASW) Method

Originally developed to analyze pavement and soil layers, the spectral analysis of surface waves (SASW) method measures the velocity of a range of frequencies present in a surface wave. In a layered system, each layer has different stiffness and body wave velocity. Because lower frequencies of a surface wave penetrate deeper into a medium (see Section 3.4.3), the variation of velocity with frequency indicates a changing stiffness with depth (Malhotra & Carino 2004). The results are often presented in a dispersion curve, or a graph of phase velocity against frequency, where the term "phase velocity" refers to the speed at which a particular frequency within a wave travels. In a homogeneous solid half space, like a concrete element, the stiffness remains the same throughout the depth. Thus, velocity is constant and does not change with frequency. This velocity will be referred to as the "surface wave velocity", as it is not related to any particular frequency.

The signal processing to compute a dispersion curve is significantly more complex than for any of the previously mentioned methods (Zhu 2005). The process is summarized graphically in Figure 3-20. First, both time domain signals are windowed so that the first arrival of the surface wave is the only portion of the wave remaining. Then, the windowed signals are converted to the frequency domain using a Fast Fourier Transform (FFT). Next, the auto-power and cross-power spectra are computed, from which the phase difference between the two signals is calculated. Finally, the phase velocity is computed as a function of the frequency. Typically, little variation in the phase velocity is seen at high frequencies in a homogeneous system when the wavelength is smaller than the thickness.

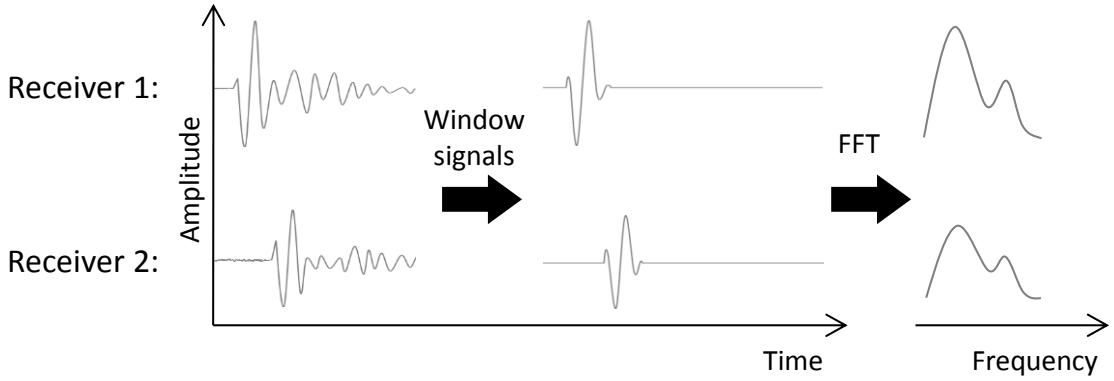

$y_1(t)$ $\quad Y_1(f) = FFT(y_1(t))$

$y_2(t)$ $\quad Y_2(f) = FFT(y_2(t))$

Auto-power and cross-power spectra:
(Note: top bar indicates the complex conjugate)

$$G_{11}(f) = Y_1(f) * \overline{Y_1(f)}$$
$$G_{22}(f) = Y_2(f) * \overline{Y_2(f)}$$
$$G_{12}(f) = Y_1(f) * \overline{Y_2(f)}$$

Phase difference:

$$\Delta\varphi(f) = \text{phase angle of } \frac{G_{12}(f)}{G_{11}(f)}$$

Phase velocity:

$$C_R(f) = \frac{2\pi f * length}{\Delta\varphi(f)}$$

Figure 3-20: Signal Processing for the SASW Method

Reports of use of the SASW method to detect ASR or DEF deterioration were not found in the literature. However, because the surface wave velocity depends on stiffness, which is affected by the cracking and expansion associated with ASR and DEF, the method may be effective in characterizing the deterioration. It is important to note that this method is most sensitive to damage closer to the surface. Lower frequency surface waves penetrate deeper into the core concrete of larger elements (see Section 3.4.3), but detecting small defects such as microcracking is more difficult with longer wavelengths.

3.6.2 Surface Wave Transmission (SWT) Method

The surface wave transmission (SWT) method is a newer method aimed at estimating the depth of a surface breaking crack by measuring the energy transmitted of a

range of frequencies across the crack. The relationship between energy transmission and crack depth has been determined by several researchers (Achenbach et al. 1980; Mendelsohn et al. 1980; Angel & Achenbach 1984; Yew et al. 1984) but has only recently been applied to concrete structures (Hevin et al. 1998; J. S. Popovics et al. 2000; W. J. Song et al. 2003; Shin et al. 2008; Kee & Zhu 2010).

Like the SASW method, the signal processing begins with taking an FFT of the windowed surface wave signal in the time domain. The transmission coefficient variation, Tr(f), is then computed as the ratio of the amplitude spectra from the two receivers.

$$Tr(f) = \frac{V_2(f)}{V_1(f)} \qquad \textit{Equation 3-5}$$

where $V_1(f)$ and $V_2(f)$ are the amplitude spectra from the receivers closer to and farther from the impact point, respectively (Kee & Zhu 2010). For comparative purposes, the transmission coefficient at the central frequency is often taken.

Initial research at the University of Texas at Austin using the SWT method on ASR and DEF damaged concrete yielded promising results (Kee 2010). Generally, a loss in energy transmission corresponded with an increase in expansion of the concrete. However, the trends varied between the tested specimens, which may potentially be explained by the different crack patterns caused by different loading histories.

One potential problem with using the SWT method on elements with distributed damage is the "near-field effect". Because the method was developed to analyze one crack located between the receivers, multiple reflections and scattering from cracks near the impact location or the receivers can make interpreting the results difficult.

3.7 NONLINEAR METHODS

All of the nondestructive methods described previously are based on linear theory of wave propagation through a material with a linear stress-strain response. These methods are very effective for locating large defects and open cracks. In recent years however, several researchers have investigated methods based on nonlinear behavior, which tend to be orders of magnitude more sensitive to microcracking and distributed

damage (Muller et al. 2005; Stauffer et al. 2005; Payan et al. 2007; Kodjo et al. 2009). Section 3.7.1 gives a brief overview of the different types of nonlinearity in solids. Sections 3.7.2 through 3.7.4 describe nonlinear NDT methods that have been recently developed.

3.7.1 Nonlinearity in Solids

There are two types of nonlinearity in solids: classical and nonclassical nonlinearity. Classical nonlinearity can be incorporated into material behavior by adding higher order terms to the stress-strain relationship. For the simple one-dimensional case, the nonlinear version of Hooke's Law is (P. A. Johnson 2007):

$$\sigma = E\varepsilon(1 + \beta\varepsilon + \delta\varepsilon^2 \ldots) \qquad \textit{Equation 3-6}$$

where E is the linear elastic modulus, and β and δ are the 2nd and 3rd order nonlinear elastic coefficients, respectively. The effects of β and δ become more prominent as the level of strain increases.

Nonclassical, or contact, nonlinearity results from the opening and closing of microcracks and small defects as a wave propagates through a material (X. Chen & Y. Wang 2009; Kazakov et al. 2002). While the compressional component of the wave can penetrate through the defect, the tensile portion is unable to pass through, creating nonlinearity in the received signal. Note that open cracks and large voids, which are easily detected with linear NDT methods, do not induce nonclassical nonlinear behavior because of the lack of contact between the surfaces during the compressional portion of the wave (Kazakov et al. 2002). Nonclassical nonlinearity is mathematically represented in the stress-strain relationship by incorporating a hysteresis function (P. A. Johnson 2007):

$$\sigma = E\varepsilon(1 + \beta\varepsilon + \delta\varepsilon^2 \ldots) + \alpha\left[\varepsilon, sign(\frac{\partial\varepsilon}{\partial t})\right] \qquad \textit{Equation 3-7}$$

where α is the hysteretic nonlinear parameter and is a function of both the magnitude of the strain and the sign of the strain rate.

The phenomenon of slow dynamics, or the gradual recovery of elastic properties over time after a disturbance, has been observed in several materials including concrete

and falls under the category of nonclassical nonlinearity (J. A. Ten Cate & Shankland 1996; J. Ten Cate et al. 2000; P. Johnson & A. Sutin 2005; Tremblay et al. 2010). The effects of slow dynamics are not captured in the higher order or hysteretic terms in Equation 3-6 and Equation 3-7. However, researchers have developed various theories and models to describe the slow dynamics behavior (Delsanto & Scalerandi 2003; O. O. Vakhnenko et al. 2004). Despite the potential for an NDT method based on slow dynamics to assess microcracking damage, it will not be further discussed here. It is likely an impractical method for use on field structures due to the continuous excitation by traffic or wind loads.

There are several indicators of nonlinear behavior that can be observed and related to the nonlinear parameters β, δ, and α to estimate the level of damage or deterioration in a material. These include the generation of higher and sub-harmonic frequencies, a shift in resonant frequency with increasing excitation amplitude, and the response of a material as a result of mixed input frequencies, among other indicators. Jhang (2009) provides a comprehensive review of nonlinear evaluation using ultrasonic methods. The following three sections summarize key points from that review as well as from several other researchers to describe the methods of harmonic generation, resonant frequency shift, and mixed frequency response (also called "frequency modulation"), including the potential application for detecting distributed damage in materials.

3.7.2 Harmonic Generation Method

When a single frequency is used to excite a specimen, integer multiples of that frequency are also present in the received signal. These integer multiples of the input frequency are called harmonics. The first harmonic is the input frequency, f_0. The second harmonic is $2f_0$, the third harmonic is $3f_0$, and so on. As the damage level increases, the nonlinearity increases, and energy is redistributed to the higher harmonic frequencies (A. A. Shah & Ribakov 2009b).

The level of nonlinearity is indicated by the nth harmonic ratio, β_n, which is defined as:

$$\beta_n = \frac{A_n}{{A_1}^n} \qquad \textit{Equation 3-8}$$

where A_n is the amplitude of the nth harmonic and A_1 is the amplitude of the fundamental frequency, f_0. β_n is proportional to the nth order nonlinear elastic coefficient in Equation 3-6. An increase in any of the harmonic ratios indicates a higher level of nonlinearity in the material and thus more damage. Results indicate that as microcracking increases, the change in the harmonic ratios is orders of magnitude higher than the change in linear parameters such as compression wave velocity or resonant frequency (Stauffer et al. 2005).

Though this method may be very sensitive to detecting microcracking in concrete, large attenuations may be a problem in the assessment of field structures. The harmonics, which have higher frequencies by definition, will experience much greater attenuation than the lower fundamental frequency. Additionally, the more microcracking in an element, the more scattering and attenuation will occur in general. As a result, very powerful excitation signals may be necessary to observe the amplitude of higher harmonics in a field structure (A. A. Shah & Ribakov 2009a).

3.7.3 Resonant Frequency Shift Method

Another way to present Equation 3-6 and Equation 3-7 is to incorporate the higher order and hysteresis terms into the elastic modulus. Because the resonant frequency depends on the elastic modulus, as described in Section 3.5, nonlinearity will be present in the resonant behavior as well. As the excitation force increases, higher values of vibrational strain are achieved, and the higher order stiffness terms are more prominent. This leads to a downward shift in the resonant frequency with increasing excitation force and strain (Muller et al. 2005). Using a linear approximation, the relationship is:

$$\frac{\Delta f}{f_0} = \frac{f - f_0}{f_0} \approx \alpha \Delta \varepsilon \qquad \textit{Equation 3-9}$$

where Δf is the shift in resonant frequency from f_0 to f, α is the hysteretic nonlinear parameter from Equation 3-7, and $\Delta\varepsilon$ is the increase in strain. Nonclassical hysteretic

nonlinearity is the dominant form of nonlinear behavior for microcracked materials at large strains, although classical nonlinearity is also present (Muller et al. 2005).

Typical results from undamaged and ASR-affected mortar bars are shown in Figure 3-21 (J. Chen et al. 2010). As the excitation force increases in both samples, the amplitude of the peak is larger and the frequency is lower. Note the difference in scale of the horizontal axes, indicating the frequency shift in the ASR-affected sample is much more prominent than that seen in the undamaged sample. Additionally, Payan et al. (2007) has shown that the resonant frequency shift is significantly more sensitive than traditional resonant frequency methods.

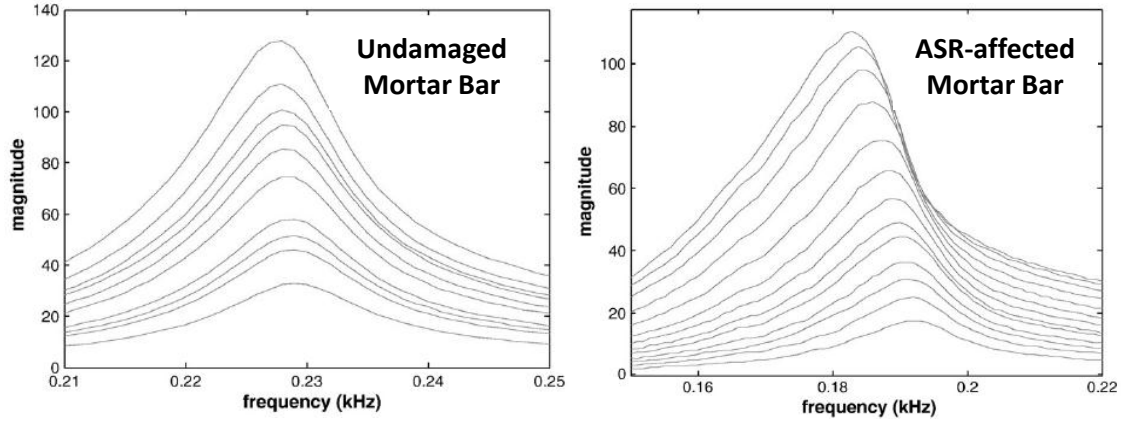

Figure 3-21: Resonant Frequency Shift Results (J. Chen et al. 2010)

3.7.4 Mixed Frequency Response Method (Frequency Modulation)

A simple and common way of evaluating the nonlinear properties is to modulate, or mix, signals of different frequencies. Typically for NDT applications, a high frequency ultrasonic signal is modulated by large amplitude, low frequency vibrations. As the cracks open and close from the low frequency excitation, the phase and amplitude of the ultrasonic wave vary (Jhang 2009). This is illustrated by the idealistic model in Figure 3-22. When the crack is closed, the high frequency wave passes through normally, with little to no amplitude loss. However, when the crack is open, the wave attenuates, resulting in amplitude modulation and creating sideband frequencies. These sideband frequencies are more pronounced as microcracking worsens (A. M. Sutin & P. A. Johnson 2004; Van Den Abeele et al. 2000).

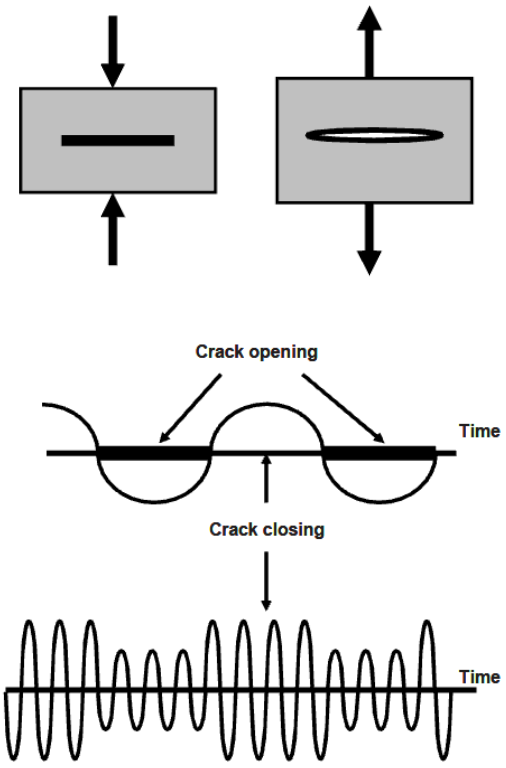

Figure 3-22: Simple Model of the Behavior of a Material with Microcracks Subjected to Mixed Frequency Excitation (Jhang 2009)

If a high frequency signal (f_{high}) is modulated by a low frequency vibration (f_{low}) in a damaged material, frequencies of $f_{high} \pm f_{low}$ will also be present in the received signal. This is evident in Figure 3-23, which shows the results of a high frequency ultrasonic signal modulated by a discrete low frequency in both a damaged and an undamaged Plexiglas sample.

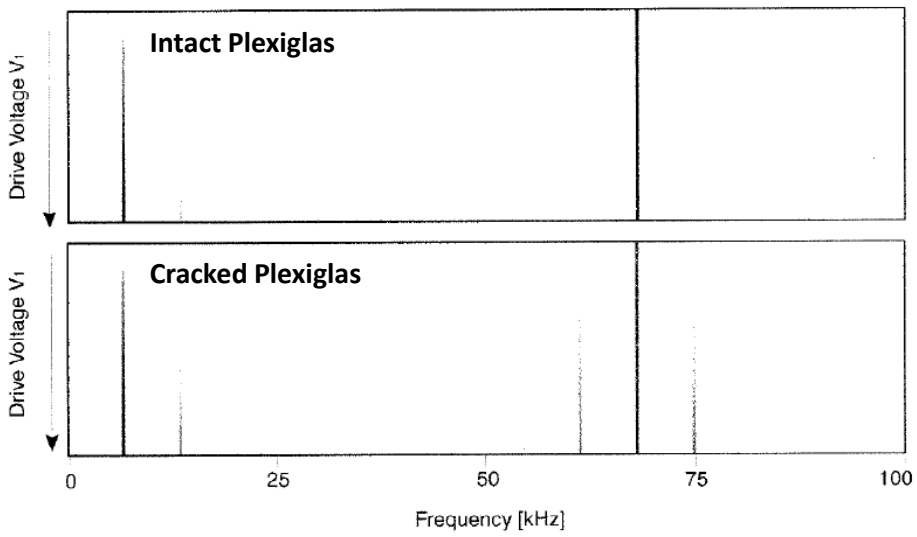

Figure 3-23: Results of a Frequency Modulation Test with Discrete Low Frequency (Van Den Abeele et al. 2000)

A more realistic way to generate large amplitude, low frequency vibration in a concrete structure is by mechanical impact, which induces a wide range of low frequencies into the specimen. An example of the response to a high frequency signal modulated by an impact-generated low frequency is depicted in Figure 3-24. Note that the sideband frequencies are still present, but the frequency distribution is much noisier because of the wide range of modulating low frequencies.

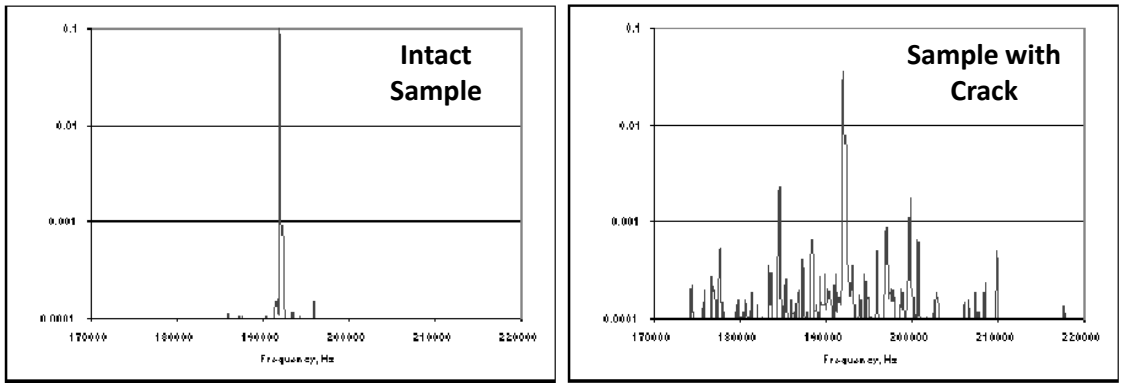

Figure 3-24: Results of a Frequency Modulation Test with Impact-Generated Low Frequency (A. M. Sutin & P. A. Johnson 2004)

Kodjo et al. (2009) has used a modified version of the mixed frequency method to analyze concrete structures and elements with several different types of damage,

including deterioration from ASR and DEF. This method will later be referred to as the "time shift nonlinear acoustic method." Instead of observing just the amplitude modulation and creation of sideband frequencies after mixing a high frequency ultrasonic signal with a low frequency mechanical impact, the travel time (or phase) of the received signal is also taken into account. The opening of a crack decreases the amplitude of the signal as well as increases the travel time, inducing a phase shift. As the effects of the impact wear off over time, both the amplitude and phase return logarithmically to the original values. This recovery of elastic properties over time is similar to the phenomenon of slow dynamics. However, this method observes the phase and amplitude shifts for a short period of time immediately after the impact (usually 0.5 to 1 second), while slow dynamics is typically observed over a period of 15 minutes to 3 hours (P. Johnson & A. Sutin 2005).

Figure 3-25 shows the typical results from a 15x15x28″ unreinforced concrete block with ASR damage (Kodjo et al. 2009). The phase dependence on signal amplitude can be observed by plotting the phase shift against the amplitude of the received wave over a short period of time after the impact (see Figure 3-25c). This yields a decreasing linear trend, with a slope that indicates the extent of the nonlinearity. As more microcracks develop and affect the wave over the travel path, the nonlinear behavior increases, and the slope of the best fit line becomes steeper. This slope is proportional to the hysteretic nonlinear parameter, α, in Equation 3-7.

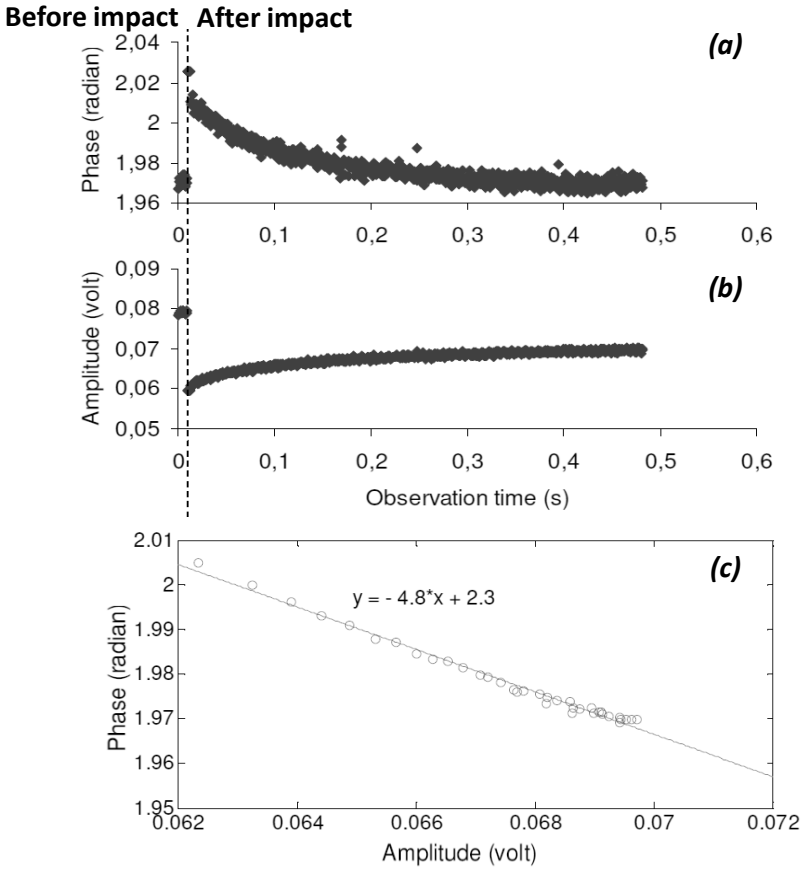

Figure 3-25: Phase and Amplitude Variation after Impact-Generated Frequency Modulation (Kodjo et al. 2009)

3.8 SUMMARY

Each of these nine methods demonstrates the potential to qualitatively assess the level of deterioration from ASR and DEF in field structures. In general, results from the literature have indicated a change in elastic properties of the deteriorated material as the level of damage increases. However, for the case of ASR and DEF deterioration in a reinforced concrete element, the presence of reinforcement also influences the behavior. For this reason, nondestructive evaluation of field structures is difficult at the present time. The current research focuses on several of the NDT methods discussed in this chapter in attempt to develop a "toolbox" for the evaluation of in-service concrete structures suffering from ASR and DEF deterioration.

CHAPTER 4
Test Specimens

4.1 OVERVIEW

To assess the use of nondestructive testing (NDT) methods to evaluate in-service concrete structures, three near-full scale bent cap specimens were fabricated at the University of Texas at Austin. Of the three specimens, two were designed and fabricated to induce accelerated deterioration from alkali-silica reaction (ASR) and delayed ettringite formation (DEF). These two will be referred to as the reactive specimens. The third was a nonreactive control specimen designed not to deteriorate. It was constructed from similar materials and stored under the same conditions as the reactive specimens. This chapter describes the design and fabrication of the test specimens in Sections 4.2 and 4.3, respectively.

4.2 DESIGN

Various bridge elements have been observed to suffer from severe ASR and DEF deterioration in Texas and around the world. The reaction is driven by the combination of the use of high early-strength cement, which introduces a large amount of alkalis and causes elevated curing temperatures, with abundant exposure to moisture from roadway runoff and drainage. Previous research at the University of Texas investigated the shear capacity of bent cap specimens subjected to moderate levels of ASR and DEF deterioration (Deschenes 2009). This research is discussed in Section 2.3.2, and served as a baseline for the current project. After nondestructive testing and monitoring of the deterioration, the specimens described in this chapter will be used to investigate the effects of deterioration on the flexural behavior. Design and fabrication of the specimens for the current project were very similar to those in the previous research in order to facilitate continuity and direct comparison between the two projects.

4.2.1 Geometry and Reinforcement Layout

The specimens were sized to behave similarly to typical bent caps in Texas. A cross section 21″ wide and 42″ deep was chosen. This depth corresponds well to bent caps found in the state, while the 21″ width was chosen to limit the specimen weight and allow for transportation in the laboratory (Deschenes 2009). Each specimen is nearly 28′ long. Figure 4-1 and Figure 4-2 show cross section and elevation views of the specimens, respectively.

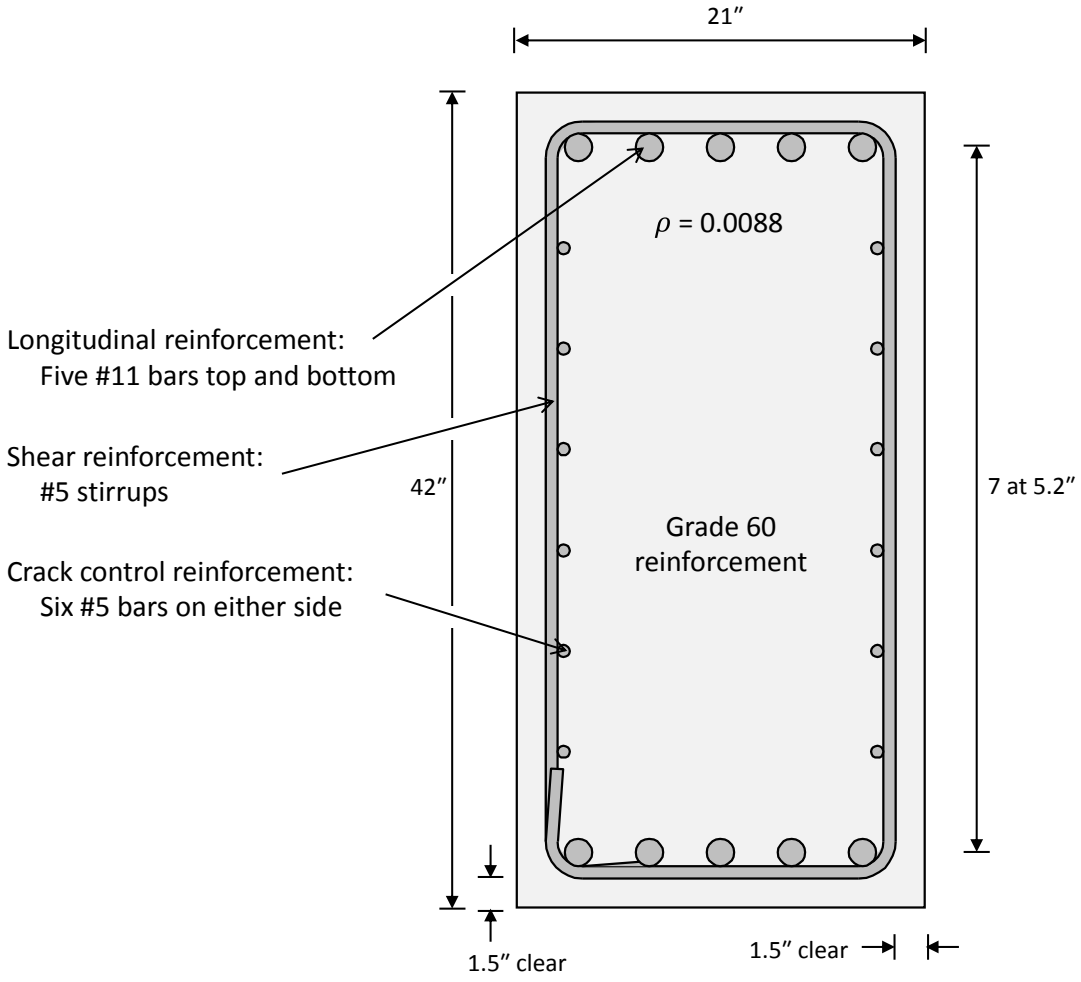

Figure 4-1: Cross Section View of Test Specimens

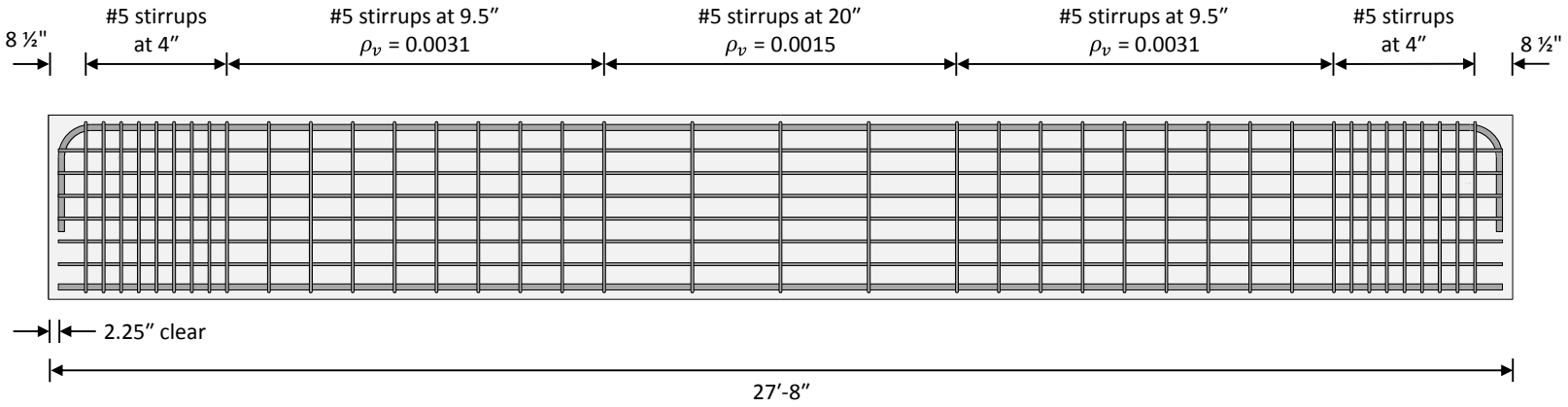

Figure 4-2: Elevation View of Test Specimens

Longitudinal reinforcement was comprised of five #11 bars in both tension and compression. Note that the tension steel is on the top side, as the specimens were fabricated, conditioned and will be tested upside down. The specimens will be tested in two-point flexure, inducing a constant maximum moment in the middle span and constant shear in the outer spans. This is discussed further in Chapter 5 (see Section 5.2.2). Adequate shear reinforcement was provided by #5 stirrups at various spacings along the specimen to ensure a flexural failure. Stirrups were spaced at 20″ in the middle test region and at 9 ½″ in the outer test region. These spacings were chosen to represent typical minimum amounts of transverse reinforcement, and to maintain compatibility with the previous research project (Deschenes 2009). To eliminate any local failure or effects outside the test regions, stirrups were spaced at 4″ at the ends of the specimens.

4.2.2 Concrete Mixtures

Design of the reactive and nonreactive concrete mixtures was also based on work done in previous research. Deschenes (2009) consulted with the Concrete Durability Center at the University of Texas at Austin to conduct several trial mixes. The concrete mixture was designed to be conducive to rapid deterioration, while maintaining representative qualities of current practices in Texas. Both the reactive and nonreactive mixes have the same proportions of cement, coarse and fine aggregate, and water. However, the type of coarse aggregate was the only constant between the mixtures. Table 4-1 gives a summary of the nonreactive and the reactive concrete mixture designs. The estimated 28-day compressive strength of both mixtures was 5000 psi, which lies within the range of typical Texas bent caps. In order to achieve this lower strength with the cement and aggregate content desired, the water-to-cement ratio was increased to 0.57. This is higher than typically used in construction, but is not expected to significantly affect the behavior.

Table 4-1: Concrete Mixture Details

Material	Mixture Proportions	Reactive Mixture Materials	Nonreactive Mixture Materials
Cement	700 lb/yd^3	Type III High-Alkali Cement from Lehigh Cement Company, Fleetwood, PA	Type III Low-Alkali Cement from Alamo Cement Company, San Antonio, TX
Water	400 lb/yd^3	Hot Tap Water (about 130°F)	Cold Tap Water
Fine Aggregate	1165 lb/yd^3	Jobe-Newman Sand from Cemex, El Paso, TX	Colorado River Sand from Texas Concrete Materials, Del Valle, TX
Coarse Aggregate	1500 lb/yd^3	¾" Crushed Limestone from Texas Crushed Stone Company, Georgetown, TX	¾" Crushed Limestone from Texas Crushed Stone Company, Georgetown, TX
Sodium Hydroxide	67.5 lb/yd^3 (reactive mixture only)	50% NaOH Solution from Fisher Scientific Company, Pittsburgh, PA	---
Water-Cement Ratio	0.57		
Est. 28-Day Strength	5000 psi		

To induce rapid ASR deterioration, Type III high-alkali cement and Jobe-Newman sand, one of the most siliceous and deleterious aggregates in the state, were used in the reactive mixture. The alkali level was boosted to a final value of 8.7 lb/yd^3 by the addition of sodium hydroxide to the fresh concrete. To accelerate DEF deterioration, the water in the reactive mixture was heated to around 130°F. A water-reducing retarder was also added to the second reactive specimen for enhanced workability. The nonreactive mixture contained low-alkali Type III cement and a local river sand to reduce the likelihood of ASR. Cold water was used during the mixing of the nonreactive specimen, and no sodium hydroxide was added. The total alkali content was only 3.4

lb/yd^3. This falls below the maximum of 4 lb/yd^3 of alkalis from cement allowed by TxDOT Special Provision 421 (TxDOT 1995).

4.3 FABRICATION

The three bent cap specimens were fabricated at the Ferguson Structural Engineering Laboratory at the University of Texas at Austin between January and May 2010. The nonreactive specimen was fabricated in January because the weather was cooler, making conditions less conducive to high curing temperatures and DEF. The reactive specimens were cast in March and in May, with more favorable ambient temperatures. The fabrication process consisted of constructing the reinforcement cage, installing instrumentation, erecting the formwork, and mixing and casting concrete. Finally, the reactive specimens were heat cured. This process is illustrated in Figure 4-3 and described in the following sections.

4.3.1 Reinforcement Cage and Instrumentation

The reinforcement cages were constructed of steel bars and stirrups of 60 ksi nominal yield strength. Testing of tensile coupons from the manufacturer confirmed this strength. A photo of a completed rebar cage is shown in Figure 4-3a. Each reinforcement cage was instrumented to measure ASR- and DEF-induced expansions, as well as with thermocouples to track curing temperatures. Strain gauges were not used for measuring expansions, because previous research indicated that the instruments were not reliable over time in the harsh, high-pH environment brought on by the deterioration (Deschenes 2009). Instead, expansions were measured mechanically with an extensometer. This required the fabrication of "targets" out of ½" stainless steel rods, PVC pipe and foam. During the specimen monitoring phase, core concrete expansions and rebar strains were measured with the extensometer from one target face to another. Curing temperatures were measured throughout the specimens with a data collection system set up outside the curing area. Figure 4-4 shows the layout of instrumentation in the specimens. The two test regions, the middle and end spans, differ only in stirrup spacing.

(a) Construct reinforcement cage

(b) Erect formwork, place cage inside

(c) Mix concrete

(d) Place concrete

(e) Heat cure (reactive specimens only)

Figure 4-3: Specimen Fabrication Process

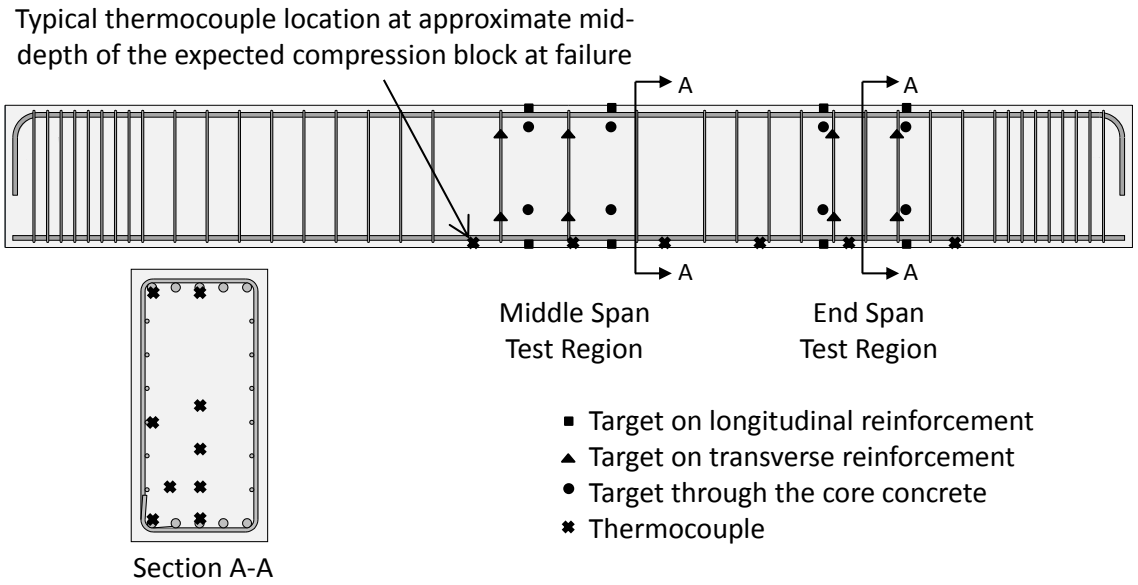

Figure 4-4: Layout of Specimen Instrumentation

The target fabrication process is depicted in Figure 4-5. After cutting the stainless steel rods to the appropriate lengths, a hole was drilled in the end of each rod to precisely match the extensometer points. Short rods were then welded to the longitudinal and transverse reinforcement for the measurement of steel strains (Figure 4-5a). To isolate the targets from the cover concrete, the rods were centered inside 1 ½" PVC pipe, and the empty space was filled by foam. This allowed the rods to move with the reinforcement without being affected by the cover concrete (Figure 4-5b). To measure core concrete expansions, long rods were fabricated to pass through the width of the specimen. These rods had holes drilled on both ends. The outer portions of these rods were isolated from the cover concrete in a similar fashion to those welded to the rebar (Figure 4-5c). The PVC pipe attached to the rods was then tied securely into the rebar cage (Figure 4-5d). A typical fully instrumented test region is depicted in Figure 4-5e. Locating the targets in this fashion allowed for the measurement of steel strains and core concrete expansions in both the longitudinal and vertical directions. No strains or expansions were measured in the width direction (21" dimension) because the gauge length of the extensometer (24") was longer than the width of the specimens. Refer to the elevation view in Figure 4-4 for the full layout of the targets in the specimens.

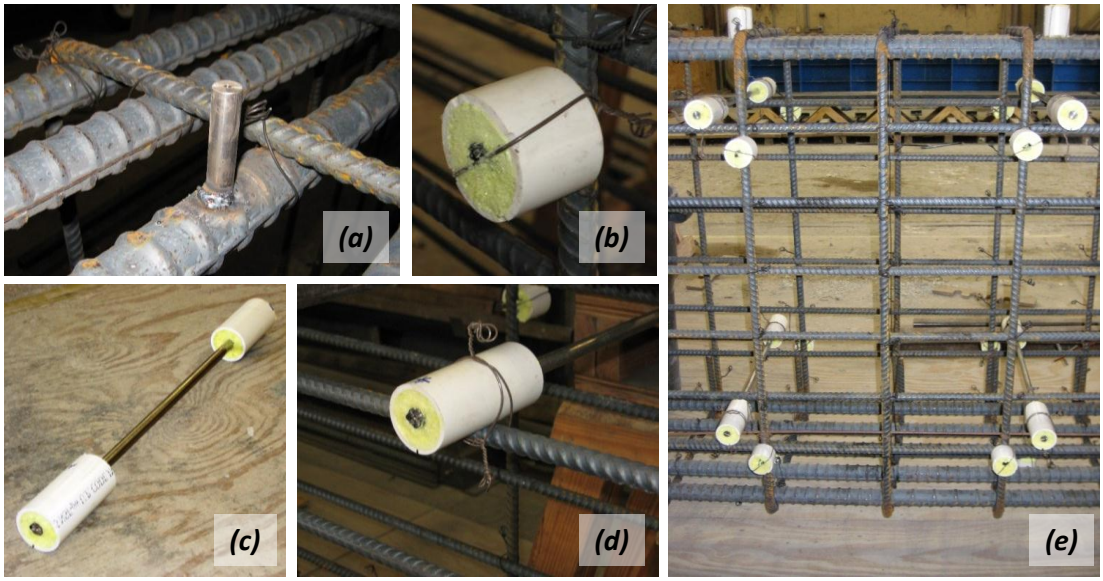

Figure 4-5: Fabrication of Targets for Mechanical Expansion Measurement

The specimens were instrumented with Type T thermocouples at several locations within the test region to measure curing temperatures, as shown in Figure 4-4. Thermocouples were placed at the quarter points along each of the two test regions, located at a depth corresponding to the approximate center of the expected compression block at flexural failure (approximately 2" from the bottom face of the specimen). Additionally, a cross section in each test region was instrumented with nine thermocouples to measure curing temperature distribution throughout the depth and width of the specimen. More details about the temperature measurements are discussed in Section 4.3.3.

The fully fabricated and instrumented reinforcement cage was then placed inside steel formwork. This is depicted in Figure 4-3b.

4.3.2 Concrete Placement

On the day of a cast, a ready-mix concrete truck arrived containing the coarse aggregate. The other materials were then added, and the concrete was mixed on-site. This was necessary for the fabrication of the reactive specimens, as workability was significantly hindered by concrete temperatures exceeding 100°F in the truck. A

retarding plasticizer was used in the mixture for the second reactive specimen to improve workability and increase time available for casting.

The first step in the concrete mixing process was to transfer the fine aggregate from storage barrels into the concrete truck using the overhead crane. The sodium hydroxide was then diluted in water and added to the reactive mixtures. During casting of the second reactive specimen, plasticizer diluted in water was also added at this stage. Next, water and cement were simultaneously placed in the truck. The cement was dumped in using the concrete bucket and the overhead crane (Figure 4-3c). The mixer was kept slowing rotating while adding materials, and was rotated rapidly for more than 200 cycles after all components had been placed in the truck. After ensuring good quality of the mixture, concrete was placed in the forms using the bucket and the overhead crane. Adequate consolidation was achieved using sideform and handheld vibrators (Figure 4-3d). After finishing the top surface with trowels, the specimens were left to cure. As-placed concrete composition was very similar to the proportions given in Table 4-1.

In addition to the large specimens, small samples were also cast according to ASTM C192 (2007). 4x8" cylinders were fabricated for determination of 28-day compressive strength, and 3x3x11¼" prisms were cast for the ASR-reactivity test defined by ASTM C1293 (2008). The actual measured 28-day compressive strengths for the three specimens are summarized in Table 4-2. More details about the ASR-reactivity test can be found in Chapter 5.

Table 4-2: 28-day Compressive Strength of Cylinders Cast with the Bent Cap Specimens

Specimen	28-day Compressive Strength (psi)
Nonreactive	6180
First Reactive	5200
Second Reactive	4700

4.3.3 High-Temperature Curing

As described in Chapter 2, curing temperatures must exceed 158°F to induce DEF deterioration. This prevents the natural formation of ettringite during the curing process. Instead it forms over a long period of time, causing expansive forces and cracking. An external heating system, shown in Figure 4-3e, was used to achieve such high curing temperatures. After placing a fireproof tarp over the formwork for insulation, kerosene and propane heaters applied external heat for the first 12-16 hours of curing. Figure 4-6 shows the temperature variation during curing for the three specimens. These temperatures were measured by the thermocouples near the bottom of the specimen, at the middle of the expected compression block at failure (see Figure 4-4). Though the maximum values are shown here, temperatures varied only a few degrees along the length of the specimens.

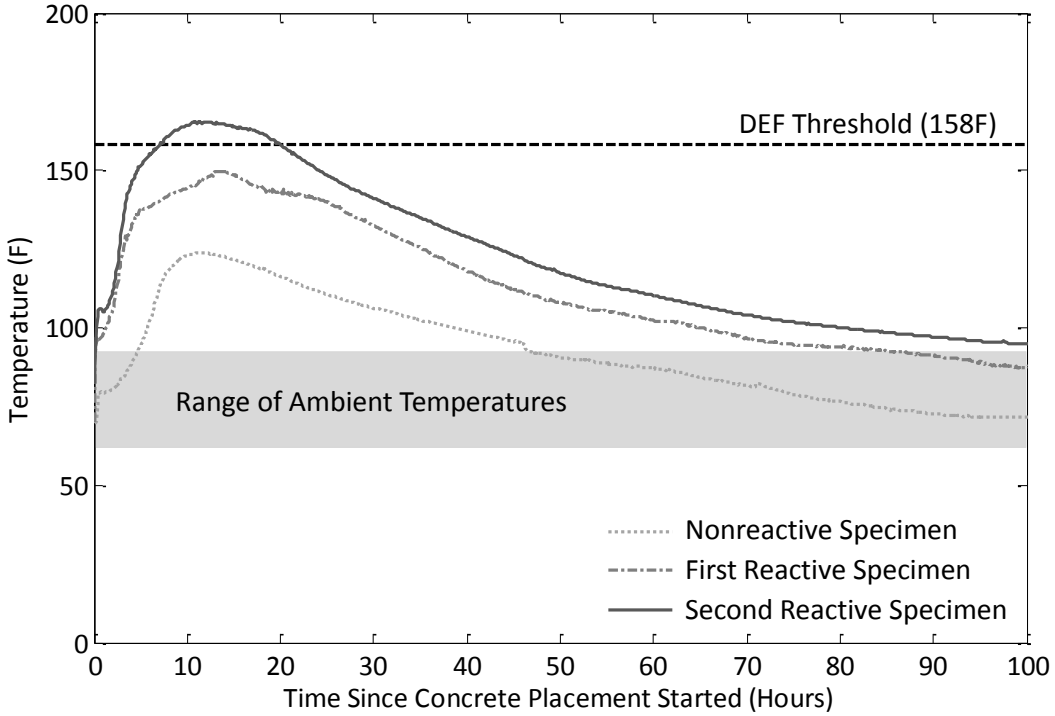

Figure 4-6: Temperature Variation through Curing Process

Distributions of the maximum temperature through the cross section are shown in Figure 4-7 for the nonreactive and second reactive specimens. Note the difference in scale between the two plots. Although the maximum curing temperature in both

specimens varied approximately 20°F throughout the cross section, the second reactive specimen experienced maximum temperatures approximately 35°F higher than did the nonreactive specimen. Unfortunately, these data were not available for the first reactive specimen, although the temperature distribution is assumed to be similar to the other specimens.

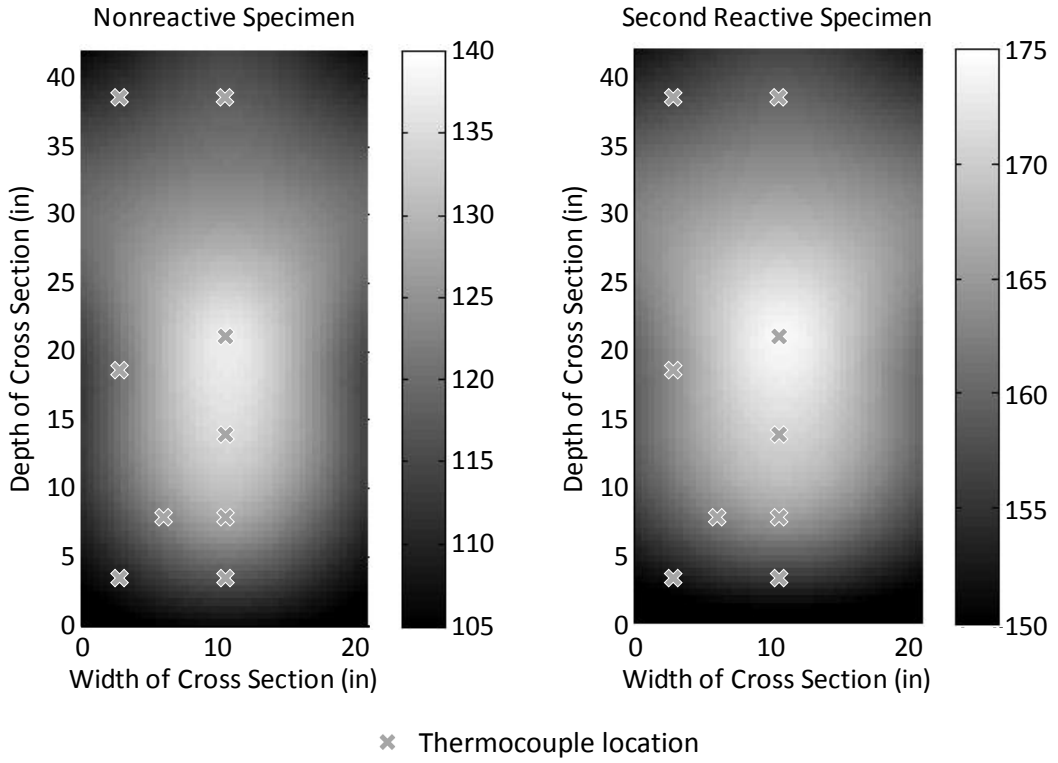

Figure 4-7: Distribution of Maximum Curing Temperatures (°F) through the Cross Section

As shown in Figure 4-6, the nonreactive specimen reached a maximum temperature of nearly 125°F near the bottom of the cross section. Because it was not subjected to external heat, temperatures through the entire cross section remained significantly lower than the DEF threshold of 158°F throughout the curing process (Figure 4-7). The first reactive specimen experienced a maximum curing temperature at the bottom of the cross section of 150°F, or slightly below the DEF threshold. However, portions of this specimen likely experienced curing temperatures at or above 158°F, as temperatures 10 to 20°F higher than those reported in Figure 4-6 occurred closer to the

middle of the cross section in the other specimens (see Figure 4-7). The second reactive specimen sustained temperatures in excess of the DEF threshold through the majority of the cross section for a minimum of 12 hours.

The small reactive concrete samples were also heat cured. A match-curing system in the laboratory (Sure Cure) ensured that the curing temperature profile of the cylinders matched that of the large specimens. The system received the temperatures measured in the large specimens via a wireless transmitter, and heated the insulated metal cylinder molds (see Figure 4-8) to match those temperatures. Thus, the cylinders were cured following the temperature profiles in Figure 4-6. For more details on the match-curing system, see Deschenes (2009). Because no insulated prism molds were available for use with the match-curing system, the prisms were manually and approximately match-cured in a small oven. The temperature of the oven was adjusted hourly to simulate the curing temperature profiles in Figure 4-6.

Figure 4-8: Match-Curing Cylinder Molds

4.4 SUMMARY

Three specimens were fabricated to investigate the effectiveness of several NDT methods in characterizing ASR and DEF deterioration. The specimens were designed as near-full scale representations of typical bent caps found in the state of Texas. Accelerated ASR and DEF deterioration was induced in two of the specimens through the use of ASR-reactive materials and high temperature curing. The third specimen was fabricated using similar non-reactive materials and was not heat-cured. Thermocouples were placed in several locations along the specimens and through the cross section to measure curing temperature, and "targets" fabricated out of stainless steel rods and studs were placed within the reinforcement cage to measure the steel strains and core concrete expansions as deterioration progresses.

CHAPTER 5
Experimental Program

5.1 OVERVIEW

After fabrication, the bent cap specimens were moved outside of the laboratory, and the conditioning and monitoring phase began. The conditioning process consisted of nightly watering cycles to accelerate the deterioration, and loading to simulate typical field stresses in the specimens. The specimens were monitored for core concrete expansions and steel strains over a period of nearly one year. Additionally, several nondestructive testing (NDT) methods were used to evaluate the specimens as deterioration progressed.

The prism samples that were cast alongside the bent cap specimens were subjected to the conditioning and expansion monitoring regime defined by ASTM C1293 (2008) . Along with this program, the prism samples were monitored over time using the resonant frequency NDT method (ASTM C215 2008).

This chapter first describes the conditioning phase of the bent cap specimens in Section 5.2. The monitoring of expansions is explained in Section 5.3, followed by a detailed description of the NDT methods used in Section 5.4. Finally, the conditioning and monitoring of the prism samples is discussed in Section 5.5. Note that the conditioning and expansion monitoring of the specimens were largely based on previous research. See Deschenes (2009) for a more detailed explanation of several of the topics covered in this chapter.

5.2 CONDITIONING OF BENT CAP SPECIMENS

ASR and DEF deterioration was accelerated in the bent cap specimens by means of a conditioning regime designed to simulate an extreme but realistic environment for a field structure. The specimens underwent both climate and load conditioning, as described in detail in the following two sections.

5.2.1 Climate Conditioning

After casting, the bent cap specimens were placed outdoors using a 15-ton forklift. Resting on concrete blocks just outside of the laboratory, the specimens were exposed to the warm climate of Austin, Texas for nearly one year. It is common for temperatures in Austin to exceed 100°F in the summer months, while winters are mild. This environment provided the warm temperatures to facilitate accelerated deterioration.

A watering system was implemented to supply adequate amounts of moisture for rapid deterioration to occur. Soaker hoses were run along the length of the specimens to evenly provide moisture to all portions of the test regions during 12-minute nightly watering cycles. Each specimen was wrapped in a curing tarp to trap in the moisture during the day (see Figure 5-1). Tarps were only removed for monitoring purposes.

Figure 5-1: Specimens Conditioning Outside of the Laboratory

5.2.2 Load Conditioning

Dead load stresses that a bent cap is likely to be subjected to in the field were induced in the specimens. External loads were applied at the third points, inducing a constant moment in the middle test region and a constant shear in the outer test regions (see Figure 5-2). As discussed previously, note that the specimens were stored and loaded upside-down (i.e. load applied from the bottom). This was done to facilitate easy application of the conditioning load. The same configuration will be used for future structural testing.

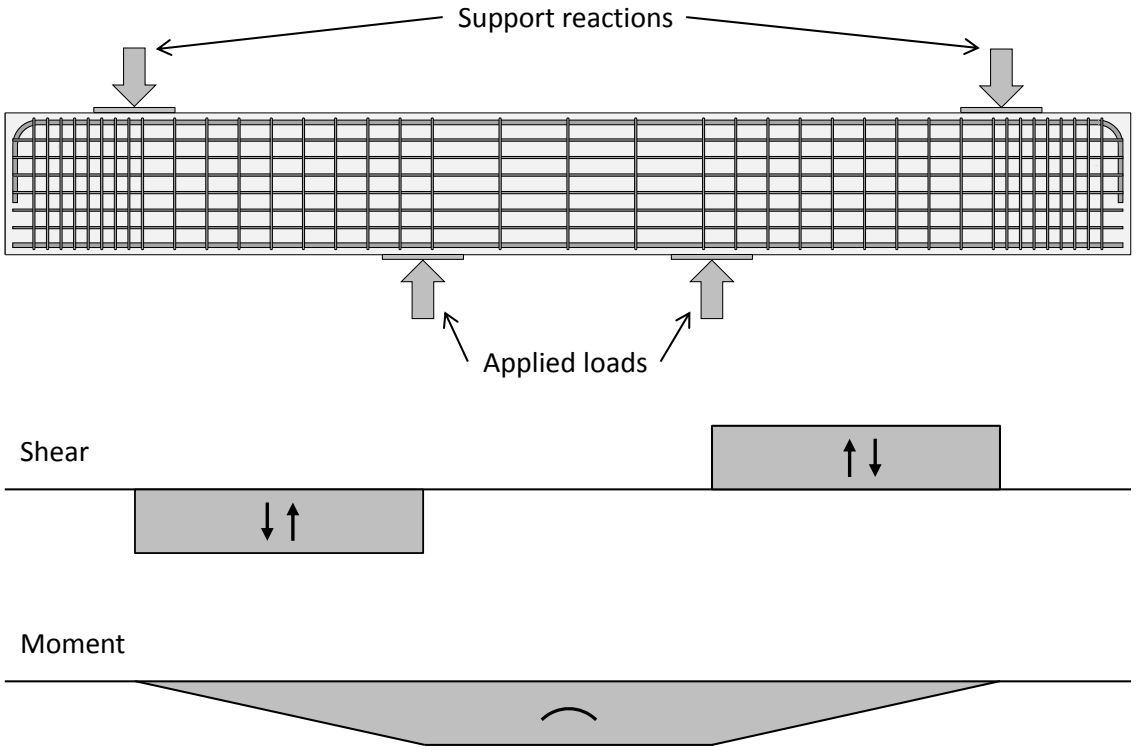

Figure 5-2: Load Conditioning of the Bent Cap Specimens

The *TxDOT LRFD Bridge Design Manual* limits the unfactored dead load stresses in the tensile steel to 22 ksi to minimize flexural cracking (TxDOT 2010). A stress value nearing this limit was targeted, resulting in an applied shear of nearly 80 kips. This force was large enough to induce some flexural cracking in the nonreactive specimen. However, no flexural cracks were observed after loading the reactive specimens, even though deterioration was minimal at the time of loading. As discussed in Chapter 2, the

reinforcement restrains the ASR and DEF induced expansion, effectively prestressing the element and increasing the cracking moment.

A steel reaction beam was placed under each specimen and was used to apply the external conditioning load. The setup is depicted in Figure 5-3. The reaction beam was separated from the specimen by two steel plates and a bearing pad at the loading points. The specimen and reaction beam were clamped together at the support points to induce stresses. Each clamping apparatus consisted of three HSS steel tubes, two above the specimen and one below the reaction beam, connected by threaded steel rods. A large spring assembly was placed between the HSS tubes and the top of the specimen. 30 ton hydraulic rams stressed the threaded rods against the springs, applying a clamping force. After tightening the nuts against the HSS tubes, the hydraulic rams and the top HSS tube were removed.

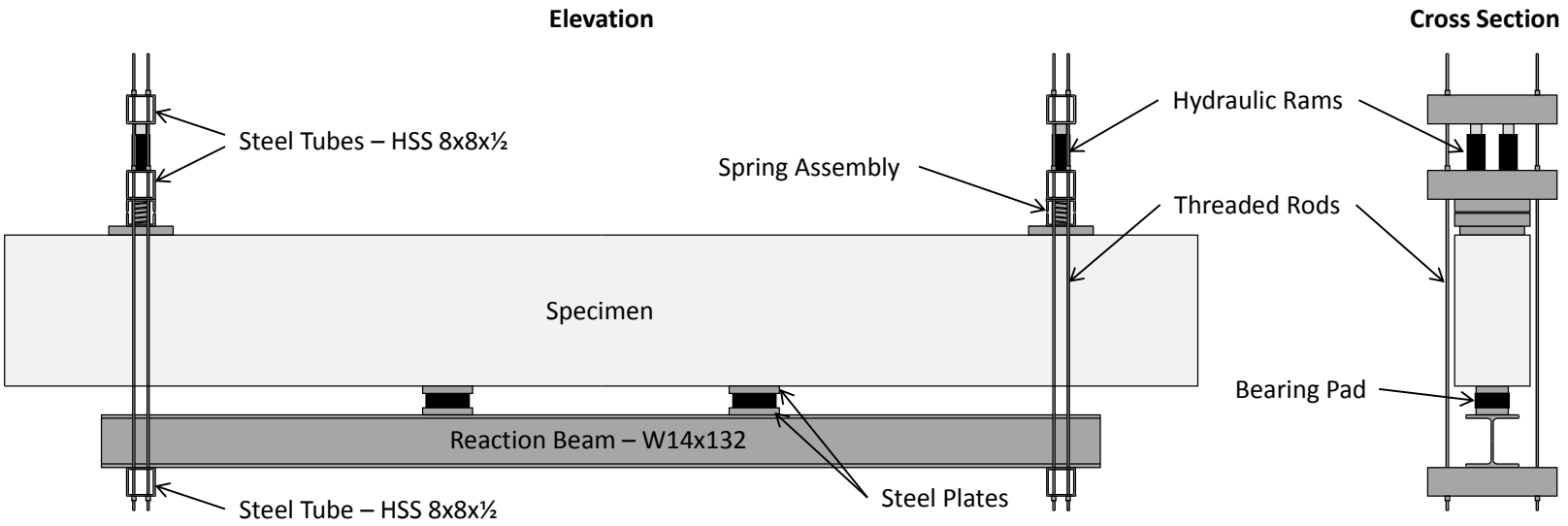

Figure 5-3: Application of the Conditioning Load

5.3 EXPANSION MONITORING OF BENT CAP SPECIMENS

The level of deterioration was quantified by measuring ASR- and DEF-induced expansions at several locations. Mechanical measurements of the steel strains and core concrete expansions were taken using the stainless steel "targets" placed in the cage during fabrication (see Section 4.3.1). An extensometer with a 24″ gauge length and 0.0025% accuracy was connected to a laptop through a National Instruments data acquisition system. Data was collected using a LabVIEW program. Photos of the equipment used and of measuring expansions are shown in Figure 5-4.

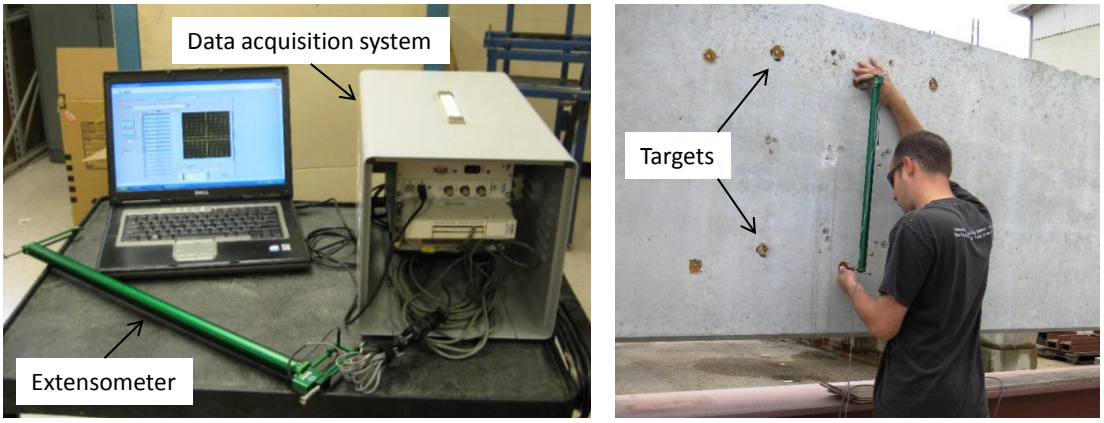

Figure 5-4: Expansion Measurements

The locations of expansion measurements are shown in Figure 5-5. Expansions were measured on both sides of the specimen, as well as on the top and bottom faces. Both longitudinal and vertical expansions were monitored. Readings were taken at temperatures as close as possible to 70°F and at times when prolonged sun exposure would not affect the results. Though insignificant compared to the ASR and DEF expansions, temperature corrections were applied using an approximate coefficient of thermal expansion of 5.5×10^{-6} °F^{-1} to normalize measurements to 70°F. Additionally, corrections were made after loading of the specimens to eliminate any effects of the applied stresses from the results. Expansions were monitored weekly in the summer months, when the warmer weather induced rapid deterioration. During the winter, measurements were taken monthly. Expansion results are given in Chapter 6.

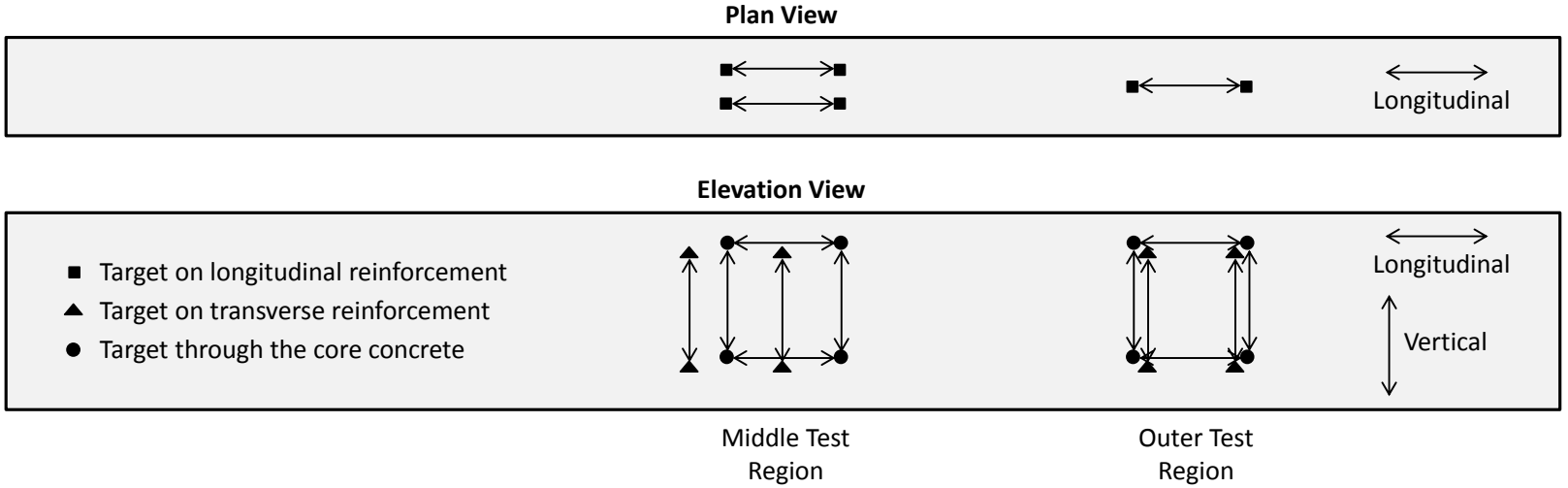

Figure 5-5: Expansion Measurement Locations

5.4 NDT MONITORING OF BENT CAP SPECIMENS

The second portion of the monitoring process consisted of performing several nondestructive tests on the deteriorating bent cap specimens, including ultrasonic pulse velocity (UPV), impact echo, and two surface wave techniques. A nonlinear acoustic technique developed by researchers at Sherbrooke University in Quebec, Canada was also used, but only at higher levels of deterioration. Chapter 3 gives an overview of each testing method, discussing previous research and applications to ASR and DEF. This section describes the details and parameters of each test method as used in the current research. All results can be found in Chapter 6.

5.4.1 Ultrasonic Pulse Velocity (UPV)

UPV travel times were measured with a Germann Instruments PUNDIT 7 test system. Procedures of ASTM C597 (2009) were followed. The velocities were computed in a Microsoft Excel spreadsheet. A photo of the system and a summary of the testing parameters are given in Figure 5-6. The test was performed using the through-transmission technique with a water-based couplant. Measurements were taken at several points both horizontally and vertically through the cross section (see Figure 5-7).

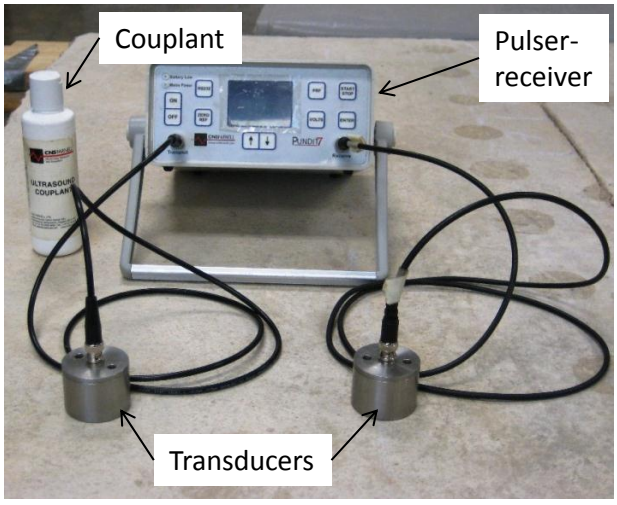

Pulse repetition frequency:	100 kHz
Excitation voltage:	100 V
Transducer frequency:	54 kHz

Figure 5-6: UPV Testing Equipment and Parameters

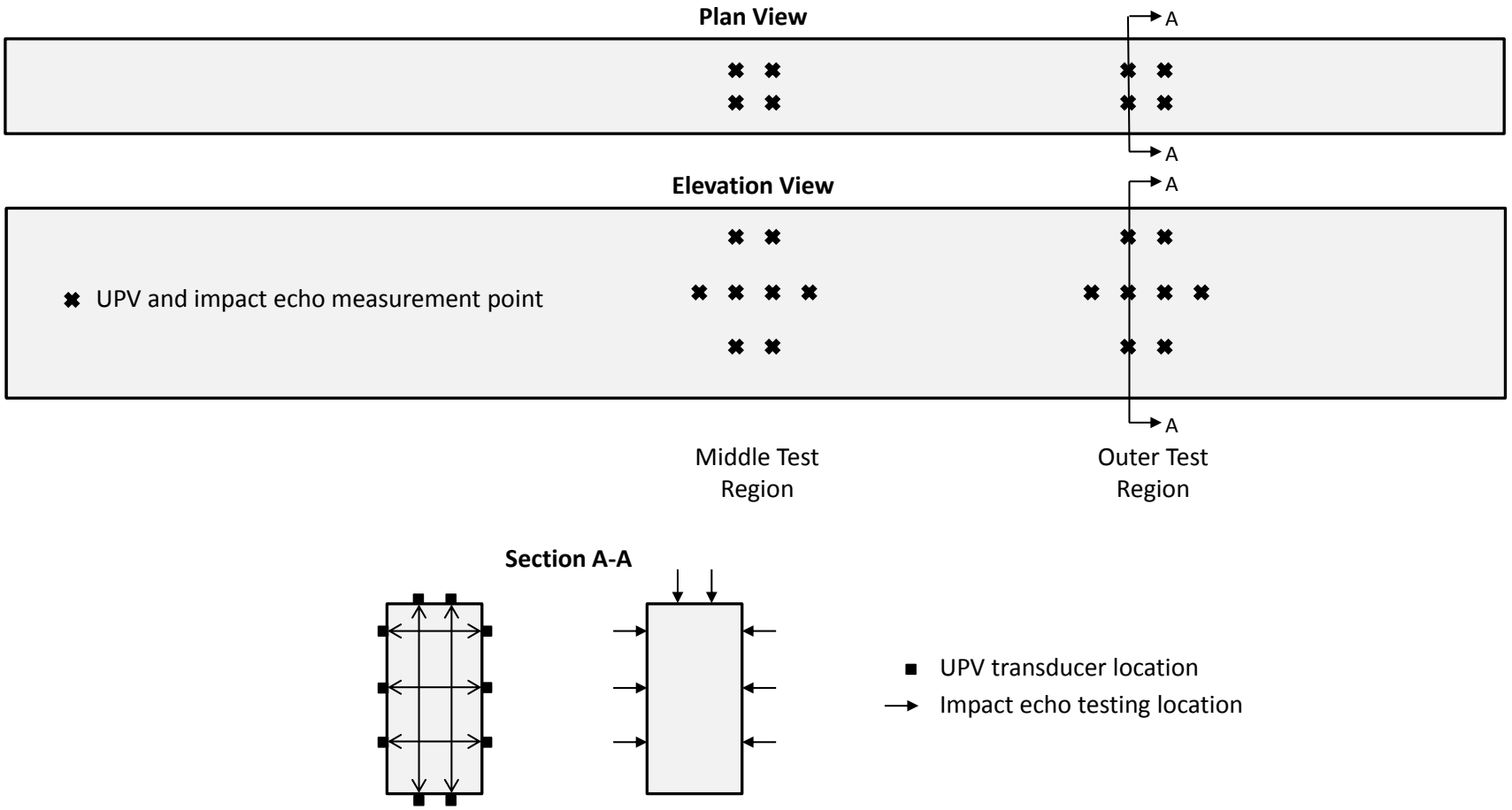

Figure 5-7: UPV and Impact Echo Testing Points

5.4.2 Impact Echo

Impact echo monitoring was performed with a Germann Instruments DOCter receiver following the procedures of ASTM C1383 (2004). The impact source was a 0.39" diameter ball-peen hammer. Data was collected through an 8-bit National Instruments digitizer using LabVIEW and later analyzed in a MATLAB program. Figure 5-8 gives an overview of the testing parameters and shows a photo of the system. The test was performed at the same points as was UPV in the middle and outer test regions (see Figure 5-7). Measurements were taken on both sides of the specimens as well as on the top face. No impact echo testing was done on the bottom face of the specimens because the loading setup did not leave enough clear space.

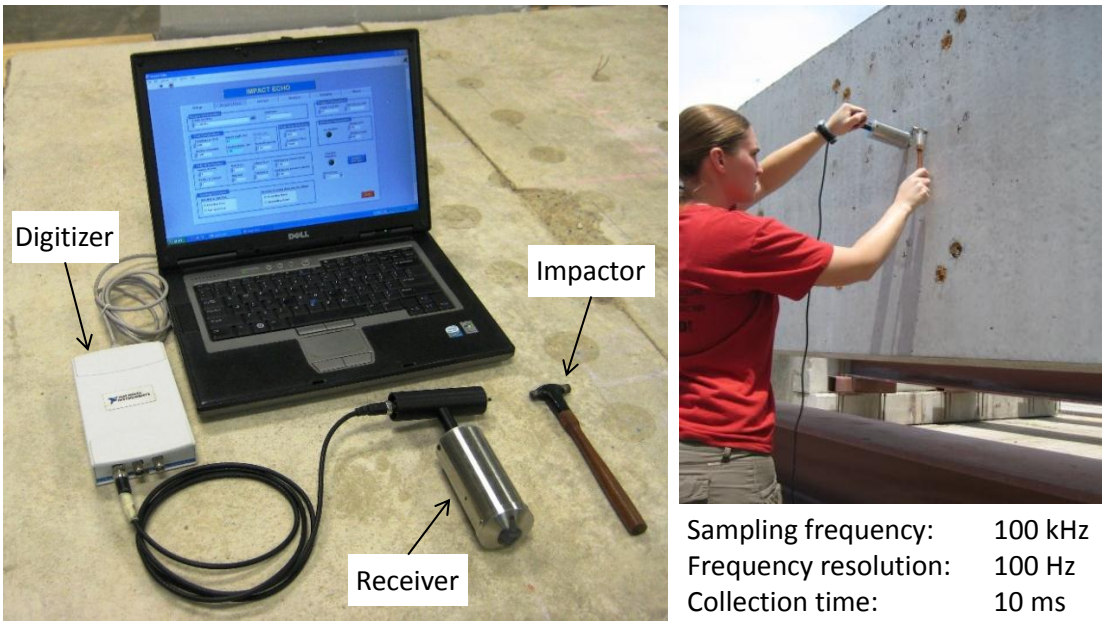

Figure 5-8: Impact Echo Testing Equipment and Parameters

5.4.3 Surface Wave Techniques

The surface wave testing was performed with two small and precise PCB microphones, which measure the air pressure caused by the surface motion of the concrete. The microphones are sensitive to frequencies from 4 Hz to 80 kHz. As discussed in Section 3.6, the use of non-contact sensors eliminates coupling issues and

speeds up the testing process. To isolate the microphones from ambient noise, a sound insulation device was fabricated (Kee & Zhu 2010).

After impacting the surface with a 0.51" steel ball, the data were collected through a 3-channel PCB signal conditioner and an 8-bit National Instruments digitizer. A LabVIEW program was used to view and save the data, which were later analyzed using MATLAB. A photo of the test setup is shown in Figure 5-9 along with a summary of the testing parameters. Figure 5-10 depicts a schematic of the surface wave testing points within each test region. The testing grid was centered within the UPV and impact echo points, and data were taken at five locations within each test region. Ten measurements were recorded at each location, five on either side of the sensors, to minimize error by averaging. Testing was limited to the side faces of the specimens. No surface wave testing was performed on the top or bottom faces.

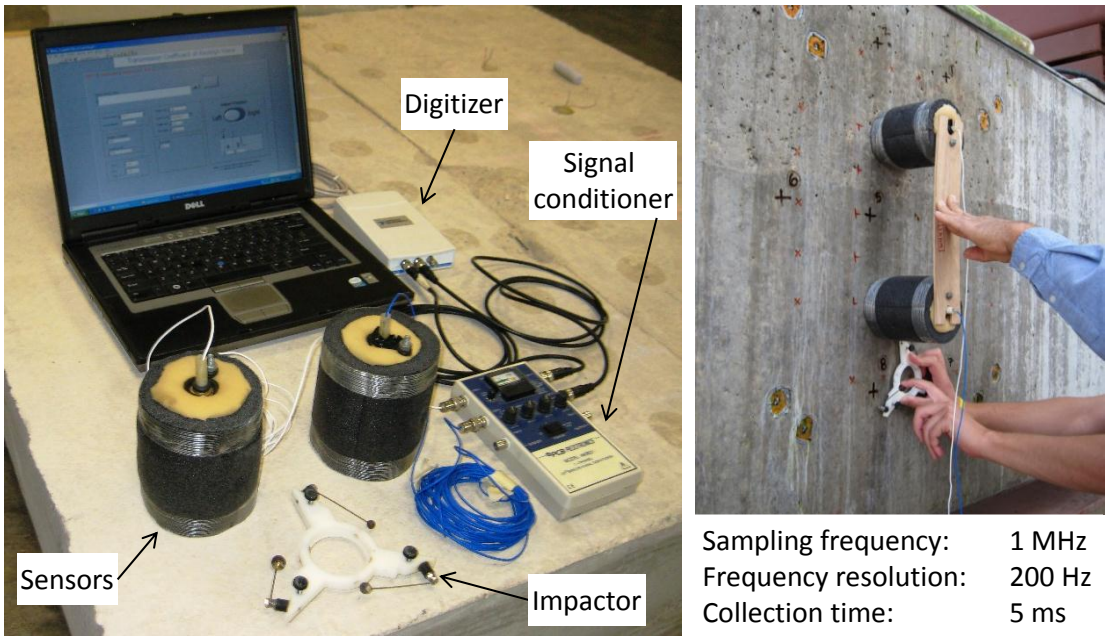

Figure 5-9: Surface Wave Testing Equipment and Parameters

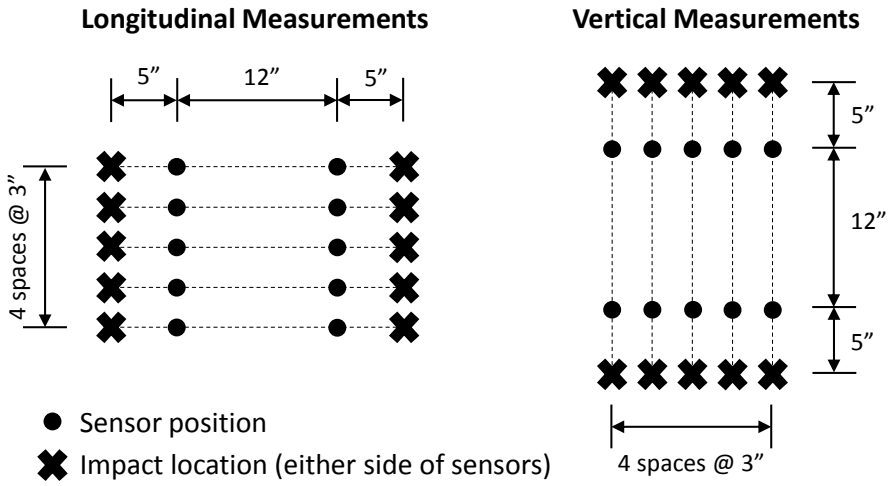

Figure 5-10: Surface Wave Testing Points in Each Test Region

5.4.4 Time Shift Nonlinear Acoustic Method

Researchers at Sherbrooke University in Quebec, Canada have recently developed a nondestructive test based on the nonlinear propagation of acoustic waves to evaluate damage from internal microcracking in concrete (Kodjo et al. 2009). This method will be referred to as the "time shift nonlinear acoustic method." Though several nonlinear testing methods have been recently developed to characterize microcracking in concrete, this method was chosen for investigation in this research because of the potential practical applicability to the evaluation of field structures. Most of the other methods are only applicable on small samples or under very controlled laboratory conditions. The basic concept is to observe an ultrasonic compression wave propagating through the material just after impacting the element with a large hammer. The impact force causes the microcracks to open, which delays the arrival and reduces the amplitude of the received wave. For a more detailed description of the method, see Section 3.7.4.

There is no test system commercially available for these measurements. Therefore, testing capability was developed in-house with guidance from the researchers at Sherbrooke University. Time shift nonlinear acoustic testing on the bent cap specimens was performed less frequently than were the other NDT methods, and most of the data were obtained at higher levels of deterioration.

The test setup and parameters are depicted in Figure 5-11. High frequency ultrasonic transducers were coupled to the surface with petroleum jelly and securely attached to the specimen with a strap. A small sledgehammer was used as the impact source. Ultrasonic pulses were generated using an Olympus square wave pulser-receiver. Data was collected through an 8-bit Agilent oscilloscope with high sampling rate capabilities. Agilent software was used to record the data, while a MATLAB program performed the analysis. Nonlinear acoustic testing was performed near the middle of each test region. Several different sensor and impact configurations were investigated. These are shown in Figure 5-12.

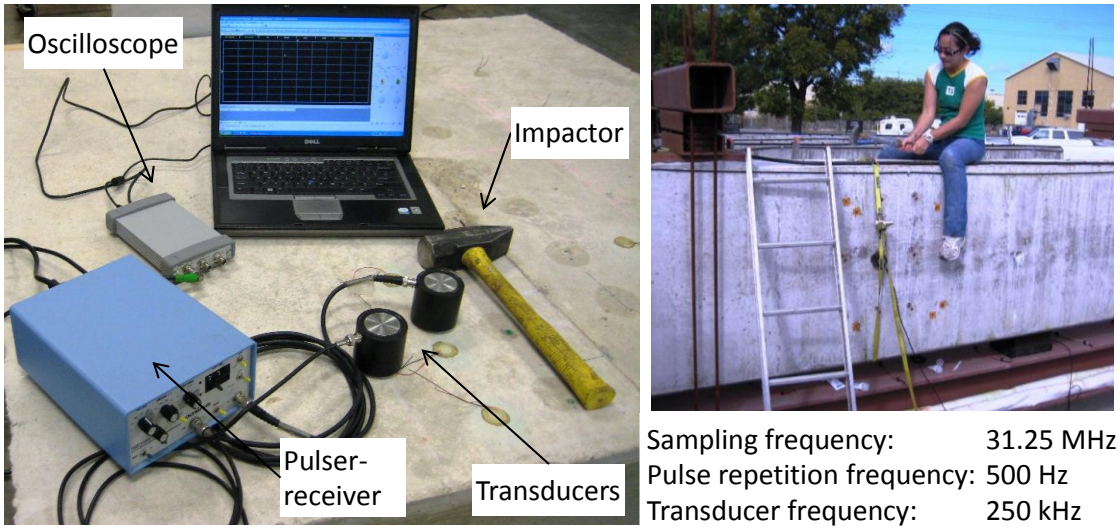

Figure 5-11: Time Shift Nonlinear Acoustic Testing Equipment and Parameters

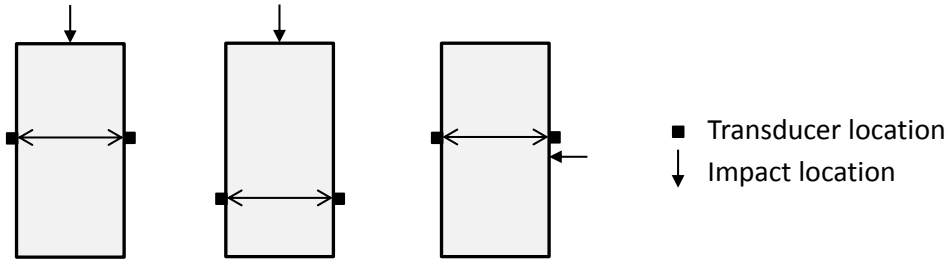

Figure 5-12: Cross Sections of Various Time Shift Nonlinear Acoustic Test Configurations

5.5 PRISM SAMPLES

Conditioning and expansion monitoring for the concrete prism samples cast alongside the large bent cap specimens were done according to ASTM C1293 (2008). This standard is used to evaluate the ASR expansive potential of a particular aggregate. In the current research, the procedures of ASTM C1293 were followed to induce rapid deterioration in the small prism samples and to monitor the expansions, even though the concrete mixture properties did not exactly adhere to those prescribed in the standard. Additionally, the prisms were monitored nondestructively using the resonant frequency method, as defined in ASTM C215 (2008).

A total of eight prism samples were fabricated for each bent cap specimen. Four samples were used for expansion monitoring, while the remaining four underwent resonant frequency testing. All prisms were conditioned according to ASTM C1293. An overview of the conditioning and expansion monitoring process is given in Section 5.5.1, and the resonant frequency monitoring is described Section 5.5.2. All monitoring results are presented in Section 6.4.

5.5.1 Conditioning and Expansion Monitoring of Prism Samples (ASTM C1293)

ASTM C1293 describes the standard procedure for measuring length change, or expansion, of prism samples with 3" square cross sections. These samples were cast with small pins in the ends for accurate length measurements. Initial length measurements were taken one day after casting. The prisms were then stored above water in sealed plastic pails in a 100°F oven (see Figure 5-13a). At an age of 7 days, the length of each sample was measured again to determine the prism expansions. The pails were removed from the oven and placed in a moist environment 12-20 hours before length measurements to allow for cooling of the samples. Immediately following the measurements, the pails were placed back into the oven. This process was repeated at ages of 14 days, 1, 2, 3, 6, 9 and 12 months. Further measurements will be taken at 6 month intervals.

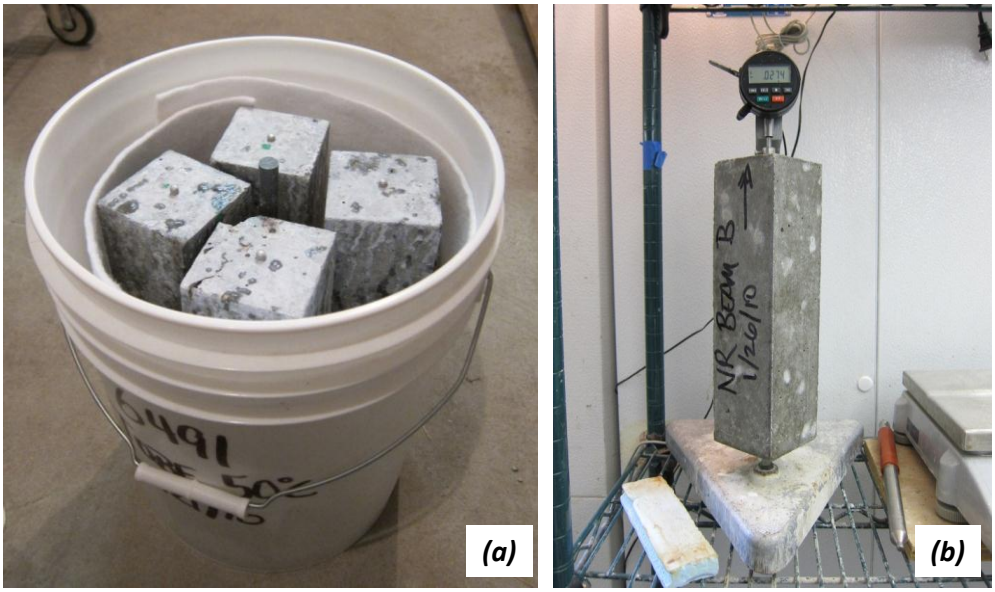

Figure 5-13: (a) Conditioning and (b) Expansion Monitoring of Prism Samples

5.5.2 Resonant Frequency Monitoring of Prism Samples (ASTM C215)

The prism samples were monitored using the resonant frequency NDT method defined by ASTM C215. Tests measuring both the transverse and longitudinal resonant frequencies were done on the same days as expansion measurements were taken. The test setup and parameters are shown in Figure 5-14. The samples rested on foam to limit vibrational constraints. To measure vibrations, a highly sensitive PCB accelerometer with a bandwidth (±10%) of 0.3 Hz to 12 kHz was attached to the surface using wax. The impact source was a 0.43" steel ball. Data were collected through a 3-channel PCB signal conditioner and an 8-bit National Instruments digitizer. The results were analyzed in a LabVIEW program. For background information and more details about the resonant frequency test, refer to Section 3.5.

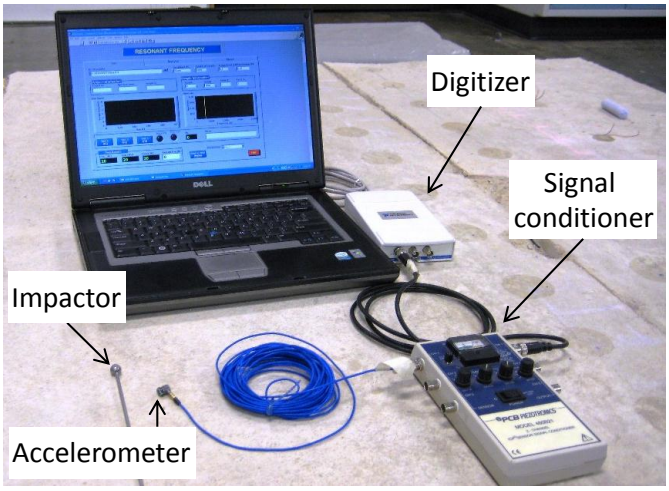

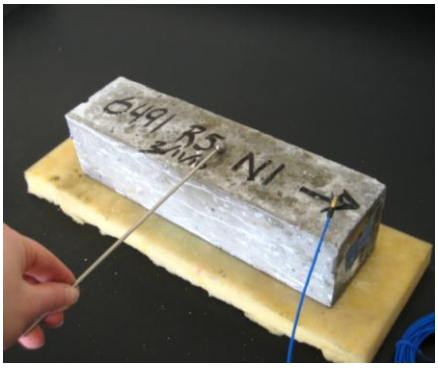

Sampling frequency: 50 kHz
Frequency resolution: 10 Hz
Collection time: 100 ms

Figure 5-14: Resonant Frequency Testing Equipment and Parameters

5.6 SUMMARY

The bent cap specimens were stored outdoors for nearly one year during the conditioning and monitoring phase. Nightly watering cycles and the warm environment induced accelerated ASR and DEF deterioration. Dead load stresses were induced in the specimens to simulate field conditions. Deterioration was quantified by measuring steel strains and core concrete expansions in several locations along the specimens. Additionally, NDT methods including UPV, impact echo, and surface wave techniques were used throughout the deterioration process. A nonlinear acoustic NDT method was also performed on the specimens at high levels of deterioration.

The prism samples were conditioned and monitored according to ASTM C1293, a standard to assess the potential of an aggregate for ASR deterioration. In addition to the expansion measurements defined in the standard, these samples were monitored using the resonant frequency NDT method.

CHAPTER 6
Experimental Results

6.1 OVERVIEW

The goal of this research was to observe trends in results from nondestructive testing as ASR and DEF deterioration progressed in concrete specimens. Ultimately, the results were used to determine the potential for using several NDT methods for evaluating field structures exhibiting symptoms of ASR and DEF. This chapter presents the results from monitoring the deterioration of and from nondestructive testing of the bent cap specimens and the prism samples. Section 6.2 discusses the deterioration of the bent cap specimens over time, and is followed by a summary of the NDT results in Section 6.3. The expansion and NDT results from testing on the prism samples are covered in Section 6.4.

6.2 BENT CAP DETERIORATION

Throughout the monitoring period, the bent cap specimens were visually observed and expansions were measured in order to quantify the damage as the deterioration progressed. Section 6.2.1 will briefly discuss the visual observations of the deterioration, and is followed by a more detailed presentation of expansions results in Section 6.2.2. Note that because this research was largely focused on NDT methods, a detailed study of crack patterns and crack widths was not performed. Deschenes (2009) provides in-depth discussions of the influence of reinforcement and external loading on the observed cracking patterns, and of the accuracy of using the crack width summation method to estimate expansion.

6.2.1 Visual Observations of Deterioration

Visual signs of deterioration were observed as early as 6 weeks after casting and 3 weeks after moving the specimens outdoors. The first visible surface cracks appeared near mid-depth of the specimens and were primarily oriented in the longitudinal direction. Over time, extensive cracking was observed on all faces of the specimens,

usually following the direction of the primary reinforcement, which provides the most restraint to the expansion.

Figure 6-1 shows photos of the second reactive specimen at an age of nearly one year. On the side face of the middle test region (Figure 6-1a), the maximum crack width is 0.025″. The cracks are oriented almost exclusively in the horizontal direction. Crack patterns on the top and bottom faces were very similar to those on the side faces. Note that in the figure, several larger cracks are highlighted in bold on the side face of the specimen. The end face of the specimen (Figure 6-1b) exhibited very wide cracks, up to 0.25″, or ten times larger than the cracks on the side faces. This is a direct result of the lack of reinforcement at the end face to control the cracking. Stirrups were stopped 8 ½″ from the end face because of the hook at the end of the tensile reinforcement (see Figure 4-2). The large horizontal crack on the end face lies just below the end of the tension steel hook. Recall that the specimens were fabricated and will later be structurally tested upside down for ease of loading, so the tension steel is on the top side (see Figure 5-2). Overall, the observed crack patterns were expected and were similar to findings in previous research.

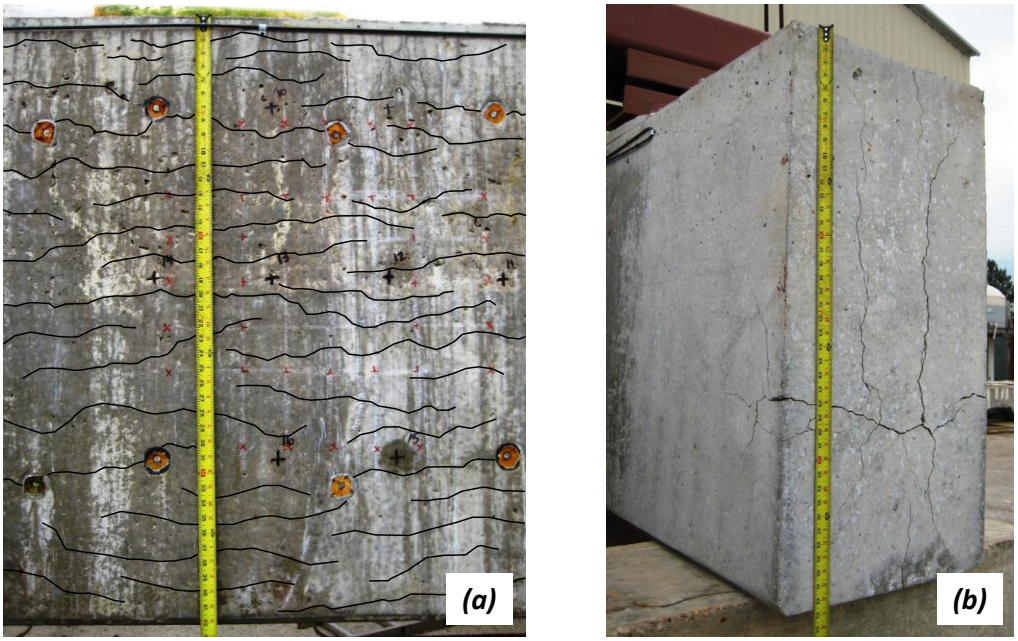

Figure 6-1: Typical Crack Patterns (Second Reactive Specimen) (a) Side Face and (b) End Face

6.2.2 Expansion Results

The timeline in Figure 6-2 illustrates the relative timeframe for casting, conditioning and expansion monitoring for the three bent cap specimens. Note that although the specimens were cast over a span of 5 months, conditioning and expansion monitoring were started at approximately the same time, just after casting of the second reactive specimen.

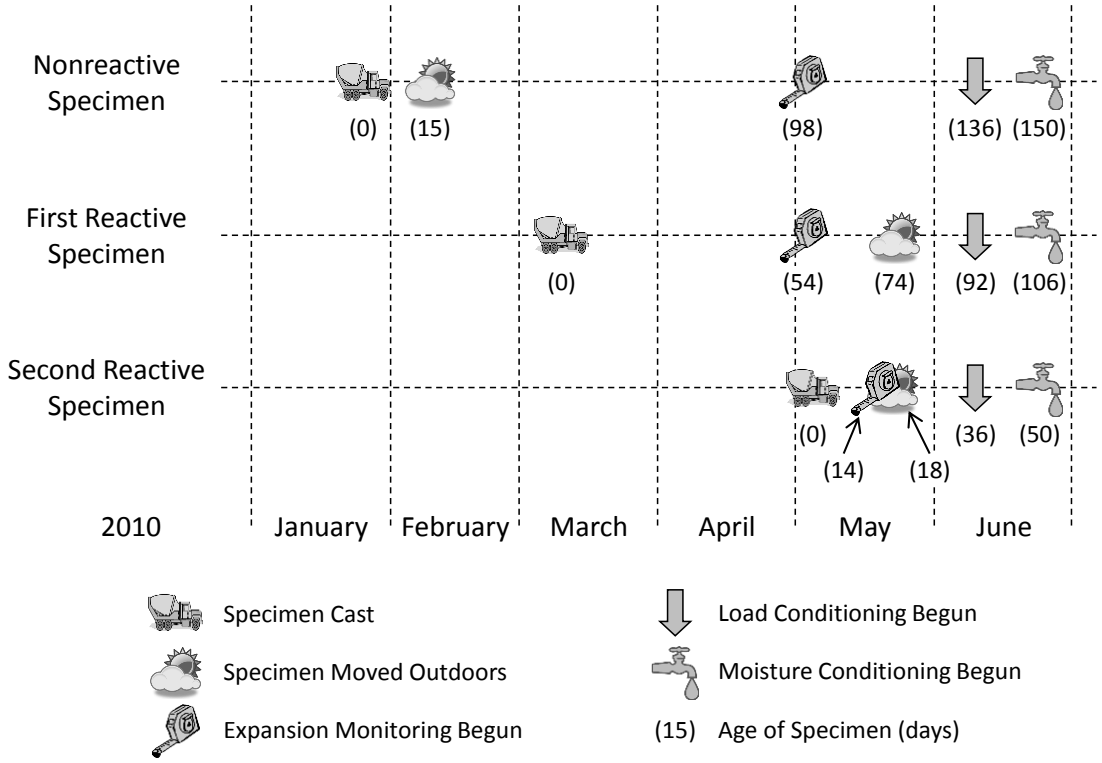

Figure 6-2: Timeline for Bent Cap Specimens

The level of ASR and DEF deterioration was quantified by measuring both the steel strains and the core concrete expansions at several different locations along the bent cap specimens. These steel strains and core concrete expansions will be collectively referred to as "expansions" throughout the rest of this chapter, as the two yielded very similar results. Measurements were taken within two test regions in each specimen: the middle test region with stirrups spaced at 20″ and the outer test region with stirrups spaced at 9 ½″. Additionally, expansions were measured in both the longitudinal and vertical directions. However, no measurements were taken over the width of the cross

section, as the gauge length used for the measurements (24″) was longer than the width of the specimens (21″). For a discussion of the instrumentation placed in the specimens to measure expansions, see Section 4.3.1. Additionally, refer to Section 5.3 for details about the location of the measurement points.

The expansion results for all three specimens during the monitoring period are presented in Figure 6-3. Six to eight measurements were taken in each direction in both test regions (longitudinal and vertical directions in the middle and outer test regions). The range of measured expansions is depicted in the figure as a shaded area for each direction. When correlating these measurements to the NDT results, the average expansion for each direction within a test region was used. The average expansion is shown by the bold black lines in the figure. These averages include both the measured steel strains and core concrete expansions. Additionally, the time at which the specimens were loaded and at which the moisture conditioning began are shown on the graphs. Recall that even though the specimens were fabricated over a period of four months, monitoring began for all shortly after casting of the second reactive specimen (see Figure 6-2). Controlled storage conditions and visual inspections ensured that no significant deterioration occurred between the time of casting and the time monitoring began.

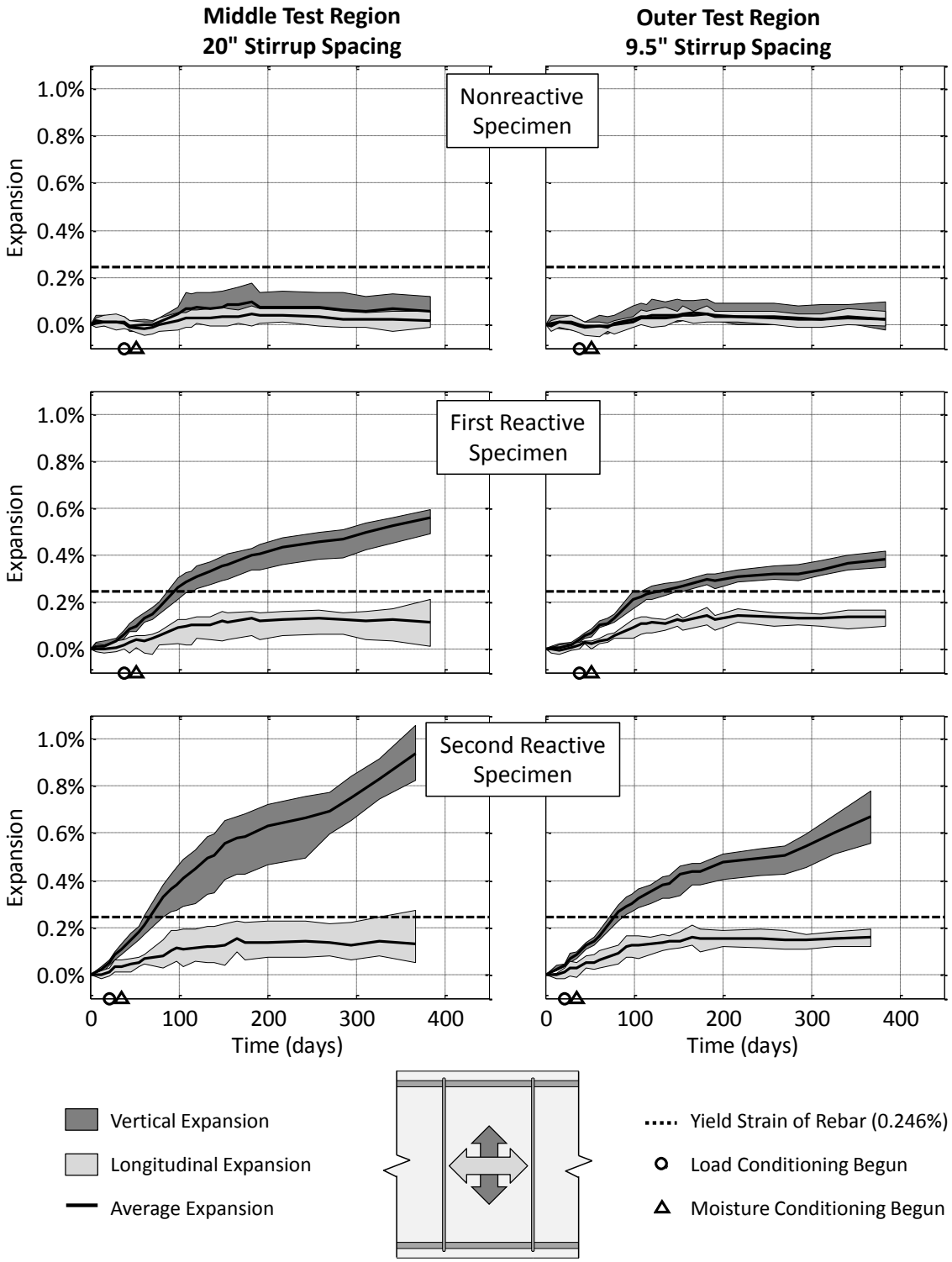

Figure 6-3: Range of Measured Bent Cap Specimen Expansions

From the plots, it is evident that the nonreactive specimen has not significantly expanded. The fluctuations seen in the graph are likely due to environmental factors including moisture content and temperature, concrete shrinkage, and measurement errors. A petrographic analysis of the concrete has yet to be completed, but it is believed that this specimen is not affected by ASR or DEF. This assumption is upheld by the NDT results, which are presented later in this chapter.

On the other hand, the reactive specimens show a significant amount of expansion, especially in the vertical direction. The second reactive specimen has expanded more rapidly than the first. This is assumed to be a direct result of curing temperature. A similar observation was made by Deschenes (2009). The second reactive specimen sustained curing temperatures above the DEF threshold throughout the majority of the cross section for at least 12 hours (see Section 4.3.3). However, only a small middle portion of the cross section of the first reactive specimen experienced such high temperatures during curing. Thus, it is likely that the first reactive specimen has been deteriorated predominantly by ASR while the second reactive specimen has been deteriorated by both ASR and DEF. Though trends in the NDT results tend to support this claim (see Sections 6.3.1 and 6.3.2.2), it cannot be confirmed until a petrographic analysis is completed.

Finally, it is important to note the effects of the reinforcement in the expansion results. As expected, the most rapid expansion took place in the middle test region of each specimen, where the reinforcement was lightest ($\rho_v = 0.15\%$). The outer test region, which had more closely spaced stirrups ($\rho_v = 0.31\%$), experienced slower expansions. Expansions in the longitudinal direction were kept under the yield strain of the reinforcement by the large amount of steel in that direction ($\rho = 2.3\%$). Note that all longitudinal steel can resist the ASR and DEF expansions. Thus, tension, compression, and crack control bars were all included in calculating the longitudinal reinforcement ratio. Despite the general trend of more rapid expansion in less heavily reinforced regions, the relationship between reinforcement ratio and expansion is complicated and

nonlinear. Therefore, it is difficult to predict the expansion rate based on the amount of steel.

6.3 RESULTS FROM NDT ON THE BENT CAP SPECIMENS

Several NDT methods were investigated to evaluate their effectiveness in the assessment of structures affected by ASR and DEF. NDT methods used include ultrasonic pulse velocity (UPV), impact echo, spectral analysis of surface waves (SASW), surface wave transmission (SWT), and the time shift nonlinear acoustic method. The results from each of these tests are presented in Sections 6.3.1 through 6.3.4. Background information on each of these methods can be found in Chapter 3. A description of the test systems and parameters used is given in Chapter 5.

There are many ways to define the level of deterioration in a structure. For the purposes of this research, the deterioration was quantified by measuring expansions throughout the specimens (see Section 6.2). The results are generally presented in this section as plots of an NDT parameter against the vertical expansion in the corresponding test region. The vertical expansion was the largest expansion measured and was thus deemed to be the most representative of the level of deterioration. It may be more appropriate to relate the NDT results to the volumetric expansion, which likely provides a better representation of the overall deterioration. However, expansions were measured in only two directions, and as discussed in the Section 6.2.2, it is difficult to estimate expansions where they are not directly measured. By using the vertical expansion to document the deterioration, the general trends of the NDT results can be observed, and the usefulness of each test can be evaluated.

6.3.1 Ultrasonic Pulse Velocity (UPV)

The ultrasonic pulse velocity (UPV) is determined by measuring the compression wave travel time of an ultrasonic pulse traversing through a material. Lower velocities indicate more damage, as it takes time for the wave to pass through or around defects.

Figure 6-4 shows the UPV results for the two reactive specimens. The data includes measurements oriented horizontally and vertically through the cross section,

taken in both the middle and outer test regions. Each data point represents an average of all measurements recorded in one direction in a test region on a given day of testing. Observations from the results are given in Section 6.3.1.1, and a discussion of the use of UPV in assessing ASR and DEF deterioration is given in Section 6.3.1.2.

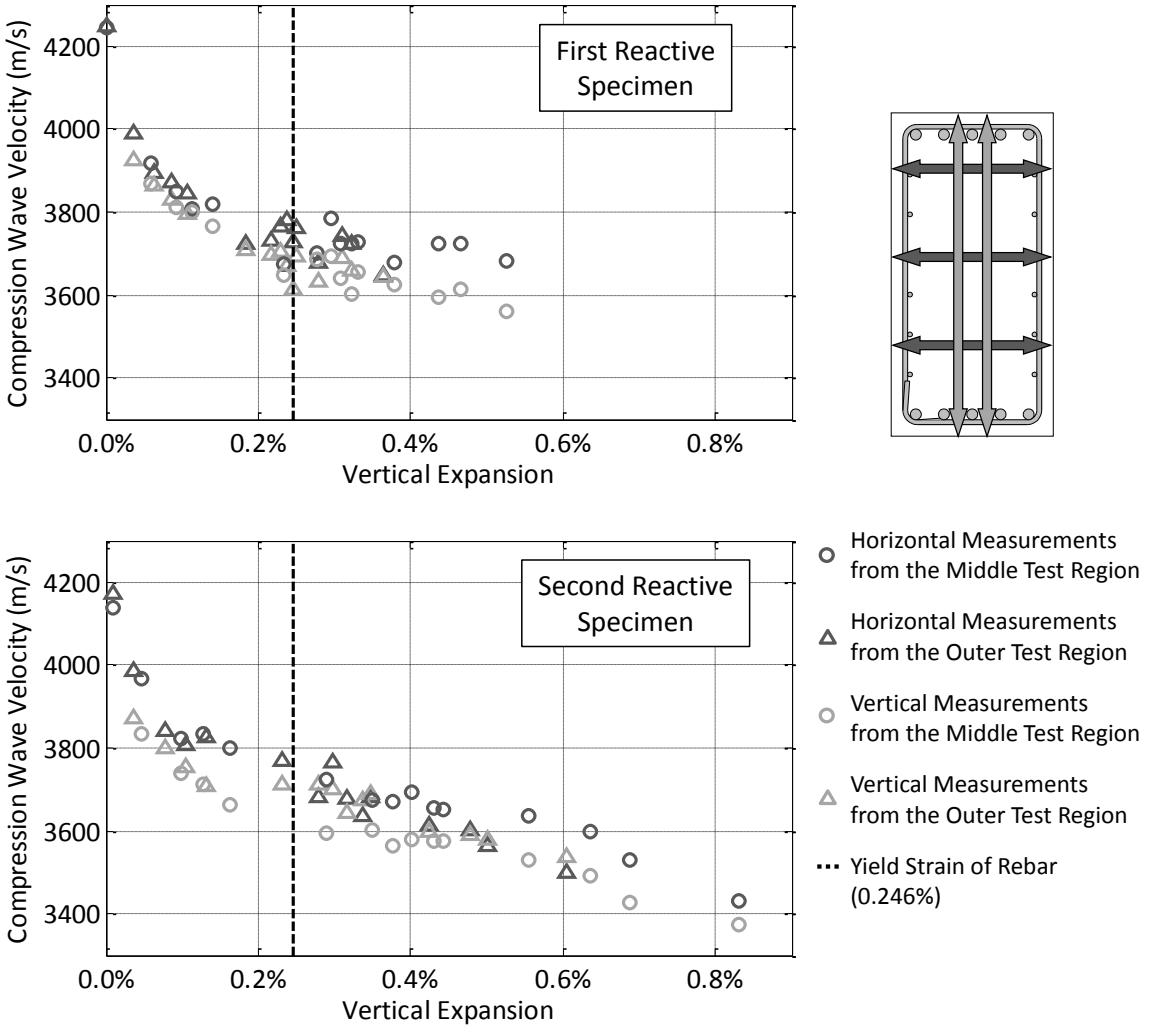

Figure 6-4: UPV Results – Variation of Compression Wave Velocity

6.3.1.1 Observations from UPV Results

The trends shown in Figure 6-4 are similar for each specimen, indicating a rapid initial drop in UPV at low levels of deterioration, with a slower loss in velocity as deterioration progressed. These trends are similar to those found in the literature (see Section 3.3.1). Velocities measured in the first reactive specimen tended to level off at

higher levels of expansion, while the UPV in the second reactive specimen continued to decrease as deterioration worsened. Over the monitoring period, the UPV measured in the nonreactive specimen varied between 4225 and 4370 m/s. Variations in this velocity are believed to be a result of environmental factors, and indicate the typical fluctuations of the compression wave velocity in good quality concrete. These measurements uphold the assumption that no ASR or DEF deterioration was present in the nonreactive specimen, as no loss in UPV was observed.

The compression wave velocity as measured by the UPV method was found to be very similar in the horizontal and vertical directions of measurement. Unfortunately, expansions were not measured in the horizontal direction. Though the horizontal expansion through the cross section is expected to be different than the vertical measured expansion, the actual relationship is unknown. However, concurrent research on ASR and DEF specimens at the University of Texas indicates that UPV is similar in all three directions, regardless of restraint from the reinforcement (Webb 2011). Though it may appear that the UPV measured in the vertical direction is slightly lower than that in the horizontal direction, this is likely a result of systematic error in the testing setup and should not be considered significant. One factor that may cause this difference is the use of the nominal dimensions of 21″ and 42″ rather than the exact initial dimensions, which were not possible to measure. In particular, the as-built vertical dimension is likely to be slightly larger than 42″ due to overfilling of the formwork during casting. A ¼″ difference in the height of the specimen would change the velocity by nearly 25 m/s, which would make up for a significant portion of the difference in UPV between the measurements in the two directions.

The decreasing negative slope of the curves as deterioration progresses indicates a slower rate of UPV loss with deterioration. This phenomenon has been observed by several researchers in tests of specimens with ASR damage (see Section 3.3.1). Most postulate that this is a result of the cracks filling with ASR gel, which has a higher compression wave velocity than air. As deterioration progresses, the gel expands to fill the already formed cracks before net volume expansion of the concrete forms new, empty

cracks. The results here are generally supportive of this theory, and the presumed presence of DEF can help to explain the slightly different trends observed for the two reactive specimens. If it is assumed that deterioration in the first reactive specimen is mostly due to ASR, the leveling off of the UPV at higher levels of deterioration is likely a result of new cracks rapidly filling with expanding ASR gel. In this case, the worsening deterioration is not well reflected in the UPV measurements at high levels of expansion. The presence of DEF and more rapid expansion seen in the second reactive specimen can explain the continued decreasing trend of UPV with deterioration. While some of the cracks are filling with the constantly expanding ASR gel, others are generated by DEF and are likely not gel-filled. Ettringite crystals formed after curing may fill or partially fill the cracks, but may not have the same stabilizing effect on UPV as does ASR gel.

An additional indication of the presence of DEF is the variation of the UPV over the height of the specimens. The data in Figure 6-4 from the horizontal direction of measurement represents the average value of UPV over all locations in the test region. This value is representative of the overall quality of the concrete in a particular area. However, the UPV measured in a test region varied up to 210 m/s in the nonreactive specimen, 300 m/s in the first reactive specimen, and 360 m/s in the second reactive specimen. Generally, the calculated velocities in the reactive specimens were lowest at mid-height, higher near the bottom, and highest near the top of the specimens. This is directly correlated to the cross-sectional distribution of curing temperature (see Figure 4-7). In locations that experienced higher curing temperatures, deterioration from DEF was more severe, yielding a lower UPV than that in the regions of the cross section that had lower curing temperatures.

6.3.1.2 Implications for Assessing ASR and DEF Deterioration with UPV

The results indicate that UPV is best suited for assessing early stages of deterioration, because it is most sensitive to low levels of expansion. An 8 to 10% loss in velocity was observed by the time the vertical expansion had reached half of the stirrup yield strain (ε_y = 0.246%). At expansions equivalent to the yield strain of the stirrups,

the velocity dropped only an additional 2%. Beyond the point of stirrup yield, the velocity either leveled out or continued to decrease slowly, depending on the specimen.

There are several things to keep in mind when extrapolating these results to the assessment of field structures. Firstly, the compression wave velocity can vary greatly in concrete depending on the composition and mixture proportions, the presence of rebar, and the moisture content (see Section 3.3.1.1). Thus, the actual measured UPV values sometimes have little meaning, and the loss in velocity is a more valuable parameter. For this reason, knowing the initial UPV before deterioration began is very helpful. This initial value is often called the "baseline." If the baseline is known, it can be compared to the measured UPV at any point in time to determine the loss in velocity, from which the extent of deterioration can be estimated. However, baseline UPV measurements are not typically available for field structures. If the concrete mixture properties and 28-day strength are known, the baseline velocity can be estimated (ACI Committee 228 2003). Alternatively, measurements from a visibly undamaged location of the structure may be used as an approximate baseline. Note that both of these estimation techniques may result in large errors. In situations where a baseline is neither known, nor can be estimated, it is difficult to assess the deterioration in a structure by taking UPV measurements at one point in time. Monitoring must be carried out over a longer period of time to effectively observe the trends. If it is not possible to maintain similar environmental conditions at each monitoring point, the various conditions should also be recorded.

The second important factor that must be considered when assessing deterioration using UPV is that the method cannot distinguish ASR and DEF deterioration from other types of defects. If the concrete was poorly consolidated, has delaminations, or is affected by other types of deterioration, the velocity and the change in velocity over time will depend on all of the defects present. Thus, the loss in UPV in a field structure with damage from several different sources likely will not adequately reflect the level of ASR and DEF deterioration.

Finally, it is important to note that the deterioration was accelerated in this study. Field structures typically deteriorate at rates that are orders of magnitude smaller than those experienced in this research. The expansions observed in these specimens in nearly one year are representative of what a field structure may see over a 20-50 year period. While all attempts were made to simulate field conditions and large discrepancies are not expected, results may differ slightly because of much slower deterioration rates in the field.

6.3.2 Impact Echo

Impact echo is a stress wave-based NDT method that was originally developed for locating defects in concrete slabs. The test consists of a receiver that measures the surface displacement of an element after a mechanical impact. Analysis of the wave reflections provides information about the wave propagation through the element. As discussed in Section 3.4, observing key features in both the time and frequency domains of the received signal can help to assess ASR and DEF deterioration. A discussion of the time domain analysis is provided in Section 6.3.2.1, while results from frequency domain analysis are presented in Section 6.3.2.2.

6.3.2.1 Time Domain Analysis

The technique proposed for assessing the level of ASR and DEF deterioration in the time domain is based on attenuation of the reflected compression waves (Kesner et al. 2004). Internal microcracking caused by ASR and DEF scatters the waves that are traveling through the concrete. As deterioration progresses and more cracks form, more scattering will occur. In theory, this phenomenon can be quantified by observing the rate at which the energy of the reflected compression waves is attenuated. More rapid attenuation indicates more scattering and thus more deterioration.

Typical time domain signals from each specimen are shown in Figure 6-5 for comparison between the initial measurements and those taken after significant deterioration had occurred in the reactive specimens. Each signal has been filtered using a 5^{th} order high-pass Butterworth filter with a cutoff frequency of 5 kHz. This eliminates

the effects of low frequency vibrations while maintaining the integrity of the signal. Each signal has been normalized by the maximum amplitude of the initial surface wave to facilitate comparison.

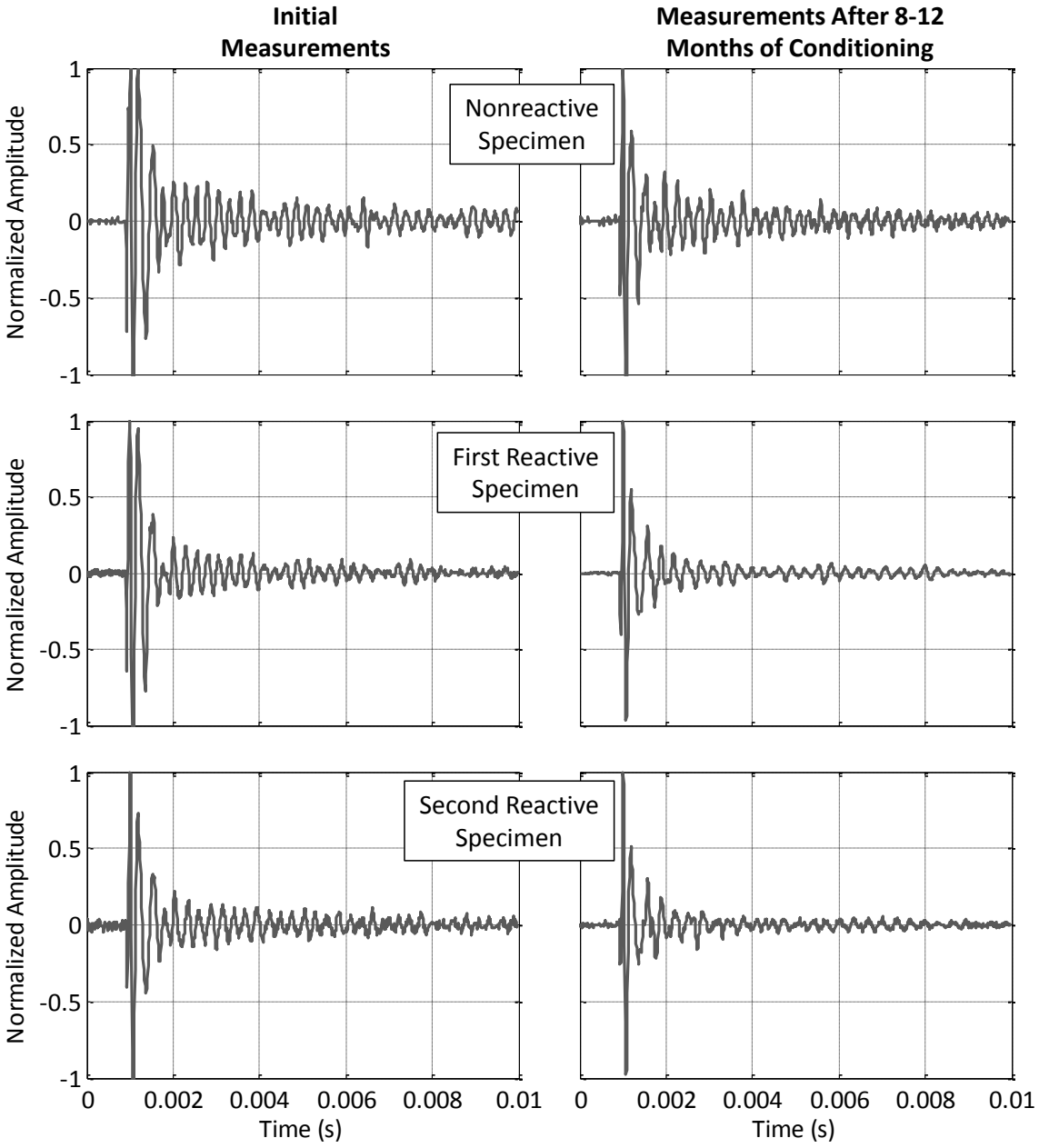

Figure 6-5: Typical Impact Echo Time Domain Signals

By visual inspection, it appears that the presence of deterioration causes more rapid attenuation. As discussed in Chapter 3, Kesner et al. (2004) proposed fitting exponential decay curves to the peaks in the signal:

$$I = I_0 e^{-\alpha t} \qquad \textit{Equation 3-3}$$

where I is the stress wave intensity at time t, I_0 is the initial stress wave intensity and α is the decay constant. Generally, this method yields higher decay constants at higher levels of deterioration. However, two important factors influence the results: the properties of the signal filter used, and the number of signal cycles included in the analysis.

Firstly, the filter order and cutoff frequency can have a significant effect on the computed decay constant. The most representative results will likely be obtained when appropriate filter properties are chosen to eliminate excessive high and low frequencies, and when these properties are maintained throughout the monitoring period.

The second and more important factor that influences the decay constant is the number of signal cycles included in the curve-fitting. Figure 6-6 shows the variation in the decay constant (α) as a result of including different numbers of cycles in the analysis. This signal is from the first reactive specimen under significantly deteriorated conditions, but the trends are typical for each of the three specimens at all levels of deterioration. As shown in the figure, the decay constant can decrease more than 15% when the number of cycles included in the analysis is increased from four to six, and over 30% when increased to eight. If all discernible signal cycles are included in the analysis, the decay constant drops by over 80% compared to including only four cycles. This variation is more significant than any consistent differences between tests on deteriorated and undamaged concrete. These results and observations are similar to those found by Tinkey et al. (2000).

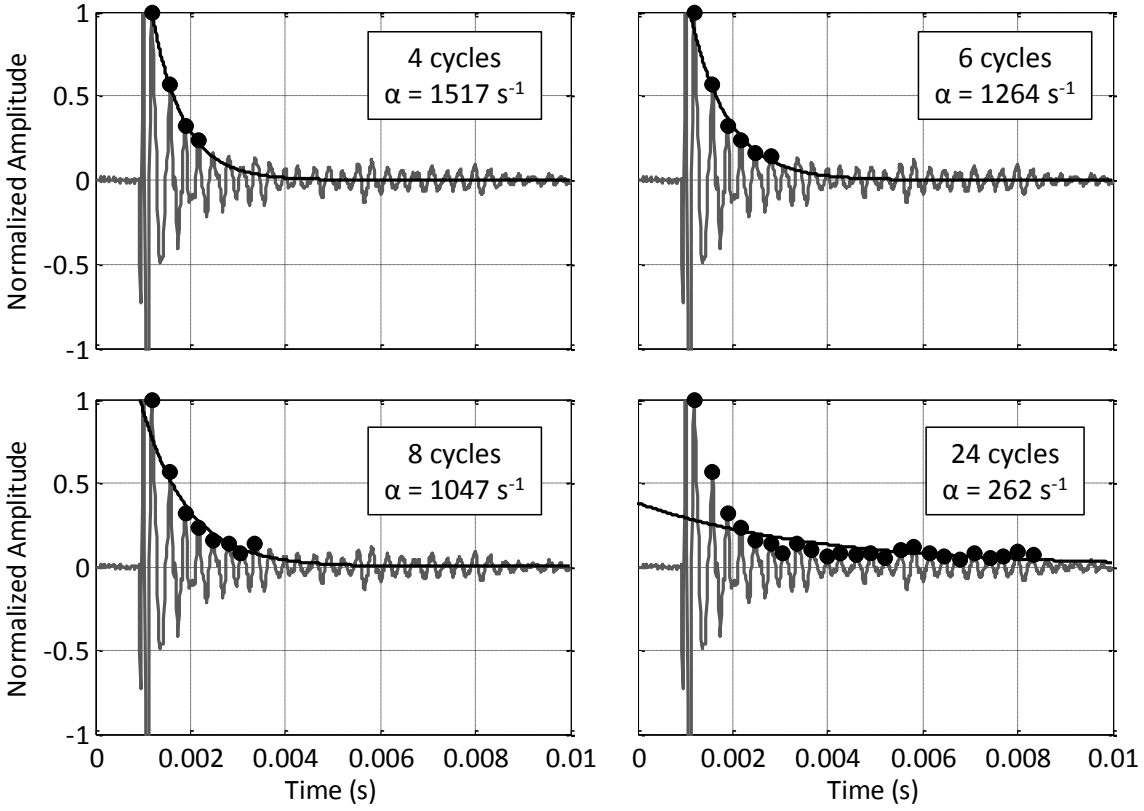

Figure 6-6: Influence of Number of Signal Cycles on Decay Constant

Using finite element modeling of infinite plates, Kesner et al. (2004) found that the signal cycles "are discernible" until 90 to 95% of the initial amplitude has been lost, and implied that all of these peaks should be used when computing the decay constant. As seen in Figure 6-6, this was found to be unrepresentative of the actual attenuation trends in the signals recorded in the current research. One reason for this is that as the energy attenuates, the signal-to-noise ratio decreases, resulting in a reduced signal quality, unless a very high vertical resolution is used. For conventional impact echo analysis, which involves observing the resonant frequency shift (see Section 6.3.2.2), such a high vertical resolution is not necessary. Another reason is that reflections from the side boundaries have a greater influence on the later portions of the signal for elements where the geometry is less similar to a plate. In an ideally infinite plate structure, as analyzed by Kesner, each peak after the initial Rayleigh wave represents consecutive arrivals of the compression wave repeatedly reflected off of the back surface.

However, in realistic elements, compression and shear waves are also reflected off of all surfaces. These reflections can alter the cycles at later times in the signal, changing the perceived arrival times and amplitudes of the compression waves, and significantly influencing the decay constant.

In general, observing the rate of attenuation in the time domain signal of an impact echo test may be able to indicate the level of ASR and DEF deterioration in an element. However, more research is needed to determine the testing parameters, most importantly the number of signal cycles to include in the analysis. Additionally, a higher vertical resolution may be needed to obtain a better quality signal for more consistent results using the time domain signals.

6.3.2.2 Frequency Domain Analysis

There are two techniques that can be used to assess ASR and DEF deterioration after transforming the signals collected during impact echo testing into the frequency domain. First, several smaller, high frequency peaks in the spectrum may be present in testing of deteriorated elements, as the incident compression wave is reflected off of the internal microcracks as well as the back surface. The second method focuses on the downward shift in the peak resonant frequency in the spectra, indicating a decreasing stiffness and a slower compression wave velocity. Figure 6-7 displays typical frequency spectra for all three beams at the time of initial measurements and after significant deterioration had occurred in the reactive specimens. These frequency spectra correspond to the time domain signals in Figure 6-5.

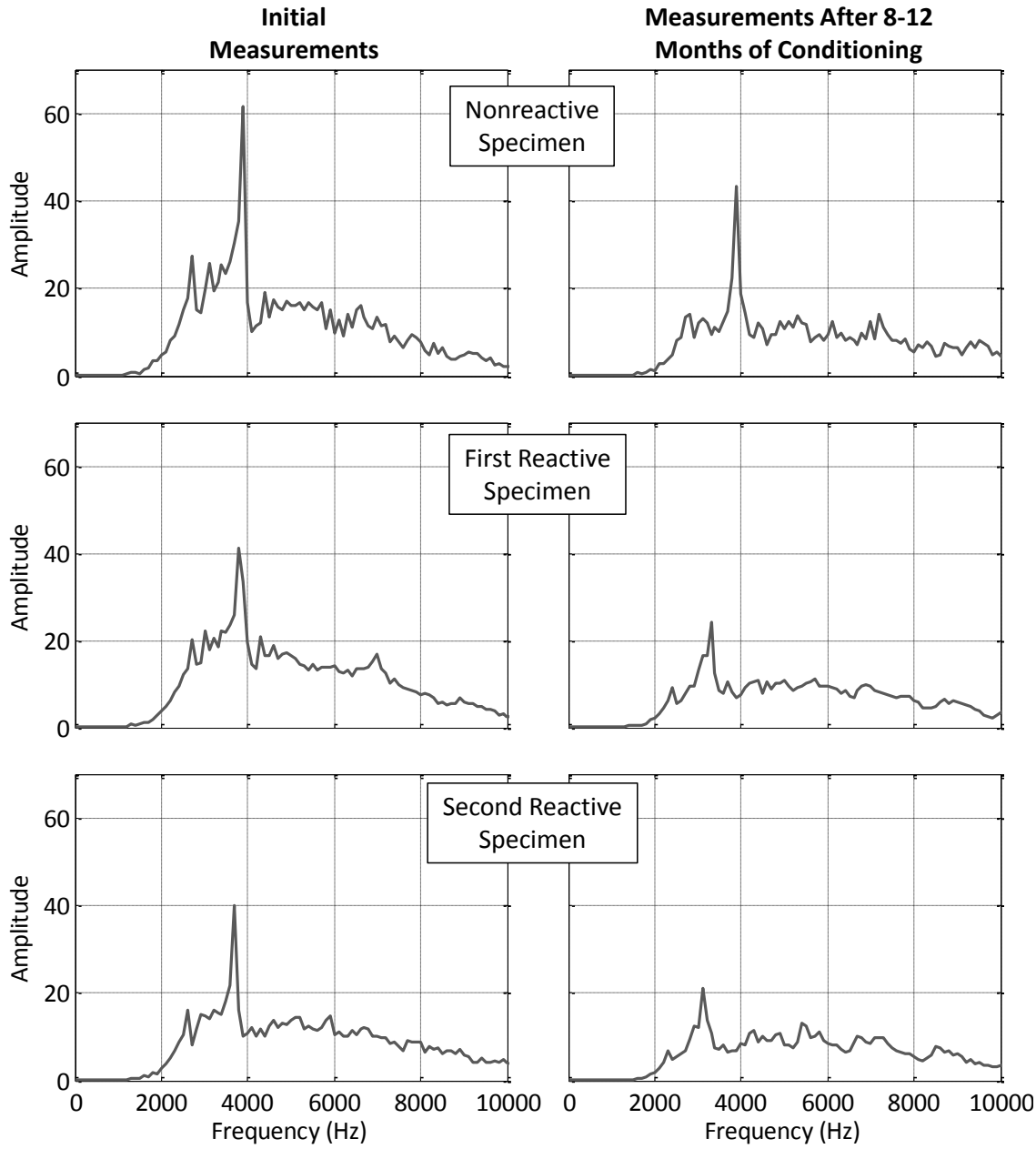

Figure 6-7: Frequency Spectra Corresponding to Time Domain Signals in Figure 6-5

There does not appear to be a significant difference in the presence of small, higher frequency peaks in the signals taken from deteriorated specimens compared to those from the nonreactive specimen or to the initial state of the reactive specimens. One reason for this may be the reflections off the side boundaries that occur as a result of the geometry of the element. If the structure tested was more plate-like, these reflections

would be less prominent in the frequency spectra, allowing for the smaller peaks indicating microcracks to be more dominant. Additionally, collecting the signal using a higher vertical resolution may eliminate some of the noise in the frequency spectrum, as well as in the time domain signal. This could also allow the smaller peaks to be more easily observed. Using a smaller impactor to induce more amplitude in the higher frequency range may also make the smaller peaks more noticeable. However, it is important to recognize that this technique is only qualitative and is more useful for determining whether or not internal microcracking may be present.

The most obvious difference between the signals from the undamaged and deteriorated specimens is the shift in the peak frequency. This corresponds to a stiffness decrease, which can be quantified by computing the compression wave velocity (see Section 3.4.1). The relationship between the vertical expansion and the velocity calculated from the impact echo measurements are given in Figure 6-8 for each of the reactive specimens. Though impact echo testing was performed at several points on both the side and top faces of the specimens, the data shown includes only the tests performed near mid-depth on the side faces in both test regions. These results were the most reliable and repeatable because the geometry most resembled a plate-like element, for which the impact echo method was developed. Also, note that the data collection parameters yielded a frequency resolution of 100 Hz (see Section 5.4.2). Even though four measurements were averaged for each data point, the trends resemble more of a stair-step than a smooth curve because of the high value of the frequency resolution. The calculated velocity in the nonreactive specimen ranged between 4220 to 4390 m/s over the monitoring period.

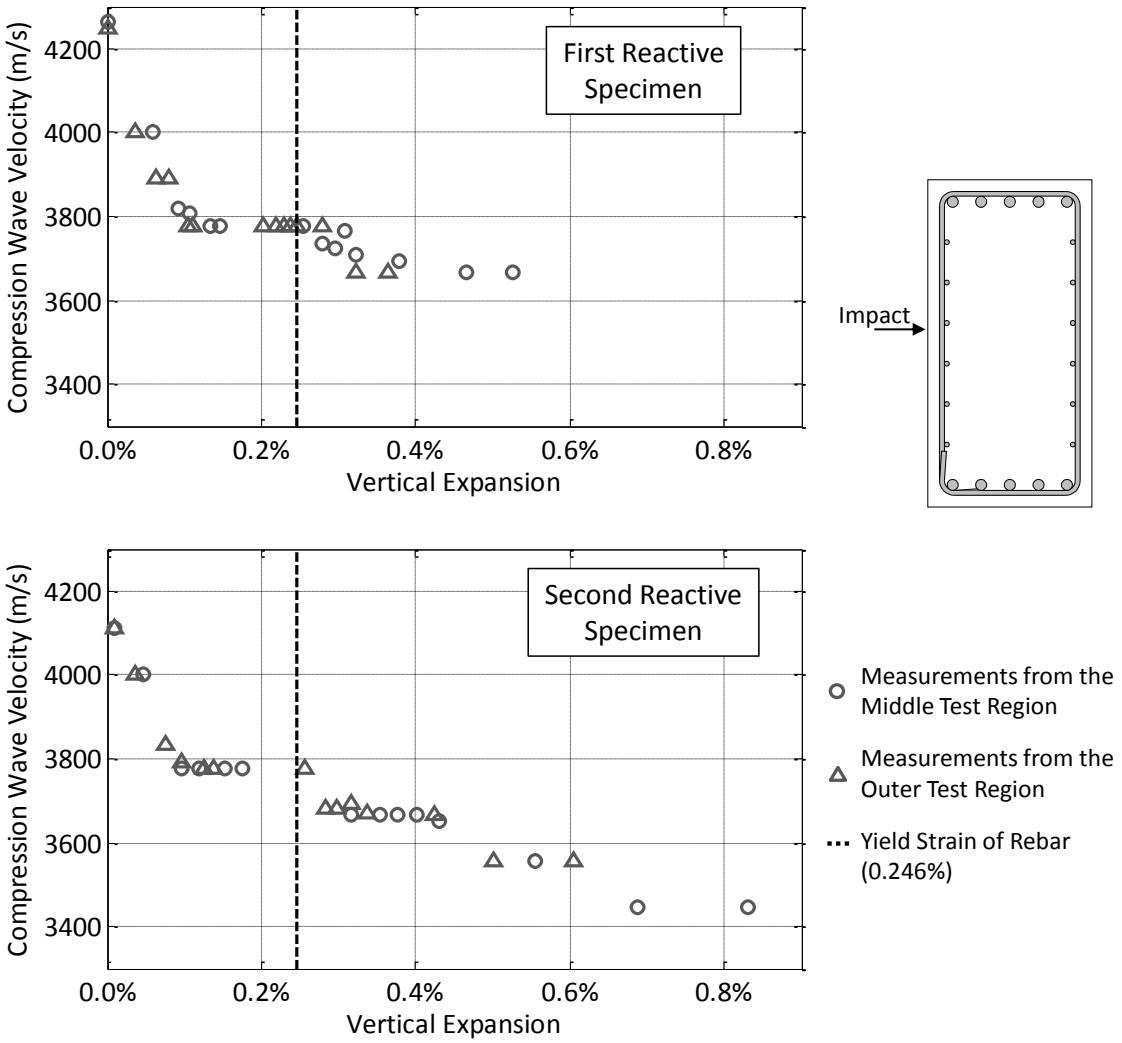

Figure 6-8: Impact Echo Results – Variation of Compression Wave Velocity

The graphs are analogous to and can be directly compared to those presenting the UPV results (Figure 6-4), as both tests measure the compression wave velocity. The trends are very similar between the UPV measurements and the velocity calculated from impact echo testing. A rapid initial decrease in velocity is observed, and the rate of velocity loss decreases as deterioration progresses. Also, note the similarity in velocity values between UPV and impact echo testing.

Like the UPV results, the impact echo velocity data are most effective in characterizing early stages of ASR and DEF deterioration (see Section 6.3.1.2). Knowing or estimating the baseline compression wave velocity is essential for assessment of the

deterioration at discrete points in time. Additionally, the general trends observed over a longer period of time can help in estimating the approximate location on the curve and the level of deterioration. Finally, recall that the compression wave velocity is a reflection of the overall quality of the concrete material, and thus cannot distinguish between various types of deterioration and defects.

6.3.3 Surface Wave Methods

Spectral analysis of surface waves (SASW) and surface wave transmission (SWT) are nondestructive techniques that measure properties of surface waves traveling through a material. Both methods use the same test setup, which consists of measuring the surface motion at two points just outside of the test region, in line with an impact point on either side. However, the signal processing and analysis differs for the two methods. After a brief overview of the typical signals collected, the SASW and SWT results are presented and discussed in Sections 6.3.3.1 and 6.3.3.2, respectively.

Figure 6-9 shows typical signals recorded during surface wave testing. Note that the same signals are used for the SASW and SWT analyses. The only portion of the signal that is analyzed is the initial arrival of the surface wave, shown as a black line in the figure. These signals illustrate the two phenomena that are observed in surface wave testing: the time delay between the arrival of the wave to the two receivers (SASW), and the difference in amplitude between the two received signals (SWT).

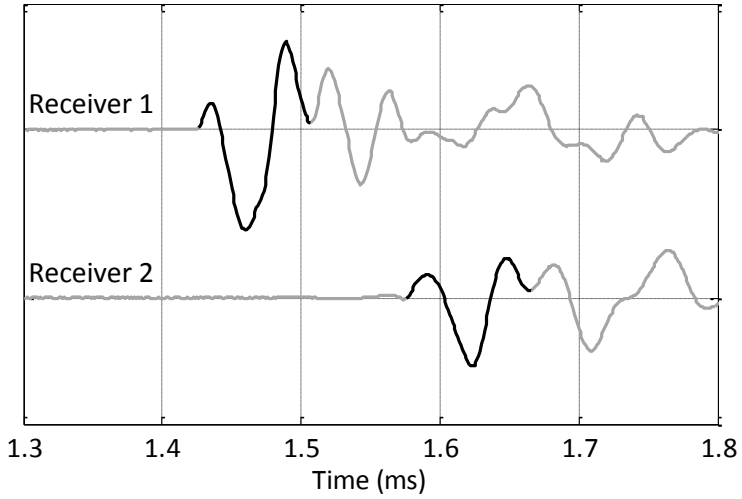

Figure 6-9: Typical Surface Wave Testing Signals

6.3.3.1 Spectral Analysis of Surface Waves (SASW)

The SASW method calculates the velocity of the different frequency components in a surface wave traveling through a material. Though the method was originally developed to distinguish between layers in pavements and soil, it may also be used for generally homogenous solids like concrete. By calculating the phase shift between the two received signals, the velocity can be obtained. As with UPV and impact echo, lower velocities indicate damage, as the wave must travel around or through the defects.

Results from an SASW analysis are often presented in the form of a dispersion curve, depicting the phase velocity as a function of frequency. A typical dispersion curve for concrete is shown in Figure 6-10. The curve on this plot represents the average of ten signals collected at one test location. Five signals are recorded from impacts on each side of the receivers, and the results from all ten signals are averaged together to minimize error caused by asymmetry in the test setup.

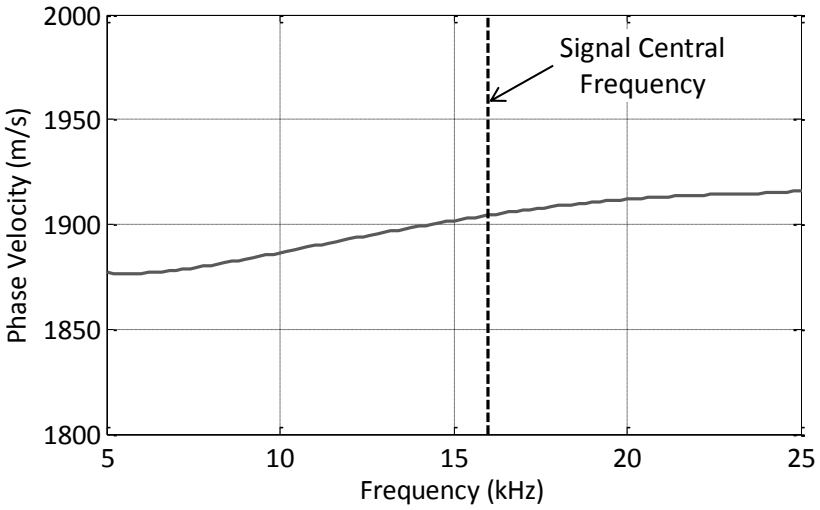

Figure 6-10: Typical Surface Wave Dispersion Curve

As can be seen in the plot, the velocity remains essentially constant through a large frequency range. The variation in phase velocity in this case is no more than 50 m/s over a range of 20 kHz. Note that the vertical axis of the plot represents a very small range. For the purposes of this research, the surface wave velocity was taken at the approximate central frequency of the received signals (16 kHz). Results from dispersion curves from five locations within a test region were averaged together to monitor the quality of the concrete in that region.

Figure 6-11 shows the results from SASW testing on the two reactive bent cap specimens. The graphs include measurements taken in both the vertical and longitudinal directions on the side faces of the specimens in the middle and outer test regions.

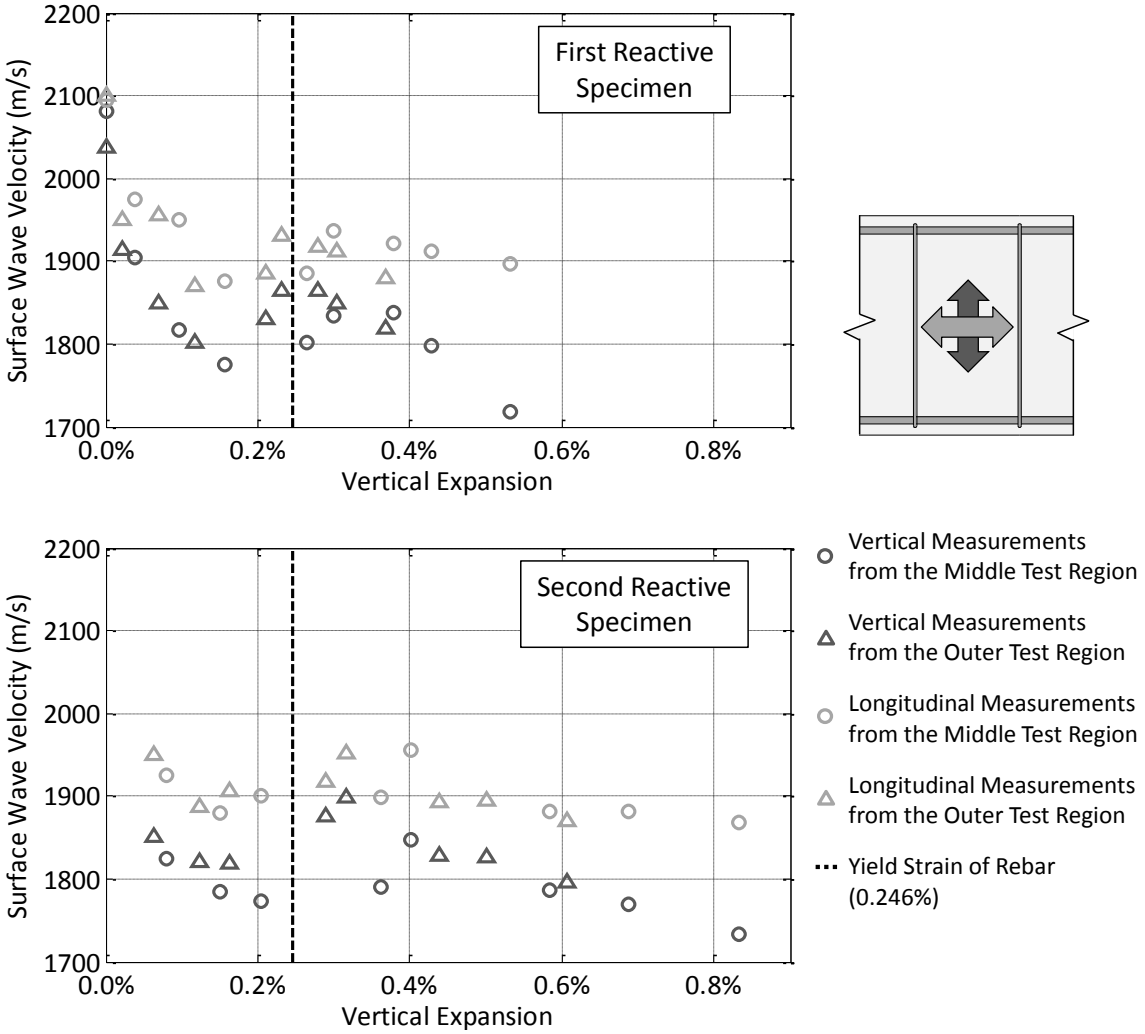

Figure 6-11: SASW Results – Variation of Surface Wave Velocity

As can be seen in the plots, the data points are widely scattered. It appears that for the first reactive specimen, a sharp drop from the initial velocity occurred at very low levels of expansions. These initial data are not available for the second reactive specimen, as deterioration began very soon after casting. However, a similar trend is predicted to have occurred. For both specimens, the trends are unclear as the deterioration progresses to higher levels.

One interesting feature of the data is that the velocities from measurements in the longitudinal direction are consistently higher than those in the vertical direction. This effect is opposite of the UPV results, where the velocity in different directions was very

similar. However, this is to be expected for surface wave measurements, as most of the surface cracking is oriented in the longitudinal direction (see Figure 6-1a), crossing the path of the vertical surface wave measurements. Very few cracks cross the path of the longitudinal measurements, leading to higher velocities in that direction.

Additionally, a discussion about the variation in the surface wave velocity measured in the nonreactive specimen over the monitoring period will illustrate the sensitivity of this method to other sources of cracking and damage. After loading the specimens, flexural cracking in the middle test region was observed in the nonreactive specimen (see Section 5.2.2). This flexural cracking penetrated into the surface wave testing area, resulting in a 5% loss in surface wave velocity in the longitudinal direction. However, this loss was recovered over time, and the surface wave velocity in both directions was similar for the remaining data points in each test region. This trend is depicted in Figure 6-12, a plot of the variation of the surface wave velocity in the nonreactive specimen against time. Though measurements were taken only four times over the monitoring period, the effects of the flexural cracking are evident.

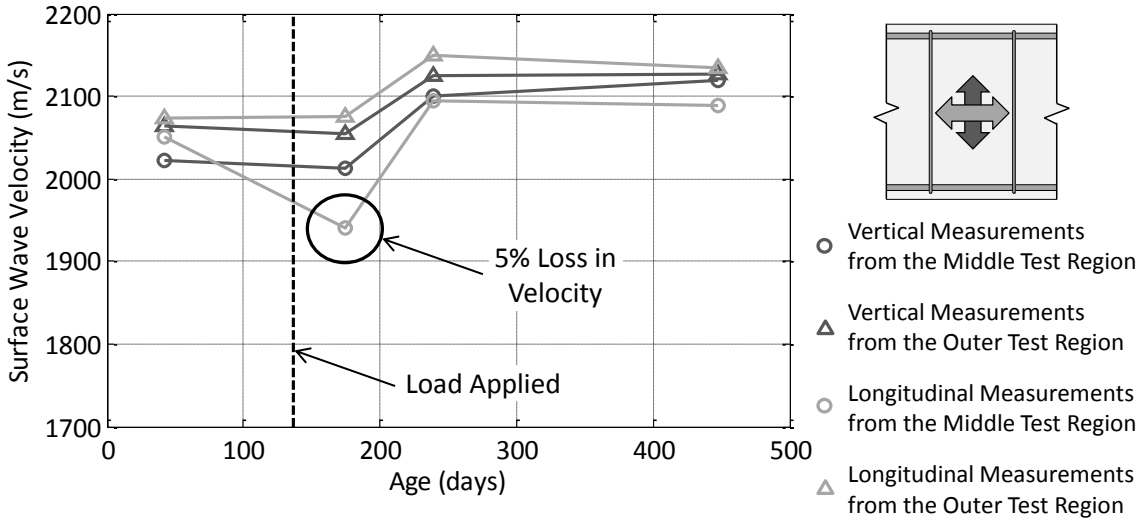

Figure 6-12: Surface Wave Velocity Variation in the Nonreactive Specimen

It is unclear what caused the surface wave velocity recovery after flexural cracking. Perhaps creep of the concrete under the load caused the cracks to slowly close, resulting in less resistance to the surface wave passing through. It is also possible that

these cracks became filled with water or other environmental debris over time, aiding the passage of the surface wave. No matter the reason, it is clear that the surface wave velocity is very sensitive to cracking from any source. Additionally, a recovery of the surface wave velocity after damage can occur over time, potentially skewing the interpretation of SASW results.

In general, these results indicate that the SASW method is not very helpful for characterizing the deterioration from ASR and DEF deterioration. Though the method appears to be effective at very early stages of deterioration, the data are widely scattered and the trends are unclear. Recovery of any loss in surface wave velocity may also occur over time. The SASW method does not seem to provide any more information than either UPV or impact echo, and is a much more time consuming method to perform because it requires data collection at several points for averaging. Additionally, the signal processing is much more complicated and requires a good deal of training to properly interpret the results.

6.3.3.2 Surface Wave Transmission (SWT)

The SWT method measures the energy transmission of the different frequency components of a surface wave between the two receivers. Lower values of transmission indicate damage, as more of the energy is scattered and attenuated by the defects. This method has been developed primarily to measure the depth of a surface breaking crack, and there were no reports found in the literature of the use of SWT for characterizing distributed cracking.

A typical variation of the surface wave energy transmission with frequency is shown in Figure 6-13. This curve represents an average of ten signals taken from one testing location. The transmission coefficient on the vertical axis is the ratio of energy present in the second receiver to that in the first. This coefficient does not take into account the geometric attenuation caused by radial spreading of the surface wave from the point impact source. It is expected that the energy present in the second received signal would be significantly lower than in the first due to the geometric attenuation. The ideal transmission coefficient, representing only the geometric attenuation, is depicted on

the graph by a horizontal dashed line. Any additional energy loss is attributed to some form of deterioration or damage in the material.

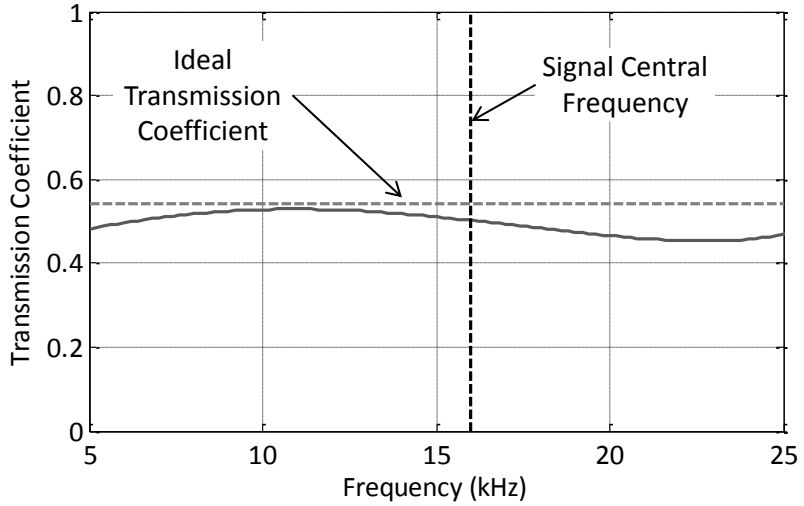

Figure 6-13: Typical Surface Wave Energy Transmission Variation

Like the surface wave velocity, the energy transmission remains fairly constant over a wide range of frequencies. For monitoring purposes, the value of the transmission coefficient was taken at 16 kHz, or the approximate central frequency of the signal. The transmission coefficients from five locations within each test region were averaged together to minimize error.

The results from the SWT testing on the two reactive specimens are depicted in Figure 6-14. The plot shows data taken in both the longitudinal and vertical directions in the middle and outer test regions.

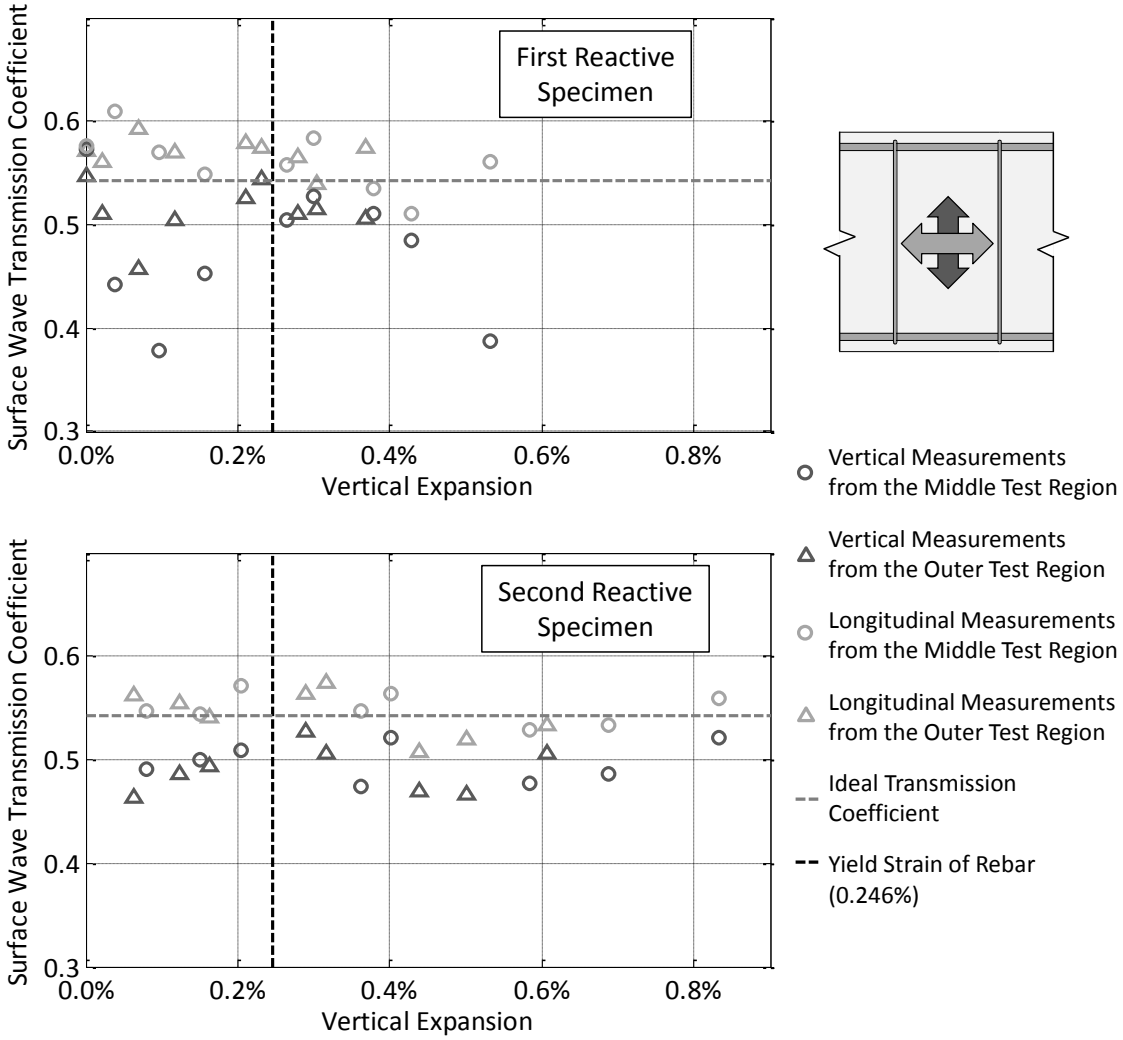

Figure 6-14: SWT Results – Variation of Surface Wave Energy Transmission

As can be seen in the plots, no discernable trends are present at any level of deterioration. The energy transmission remains relatively constant as deterioration progressed, although the data points are widely scattered. Like with the SASW results, the measurements taken in the longitudinal direction have generally higher transmission coefficients than those taken in the vertical direction, because the surface cracks in both specimens run largely in the longitudinal direction (see Figure 6-1a).

The energy transmission in the nonreactive beam followed similar trends to those of the surface wave velocity, as seen in Figure 6-15. The transmission dropped 20% as a result of flexural cracking in the middle region of the specimen after applying the

simulated service load. This loss was recovered over time, just as the loss in surface wave velocity was.

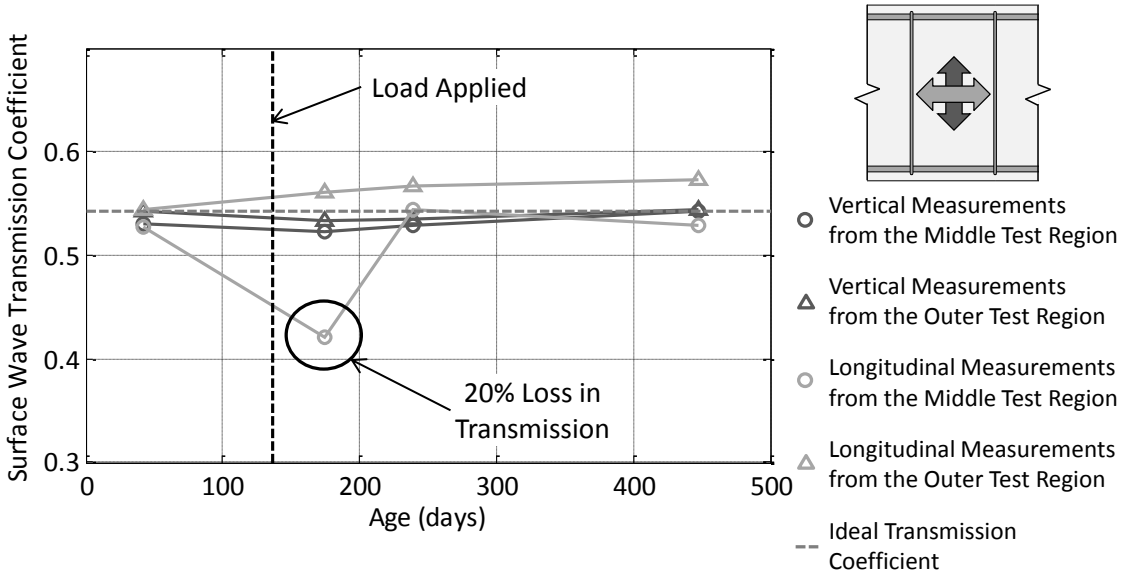

Figure 6-15: Surface Wave Energy Transmission Variation in the Nonreactive Specimen

From observing these results, it is clear that the SWT method does not provide valuable information for characterizing the level of ASR and DEF deterioration in an element. Although a decrease in energy transmission is expected as the deterioration worsens and more cracks are forming, this was not observed in the testing. One likely reason for this is the "near-field effect". As Kee and Zhu (2010) explain, interactions between the incident surface wave and other body wave reflections can amplify the apparent surface wave and make the signals difficult to interpret. This effect is prominent when the receivers are located close to surface breaking cracks. The random distribution of cracking from ASR and DEF deterioration makes it difficult to place the receivers outside of the "near-field" area.

6.3.4 Time Shift Nonlinear Acoustic Method

The advantage of using NDT methods based on nonlinear wave propagation to assess ASR and DEF deterioration is that they are more sensitive to small defects like microcracks. Traditional linear methods, including all other techniques discussed in this

chapter, are better at detecting large cracks and voids. Though several nonlinear NDT methods are in development (see Section 3.7), only one was chosen for investigation in this research. This "time shift nonlinear acoustic method" was developed at Sherbrooke University in Quebec, Canada and seemed to be the most feasible method for testing field structures (Kodjo et al. 2009). The method is based on observing the time delay and amplitude loss of ultrasonic pulses following a mechanical impact which imparts enough force to open the microcracks. Opening of the cracks reduces the amplitude of the received wave as a result of attenuation through and scattering around the cracks. A phase shift is caused by the delayed arrival of the wave. As the impact effects wear off, the cracks close and both properties return logarithmically to the original values.

A typical set of results from tests on the nonreactive and first reactive specimens near the end of the monitoring period are summarized in Figure 6-16 and Table 6-1. The plots in the figure depict the variation of the phase shift and amplitude of the received ultrasonic pulses over time. The amplitude is normalized by that of the first received pulse. The level of nonlinearity is quantified by the slope of the linear portion of the phase shift vs. amplitude plot. This portion of the plot is depicted as dark grey data points in the figure. For comparison between different elements, this slope is normalized by the linear compression wave velocity, the central frequency of the signal before impact, and the travel path length. Thus, the nonlinear parameter, α, is defined as:

$$\alpha = \frac{mV_p}{\pi f L} \qquad \textit{Equation 6-1}$$

where m is the slope of the phase shift vs. amplitude plot, V_p is the linear compression wave velocity, f is the central frequency of the pulse before impact, and L is the travel path length. Higher values of the nonlinear parameter indicate more microcracking and deterioration. Note that this nonlinear parameter is many orders of magnitude smaller than those calculated by Kodjo et al. (2009) because of a slight difference in the data manipulation. Kodjo et al. introduces a factor to relate the amplitude of the ultrasonic input signal to the strain amplitude imparted into the specimen, rather than normalizing the amplitude. Although the values cannot be directly compared, the trends can be.

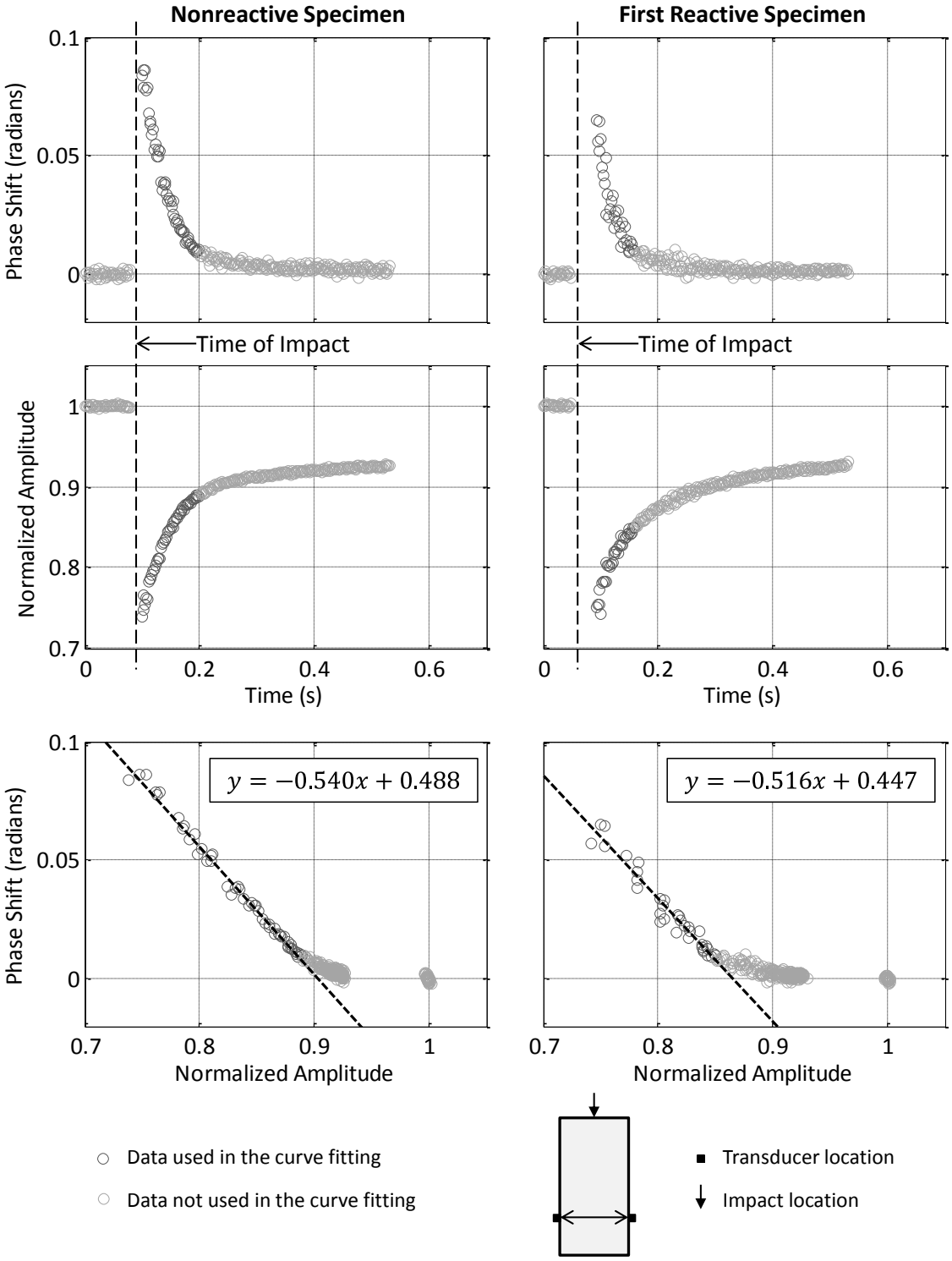

Figure 6-16: Time Shift Nonlinear Acoustic Method Results

Table 6-1: Time Shift Nonlinear Acoustic Method Results

Property	Nonreactive Specimen	First Reactive Specimen
Linear Velocity, V_p (m/s)	4290	3670
Travel Path Length, L (in)	21	21
Central Frequency, f (kHz)	89.5	57.0
Slope, m (radians)	-0.540	-0.516
Nonlinear parameter, α	0.0154	0.0198

As can be seen in the table, the linear velocity, as measured by UPV, is lower in the reactive specimen than in the nonreactive specimen. Additionally, the central frequency of the received ultrasonic signal before impact is significantly lower in the reactive specimen. Both of these observations indicate deterioration based on linear wave propagation before the mechanical impact, and are congruent with the results presented in previous sections. Additionally, the nonlinear parameter is higher for the first reactive specimen than for the nonreactive specimen. This indicates a larger amount of nonlinear behavior and microcracking in the specimen deteriorated by ASR and DEF.

Though these are results from only two tests, they indicate that this method may be useful in characterizing ASR and DEF deterioration in field structures. Unfortunately, no data were collected at low levels of expansion, as this method is not commercially available and had to be developed in-house over the course of this project. To adequately evaluate this method for assessing field structures, more research is needed to refine the most effective parameters to use during data collection and analysis, and to track the results through various levels of deterioration.

Important parameters to consider in the data collection include the sampling frequency, the vertical range and resolution, and the testing configuration. A high sampling frequency is necessary to accurately observe the very small time delays in the signal arrival. To collect a signal for a long period of time, higher sampling frequencies

require more memory to store the collected data. Similarly, a large vertical range and small vertical resolution will more accurately depict the amplitude changes. Without the proper data acquisition equipment, it is not possible to obtain high-quality data to analyze. Additionally, three testing configurations were used, as described in Section 5.4.4. To determine the most effective locations of the transducers and impact, these different configurations need to be investigated.

Several parameters must also be considered in the data analysis. Firstly, determining the amount of data points to be included in the curve fitting to determine the nonlinear parameter can widely affect the results. It is clear from the phase vs. amplitude plots in Figure 6-16 that it is unreasonable to include all of the data points in computing the slope of the best fit line. However, the exact cut-off point is unclear, and small variations can have a significant effect on the nonlinear parameter. Secondly, it is often necessary to filter the received signal to facilitate data analysis. A bandpass Butterworth filter was used to remove both high and low frequencies from the signals in the data presented here. However, changing the filter properties can also affect the results. Finally, the initial arrival of the ultrasonic compression wave has a different shape in a variety of concrete mixes. Typical received signals from the nonreactive and first reactive specimens are shown in Figure 6-17. The longer time delay and lower frequency of the signal in the first reactive specimen are evident in the figure. Additionally, while the initial arrival of the pulse is well defined in the nonreactive specimen, it is not for the first reactive specimen. Based on these differences, it is unclear how much of the signal should be included in the analysis as the first arrival of the ultrasonic wave.

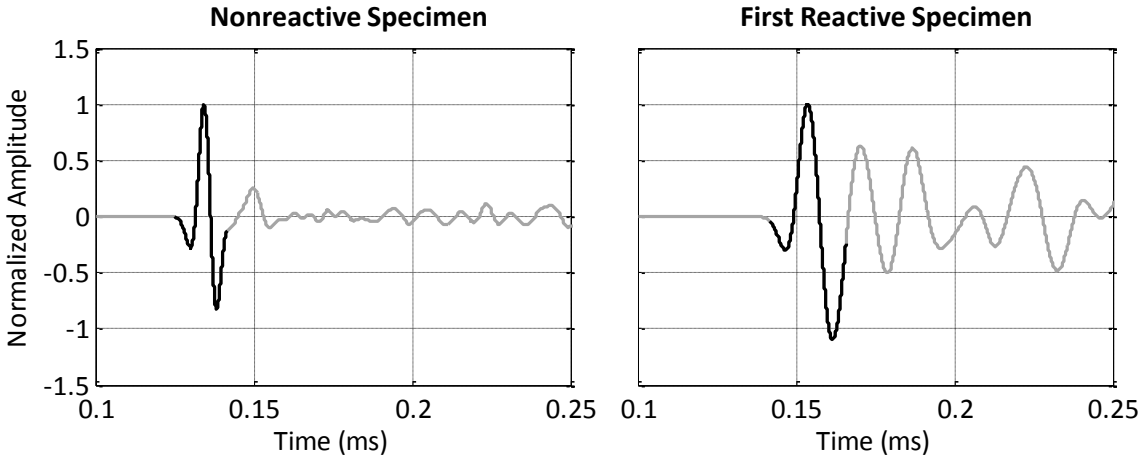

Figure 6-17: Typical Time Shift Nonlinear Acoustic Method Received Signals

Although this method may have potential for field assessment of elements affected by ASR and DEF, there are a few foreseeable problems that may arise and need to be addressed. Firstly, significantly lower received signal amplitude was observed in the reactive specimens. This indicates that the extensive microcracking damage is leading to large amounts of attenuation, which may be a problem in testing very thick elements. Additionally, it may be difficult to impart enough force into a large field structure to open the microcracks and cause a discernable nonlinear response. A small sledgehammer was used for the testing in this near-full scale study, but a larger impactor may be necessary in certain cases. Also, the effects of environmental conditions, such as moisture content and temperature, have not yet been investigated. Finally, as with all NDT methods, this technique is sensitive to many different sources of deterioration, and the results may reflect multiple types of damage.

Despite the small amount of results obtained and the potential problems associated with applying the technique on field structures, a significant benefit of nonlinear methods in general is that they are orders of magnitude more sensitive than linear methods. Thus, the importance of accurate baseline measurements is greatly diminished.

6.4 RESULTS FROM PRISM SAMPLES

Expansion and NDT monitoring of the small prism samples cast with the bent cap specimens was performed over a period of one year. The results from the expansion monitoring are presented in Section 6.4.1, followed by the NDT results from the resonant frequency testing in Section 6.4.2.

6.4.1 Expansion Results

The deterioration in the small prism samples cast alongside the bent cap specimens was quantified by measuring the length change, or expansion, of the prisms according to the provisions of ASTM C1293 (2008) (see Section 5.5.1). The results are presented in Figure 6-18, which shows the range of expansions of the four prisms cast with each bent cap specimen, as well as the average expansion over the monitoring period. The NDT results were compared with the average expansions.

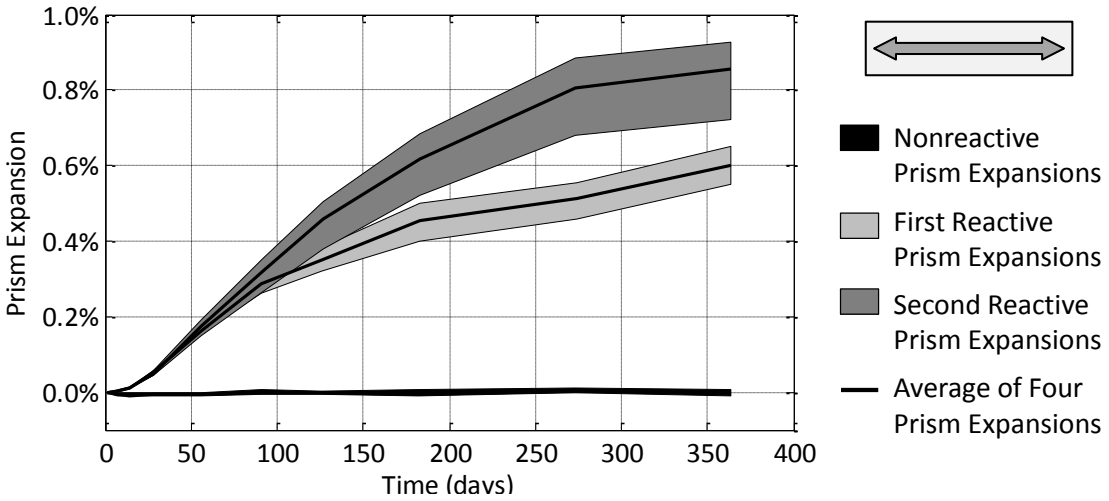

Figure 6-18: Range of Measured Prism Sample Expansions

As can be seen in the figure, the trends are very similar to the bent cap expansions. The nonreactive prisms have not shown any signs of expansion, confirming that no ASR or DEF is present in the control prisms. The reactive prisms, on the other hand, have expanded significantly over the monitoring period. The prism expansions are comparable, but slightly higher than the largest measured expansions in the bent cap specimens. This is to be expected, as the prisms are not reinforced and experience

unrestrained expansion. Additionally, the prisms corresponding to the second reactive concrete mixture have expanded more rapidly than those fabricated from the first reactive mixture. This is attributed to the difference in curing temperatures of the prisms, which were approximately match-cured to the bent cap specimens in an oven (see Section 4.3.3). Like the bent cap specimens, the second reactive prisms sustained temperatures above the DEF threshold for at least 12 hours, while the maximum temperatures in the first reactive prisms hovered around the DEF threshold, but were not sustained for a significant amount of time. Thus, it is expected that the higher rate of expansion in the second reactive prisms is a result of a combination of ASR and DEF deterioration, while the expansion in the first reactive prisms is attributed mostly to ASR deterioration.

6.4.2 Resonant Frequency NDT Results

The resonant frequency NDT method, as defined by ASTM C215 (2008), was performed on the prism samples as deterioration progressed. The concept of the test is to record the motion of an element after a mechanical impact to determine the resonant frequencies of vibration. As discussed in Chapter 3, the dynamic elastic modulus, E_d, can be computed by:

$$E_d = CMn^2 \qquad \textit{Equation 3-4}$$

where n is the measured fundamental frequency of a particular mode of free vibration, M is the mass of the element, and C is a constant based on the geometry. A lower resonant frequency results in a lower modulus, indicating a reduced stiffness and increased deterioration. Results from the resonant frequency testing on the reactive prisms are shown in Figure 6-19, which depicts the variation in the dynamic elastic modulus with deterioration. The data include results from testing in both the transverse and longitudinal directions. The average dynamic moduli calculated for the nonreactive prisms ranged from 5200 to 5400 ksi, although resonant frequency testing was not performed for the first three months of monitoring of these prisms.

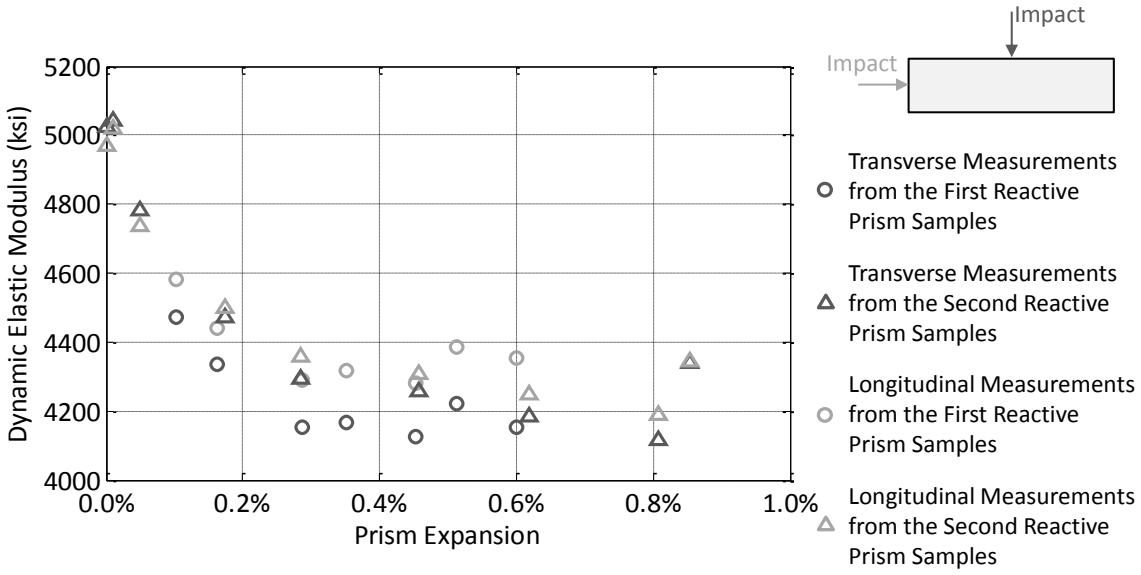

Figure 6-19: Resonant Frequency Results – Variation of Dynamic Elastic Modulus

The trends from the resonant frequency results are very similar to the variation in compression velocity measured using UPV and impact echo. An initial drop in the modulus was observed with low levels of expansion. As the deterioration progressed, the modulus tended to level off and the data points became more widely scattered. One possible explanation for the flattening of the curve at higher expansions is that the cracks were filled with ASR gel, effectively stiffening the element. This is the same reasoning that is often given for the leveling off of the compression wave velocity at high levels of expansion. Additionally, the dynamic elastic modulus was similar for testing in the transverse and longitudinal directions. The data indicate that the modulus may tend to be slightly higher when computed from the longitudinal resonant frequency (shown as light grey data points), but this is likely due to small errors in the calculations, as approximate nominal dimensions of the prisms were used.

These results indicate that the resonant frequency method, like UPV and impact echo, is most effective at low levels of deterioration. However, this method cannot be easily and directly performed on field structures, as can UPV and impact echo. Instead, cores must be taken for resonant frequency testing, making it actually a semi-destructive method. Additionally, when the core is removed from the element, the effects of

confinement by the reinforcement and load-induced stresses are also removed, and the core becomes less representative of the field structure. Note that it is possible to perform a modified version of resonant frequency testing on a field structure, but computer modeling is required to relate the measured resonant frequencies to the dynamic elastic modulus when the geometry and boundary conditions are more complex.

6.5 SUMMARY

Over a period of approximately one year, the bent cap specimens and small prism samples were monitored as ASR and DEF deterioration progressed. Along with visual observation, expansions were measured to quantify the level of deterioration, and several NDT methods were performed to determine which methods may be useful for characterizing deterioration in field structures.

All reactive specimens exhibited significant amounts of visible surface cracking and expansion as a result of the ASR and DEF deterioration, while the nonreactive controls showed no signs of deterioration. Note that the deterioration was accelerated in this study and is analogous to what a field structure would see over a much longer period of time. In general, more rapid expansion was observed in the second reactive specimen and prisms, which sustained curing temperatures above the DEF threshold for at least 12 hours, while the first reactive specimen and prisms did not. Also, more rapid expansion was measured in locations and directions of less restraining reinforcement.

The compression wave velocity, measured by either UPV or impact echo, seems to be the most effective NDT parameter for the assessment of deterioration in field structures, at least at low levels of expansion. As the deterioration progresses, however, the velocity is less sensitive to increasing expansions and becomes a less useful assessment tool. The surface wave velocity, measured using the SASW method, showed similar trends to the compression wave velocity, but the results were more scattered and the test is more time-consuming to perform and analyze. Computing the dynamic elastic modulus from the measured resonant frequencies also exhibited similar trends to the compression and surface wave velocities. However, this method requires drilling cores from the structure, which makes it a semi-destructive method and removes the test

specimen from the field conditions. Additionally, having baseline measurements, or knowing what the value of the velocity or modulus would have been if there was no deterioration, is important for all of these methods.

The alternate methods of analyzing the impact echo data were less useful than computing the compression wave velocity. The time domain method based on attenuation of reflected compression waves needs more refinement to clarify the proper parameters to be used in the analysis. Observing the amount of smaller peaks in the frequency spectrum may be a helpful diagnostic tool if high quality data are obtained, but cannot be used as a quantitative measure of deterioration. Similarly, measuring the energy transmission of a surface wave using the SWT method gave poor results, as the extensive network of cracks reflected various waves that interfered with the analyzed surface wave.

Finally, the time shift nonlinear acoustic method showed some promise for assessing the deterioration, although more research is needed to determine the most effective data collection and analysis parameters. The benefits to using nonlinear methods are that they are more sensitive to microcracking than are linear methods, meaning that baseline measurements and small errors in the testing are less important. However, the method requires complex data processing and very precise equipment, and the results may be affected by environmental factors.

CHAPTER 7
Summary, Conclusions, and Recommendations

7.1 SUMMARY

Alkali-silica reaction (ASR) and delayed ettringite formation (DEF) are responsible for the deterioration of many highway structures throughout the state of Texas and around the world in recent decades. Several researchers have indicated that the expansions and cracking caused by ASR and DEF may not adversely affect the structural performance of a reinforced concrete element. Even though the strength and stiffness of plain concrete are significantly reduced by the deterioration, the restraint and confinement provided by the reinforcement helps to maintain the integrity of the structure. The current greatest concern for structural performance is the potential for rebar fracture, which may eliminate the beneficial effects of the reinforcement. Additionally, the extensive surface cracking presents a serviceability problem, as water and other contaminants can penetrate the element through the cracks.

A considerable amount of research has been performed regarding ASR and DEF in the state of Texas and around the world. For the most part, the prevention of ASR and DEF in new structures has been achieved. A significant concern remains with the evaluation of in-service structures suffering from various levels of deterioration. This evaluation process consists of diagnosing the source of deterioration, assessing the current level of deterioration, predicting the future deterioration, and determining plans for mitigation or repair. The goal of this research was to determine how nondestructive testing (NDT) can supplement the methods already used in this process. The NDT methods discussed here largely fall into the category of assessment of the level of deterioration in a structure at discrete points in time, as well as tracking and predicting the future deterioration.

To evaluate the capability of various NDT methods to characterize ASR and DEF deterioration, three near full-scale reinforced concrete specimens were fabricated,

representing bent caps typically found in the state of Texas. Accelerated ASR and DEF deterioration was induced in the two reactive specimens by carefully selecting materials, ensuring high curing temperatures, and providing a warm, high humidity conditioning environment. The third specimen was a nonreactive control which exhibited no signs of ASR or DEF deterioration. All specimens were subjected to the same conditioning regime, which included providing a constant supply of moisture and applying a service load to simulate stress conditions seen in the field. Over the monitoring period of approximately one year, deterioration was quantified by measuring expansions in several locations on each specimen. Several NDT methods were performed as deterioration progressed, namely ultrasonic pulse velocity (UPV), impact echo, spectral analysis of surface waves (SASW), surface wave transmission (SWT) and a nonlinear acoustic method. Additionally, small prism samples were fabricated alongside the bent cap specimens. Monitoring included measuring prism expansions and performing the resonant frequency NDT method.

7.2 CONCLUSIONS AND RECOMMENDATIONS

Based on the results from this research, the following conclusions and recommendations are made in regards to using NDT methods to evaluate in-service concrete structures affected by ASR and DEF:

1. ***A loss in compression wave velocity, measured by either UPV or impact echo, was found to be the best and most consistent indicator at <u>low</u> levels of deterioration.*** Both UPV and impact echo are easy and quick methods to perform. However, UPV is recommended over impact echo because of the simpler and more consistent analysis that does not require performing a Fourier Transform. Impact echo can be used in cases when access to only one side of the element is available. One disadvantage to measuring the compression wave velocity is that it is less sensitive to higher levels of deterioration. Results from this research indicated that the velocity remains fairly constant as expansions increase beyond approximately the yield strain of the transverse reinforcement. Additionally, the velocity is dependent on many factors, most importantly the

concrete composition and moisture content. Thus, it is important to know or estimate a "baseline" velocity, or what the velocity was before deterioration occurred, for comparison. Finally, as with most NDT methods, the compression wave velocity is sensitive to all types of damage and cannot distinguish ASR and DEF deterioration from other damage.

2. ***Reductions in the surface wave velocity, measured using the SASW method, and in the dynamic elastic modulus, measured using the resonant frequency method, indicated similar trends to the compression wave velocity, but are not as highly recommended.*** The surface wave velocity data were more scattered, and different results were obtained for measurements in two directions, depending on the surface crack pattern. Also, a recovery of any loss in surface wave velocity may occur over time, as observed in the research presented here. The resonant frequency method can only be performed on small samples and requires cores to be taken from the structure, making it a semi-destructive method. Removing a core for testing also eliminates the effects of internal stresses and restrained expansion, limiting the comparability of the core to the field structure
3. ***The impact echo techniques of time domain attenuation analysis and observation of smaller peaks in the frequency spectrum did not yield reliable results.*** Though the time domain analysis generally indicated more attenuation when deterioration was present, the results are greatly affected by the number of compression wave arrivals to include in the analysis. Reflections off side boundaries and noise in the received signal can also affect the results. Additional small frequency peaks were not observed in the spectra of signals from deteriorated specimens. The presence of small peaks may have been overshadowed by boundary reflections or by noise in the collected signal.
4. ***The energy transmission of surface waves using the SWT method was not sensitive to ASR and DEF deterioration.*** This is likely due to the near-field effect, in which reflections of body waves off cracks interfere with the analyzed

surface wave. Because of the vast network of surface cracking caused by ASR and DEF, it is difficult to locate the receivers to avoid this effect.

5. ***The time shift nonlinear acoustic method may have the potential to evaluate ASR and DEF deterioration, but more research is needed to refine the parameters of the test and to track the results as deterioration progresses.*** Nonlinear propagation of waves is more sensitive to microcracking than traditional linear methods, including all other methods discussed here, which are more effective at detecting larger defects. This also means that having a baseline value is less important than with linear methods. However, the method requires high-powered, precision equipment, as very large data files must be collected, stored and analyzed. Another potential problem is safely impacting the structure with enough force to induce measureable nonlinear behavior. Effects of environmental conditions, such as moisture content, have not yet been studied. Finally, more data need to be collected to understand the trends as deterioration progresses.

6. ***None of the NDT methods investigated in this study are expected to be effective evaluation tools at high levels of expansion or for predicting structural performance.*** Many of the NDT methods (UPV, impact echo, SASW and resonant frequency) are sensitive to early ASR and DEF deterioration, but the subsequent loss in velocity or modulus becomes less significant as expansion increases. Additionally, NDT results will likely not be able to adequately predict structure performance. This is because the parameters measured with the nondestructive tests, like wave velocity, are associated primarily with properties of only the concrete. The interaction between the expanding concrete and the restraining reinforcement is not adequately represented in the NDT results.

7.3 FUTURE WORK

The NDT results obtained in this research may be helpful in the assessment of current and future ASR and DEF deterioration in the field if applied appropriately. However, predicting structural performance is not possible using the NDT methods

investigated in this research, because the NDT parameters reflect only the concrete properties and do not take into account the interaction between the expanding concrete and the restraining reinforcement. It is also important to consider the differences between field and laboratory testing when relating these findings to field testing. Additional research to connect laboratory and field testing will be helpful in making this transition. Also, methods of diagnosing and mitigating ASR and DEF deterioration are key components in the evaluation process. In particular, effective mitigation methods need to be developed to reduce any potential threats to public safety that may be caused by ASR and DEF. Finally, more structural testing of full scale deteriorated elements should be performed to fully understand the implications of ASR and DEF expansions and cracking on the structural behavior. This includes investigating the potential for rebar fracture and its implications on behavior.

References

Achenbach, J.D., Keer, L.M. & Mendelsohn, D.A., 1980. Elastodynamic analysis of an edge crack. Journal of Applied Mechanics, 47(3), pp.551-556.

ACI Committee 228, 1998. ACI 228.2R Nondestructive Test Methods for Evaluation of Concrete in Structures, Report No 228.2R. Nondestructive Testing of Concrete, American Concrete Institute.

ACI Committee 228, 2003. In-place methods to estimate concrete strength, Report No 228.1R. Nondestructive Testing of Concrete, American Concrete Institute.

Ahmed, T., Burley, E. & Rigden, S., 1998. The Static and Fatigue Strength of Reinforced Concrete Beams Affected by Alkali-Silica Reaction. ACI Materials Journal, 95(4), pp.376-388.

Alexander, M.G., Blight, G.E. & Lampacher, B.J., 1992. Pre-demolition tests on structural concrete damaged by AAR. In 9th International Conference on Alkali-Aggregate Reaction in Concrete. London: Concrete Society, pp. 1-8.

Angel, Y.C. & Achenbach, J.D., 1984. Reflection and transmission of obliquely incident Rayleigh waves by a surface-breaking crack. The Journal of the Acoustical Society of America, 75(2), pp.313-319.

ASTM C1293, 2008. Standard Test Method for Determination of Length Change of Concrete Due to Alkali-Silica Reaction, American Society for Testing and Materials.

ASTM C1383, 2004. Standard test method for measuring the P-wave speed and the thickness of concrete plates using the impact-echo method, American Society for Testing and Materials.

ASTM C192, 2007. Standard Practice for Making and Curing Concrete Test Specimens in the Laboratory, American Society for Testing and Materials.

ASTM C215, 2008. Standard Test Method for Fundamental Transverse, Longitudinal, and Torsional Resonant Frequencies of Concrete Specimens, American Society for Testing and Materials.

ASTM C597, 2009. Standard test method for pulse velocity through concrete, American Society for Testing and Materials.

Bach, F., Thorsen, T.S. & Nielsen, M.P., 1992. Load carrying capacity of structural members subjected to alkali-silica reactions. In 9th International Conference on Alkali-Aggregate Reaction in Concrete. London: Concrete Society, pp. 9-21.

Bauer, S., Cornell, B. Figurski, D., Ley, T., Miralles, J. & Folliard, K., 2006. Alkali-silica reaction and delayed ettringite formation in concrete: A literature review, Report No 0-4085-1. Center for Transportation Research, The University of Texas at Austin, Austin, TX.

Blight, G.E., Alexander, M.G., Schutte, W.K. & Ralph, T.K., 1983. The effect of alkali-aggregate reaction on the strength and deformation of a reinforced concrete structure. In 6th International Conference on Alkali-Aggregate Reaction. Copenhagen: Technical University of Denmark, pp. 401-410.

Boenig, A., 2000. Bridges with Premature Concrete Deterioration: Field Observations and Large-Scale Testing, MS Thesis, The University of Texas at Austin.

Bungey, J.H., 1991. Ultrasonic testing to identify alkali-silica reaction in concrete. British Journal of NDT, 33(5), pp.227-231.

Chana, P.S. & Korobokis, G.A., 1992. The structural performance of reinforced concrete affected by alkali silica reaction: Phase II, Contractor Report 311. Transport and Road Research Laboratory, Crowthorne, Berkshire, United Kingdom.

Chen, J., Jayapalan, A., Kim, J., Kurtis, K.E. & Jacobs, L.J., 2010. Rapid evaluation of alkali–silica reactivity of aggregates using a nonlinear resonance spectroscopy technique. Cement and Concrete Research, 40(6), pp.914-923.

Chen, X. & Wang, Y., 2009. Experimental and numerical study on microcrack detection using contact nonlinear acoustics. Frontiers of Architecture and Civil Engineering in China, 3(2), pp.137-141.

Clark, L.A., 1989. Critical review of the structural implications of the alkali silica reaction in concrete, Contractor Report 169. Transport and Road Research Laboratory, Crowthorne, Berkshire, United Kingdom.

Delsanto, P. & Scalerandi, M., 2003. Modeling nonclassical nonlinearity, conditioning, and slow dynamics effects in mesoscopic elastic materials. Physical Review B, 68(6), pp.1-9.

Deschenes, D.J., 2009. ASR/DEF-Damaged Bent Caps: Shear Tests and Field Implications, MS Thesis, The University of Texas at Austin.

Fan, S. & Hanson, J.M., 1998. Effect of Alkali Silica Reaction Expansion and Cracking on Structural Behavior of Reinforced Concrete Beams. ACI Structural Journal, 95(5), pp.498-505.

Gibson, A., 2004. Advances in nondestructive testing of concrete pavements, PhD Dissertation, University of Illinois at Urbana-Champaign.

Gibson, A. & Popovics, J.S., 2005. Lamb wave basis for impact-echo method analysis. Journal of Engineering Mechanics, 131(4), pp.438-443.

Hajighasemali, S., Ramezanianpour, A.A. & Lotfi, V., 2008. Flexural strength and numerical simulation of ASR affected beams. In 13th International Conference on Alkali-Aggregate Reaction in Concrete. Trondheim: CD-ROM.

Henriksen, C., 1995. Impact-echo testing. Concrete International, 17(5), pp.55-58.

Hevin, G., Abraham, O., Pedersen, H. & Campillo, M., 1998. Characterisation of surface cracks with Rayleigh waves : A numerical model. NDT & E International, 31(4), pp.289-297.

Imai, H., Yamasaki, T., Maehara, H. & Miyagawa, T., 1983. The deterioration by alkali-silica reaction of Hanshin Expressway concrete structures. In 6th International Conference on Alkali-Aggregate Reaction. Copenhagen: Technical University of Denmark, pp. 131-135.

Ishizuka, M., Utho, D., Kuzume, K., Sugimoto, M. & Nishiboshi, M., 1989. Characteristics of road structures damaged by AAR on the Hanshin Expressway due to continuous observation. In 8th International Conference on Alkali-Aggregate Reaction. Kyoto: Spon Press, pp. 771-778.

Jhang, K., 2009. Nonlinear Ultrasonic Techniques for Non- destructive Assessment of Micro Damage in Material: A Review. International Journal of Precision Engineering and Manufacturing, 10(1), pp.123-135.

Johnson, P.A., 2007. Nonequilibrium nonlinear-dynamics in solids: State of the art. In P. P. Delsanto, ed. Universality of Nonclassical Nonlinearity: Applications to Non-Destructive Evaluation. Dordrecht: Springer.

Johnson, P. & Sutin, A., 2005. Slow dynamics and anomalous nonlinear fast dynamics in diverse solids. The Journal of the Acoustical Society of America, 117(1), pp.124-130.

Kazakov, V.V., Sutin, A. & Johnson, P., 2002. Sensitive imaging of an elastic nonlinear wave-scattering source in a solid. Applied Physics Letters, 81(4), pp.646-648.

Kee, S., 2010. Personal Communication.

Kee, S. & Zhu, J., 2010. Using air-coupled sensors to determine the depth of a surface-breaking crack in concrete. The Journal of the Acoustical Society of America, 127(3), pp.1279-1287.

Kesner, K., Sansalone, M. & Poston, R.W., 2004. Detection and quantification of distributed damage in concrete using transient stress waves. ACI Materials Journal, 101(4), pp.318-326.

Kodjo, A., Rivard, P., Cohen-Tenoudji, F. & Gallias, J.L., 2009. Evaluation of damages due to alkali-silica reaction with nonlinear acoustics techniques. In XIV International Conference on Nonlinear Elasticity in Materials. Lisbon: Acoustical Society of America, pp. 1-10.

Larson, N.A., 2010. Structural Performance of ASR/DEF Damaged Prestressed Concrete Trapezoidal Box Beams with Dapped Ends, MS Thesis, The University of Texas at Austin.

Livingston, R.A., Ornsby, C., Amde, A.M., Ceary, M., McMorris, N. & Finnerty, P., 2010. Field survey of delayed ettringite formation related damage in concrete bridges in the state of Maryland, Federal Highway Administration. Available at: http://www.pooledfund.org/documents/solicitations/1138.pdf.

Malhotra, V.M. & Carino, N.J., 2004. Handbook on Nondestructive Testing of Concrete 2nd ed., West Conshohocken: CRC Press.

Mendelsohn, D.A., Achenbach, J.D. & Keer, L.M., 1980. Scattering of elastic waves by a surface-breaking crack. Wave Motion, 2(3), pp.277-292.

Miyagawa, T., Seto, K., Sasaki, K., Mikata, Y., Kuzume, K. & Minami, T., 2006. Fracture of Reinforcing Steels in Concrete Structures Damaged by Alkali-Silica Reaction - Field Survey , Mechanism and Maintenance. Journal Of Advanced Concrete Technology, 4(3), pp.339-355.

Monette, L., Gardner, J. & Grattan-Bellew, P., 2000. Structural effects of the alkali-silica reaction on non-loaded and loaded reinforced concrete beams. In 11th International Conference on Alkali-Aggregate Reaction. Quebec: Centre de Recherché Interuniversitaire sur le Beton, pp. 999-1008.

Muller, M., Sutin, A., Guyer, R., Talmant, M., Laugier, P. & Johnson, P., 2005. Nonlinear resonant ultrasound spectroscopy (NRUS) applied to damage assessment in bone. The Journal of the Acoustical Society of America, 118(6), pp.3946-3952.

Ohdaira, E. & Masuzawa, N., 2000. Water content and its effect on ultrasound propagation in concrete - the possibility of NDE. Ultrasonics, 38(1), pp.546-552.

Ono, K., 2000. Long-term behavior of AAR bridge pier and the internal deterioration. In 11th International Conference on Alkali-Aggregate Reaction. Quebec: Centre de Recherché Interuniversitaire sur le Beton, pp. 1167-1174.

Ono, K., 1992. Monitoring of AAR bridge pier by vibration measurement. In 9th International Conference on Alkali-Aggregate Reaction in Concrete. London: Concrete Society, pp. 758-765.

Payan, C., Garnier, V., Moysan, J. & Johnson, P.A., 2007. Applying nonlinear resonant ultrasound spectroscopy to improving thermal damage assessment in concrete. The Journal of the Acoustical Society of America, 121(4), p.EL125-EL130.

Petersen, C.G., 2000. Impact-echo testing of railway tunnels for cracking caused by ASR, Germann Instruments A/S, Copenhagen, Denmark.

Pleau, R., Berube, M.A., Pigeon, M., Fournier, B. & Raphael, S., 1989. Mechanical behavior of concrete affected by ASR. In 8th International Conference on Alkali-Aggregate Reaction. Kyoto: Spon Press, pp. 721-726.

Popovics, J.S., Song, W., Ghandehari, M., Subramaniam, K.V., Achenbach, J.D. & Shah, S.P., 2000. Application of surface wave transmission measurements for crack depth determination in concrete. ACI Materials Journal, 97(2), pp.127-136.

Popovics, S. & Popovics, J.S., 1991. Effect of stresses on the ultrasonic pulse velocity in concrete. Materials and Structures, 24(1), pp.15-23.

Ravindrarajah, R.S., Khan, A.S. & Pathmasiri, M., 2002. Properties of high-strength high-performance concrete for marine environment. In International Conference on Concrete in Marine Environment. Hanoi: IABSE Vietnam National Center for Natural Science and Technology, pp. 1-10.

Rivard, P. & Saint-Pierre, F., 2009. Assessing alkali-silica reaction damage to concrete with non-destructive methods: From the lab to the field. Construction and Building Materials, 23(2), pp.902-909.

Saint-Pierre, F., Rivard, P. & Ballivy, G., 2007. Measurement of alkali–silica reaction progression by ultrasonic waves attenuation. Cement and Concrete Research, 37(6), pp.948-956.

Sansalone, M., 1997. Impact-echo: The complete story. ACI Structural Journal, 94(6), pp.777-786.

Sansalone, M. & Streett, W.B., 1997. Impact-Echo: Non-Destructive Evaluation of Concrete and Masonry, Jersey Shore: Bullbrier Press.

Schubert, F. & Köhler, B., 2008. Ten Lectures on Impact-Echo. Journal of Nondestructive Evaluation, 27(1-3), pp.5-21.

Shah, A.A. & Ribakov, Y., 2009a. Non-destructive evaluation of concrete in damaged and undamaged states. Materials and Design, 30(9), pp.3504-3511.

Shah, A.A. & Ribakov, Y., 2009b. Non-linear ultrasonic evaluation of damaged concrete based on higher order harmonic generation. Materials and Design, 30(10), pp.4095-4102.

Shin, W., Zhu, J., Min, J. & Popovics, J.S., 2008. Crack depth estimation in concrete using energy transmission of surface waves. ACI Materials Journal, 105(5), pp.510-516.

Song, W.J., Popovics, J.S, Aldrin, J.C. & Shah, S.P., 2003. Measurement of surface wave transmission coefficient across surface-breaking cracks and notches in concrete. The Journal of the Acoustical Society of America, 113(2), pp.717-725.

Stauffer, J.D., Woodward, C.B. & White, K.R., 2005. Nonlinear Ultrasonic Testing with Resonant and Pulse Velocity Parameters for Early Damage in Concrete. ACI Materials Journal, 102(2), pp.118-121.

Sutin, A.M. & Johnson, P.A., 2004. Nonlinear Elastic Wave NDE II. Nonlinear Wave Modulation Spectroscopy and Nonlinear Time Reversed Acoustics. In Review of Progress in Quantitative Nondestructive Evaluation. Golden: American Institute of Physics, pp. 385-392.

Swamy, R.N. & Al-Asali, M.M., 1989. Effect of alkali-silica reaction on the structural behavior of reinforced concrete beams. ACI Structural Journal, 86(4), pp.451-459.

Ten Cate, J., Smith, E. & Guyer, Ra, 2000. Universal slow dynamics in granular solids. Physical Review Letters, 85(5), pp.1020-1023.

Ten Cate, J.A. & Shankland, T.J., 1996. Slow dynamics in the nonlinear elastic response of Berea sandstone. Geophysical Research Letters, 23(21), pp.3019-3022.

The Institute of Structural Engineers, 1992. Structural effects of alkali-silica reaction, London: SETO Ltd.

Tinkey, B.V., Fowler, T.J. & Klingner, R.E., 2000. Nondestructive testing of prestressed bridge girders with distributed damage, Report No 1857-2. Center for Transportation Research, The University of Texas at Austin, Austin, TX.

Torii, K., Wasada, D., Sasatani, T. & Minato, T., 2008. A survey on ASR-affected bridge piers with fracture of steel bars on Noto Expressway. In 13th International Conference on Alkali-Aggregate Reaction in Concrete. Trondheim: CD-ROM.

Tremblay, N., Larose, E. & Rossetto, V., 2010. Probing slow dynamics of consolidated granular multicomposite materials by diffuse acoustic wave spectroscopy. The Journal of the Acoustical Society of America, 127(3), pp.1239-1243.

TxDOT, 2010. LFRD Bridge Design Manual, Texas Department of Transportation.

TxDOT, 1995. Portland Cement Concrete, Special Provision 421---028, Texas Department of Transportation.

Vakhnenko, O.O., Vakhnenko, V.O., Shankland, T.J. & TenCate, J.A., 2004. Strain-induced kinetics of intergrain defects as the mechanism of slow dynamics in the nonlinear resonant response of humid sandstone bars. Physical Review E, 70(1), pp.1-4.

Van Den Abeele, K.E., Johnson, P.A. & Sutin, A., 2000. Nonlinear Elastic Wave Spectroscopy (NEWS) Techniques to Discern Material Damage, Part I : Nonlinear Wave Modulation Spectroscopy (NWMS). Research in Nondestructive Evaluation, 12(1), pp.17-30.

Webb, Z., 2011. Experimental Investigation of ASR/DEF-Induced Rebar Fracture, MS Thesis, The University of Texas at Austin.

Yew, C.H., Chen, K.G. & Wang, D.L., 1984. An experimental study of interaction between surface waves and a surface breaking crack. The Journal of the Acoustical Society of America, 75(1), pp.189-196.

Zhu, J., 2005. Non-contact NDT of concrete structures using air-coupled sensors, PhD Dissertation, University of Illinois at Urbana-Champaign.